NORTHWESTERN UNIVERSITY

On Cyclic Robots for the Lower Limb

A DISSERTATION

SUBMITTED TO THE GRADUATE SCHOOL
IN PARTIAL FULFILLMENT OF THE REQUIREMENTS

for the degree

DOCTOR OF PHILOSOPHY

Field of Mechanical Engineering

By

Brian P. DeJong

EVANSTON, ILLINOIS

December 2007

ABSTRACT

On Cyclic Robots for the Lower Limb

Brian P. DeJong

There is a need for cyclic robots that interact with lower limbs. Such robots will bring new programmability to exercise, rehabilitation, psychophysiology, and physiology, allowing for complete customization of the foot pedal path and dynamics. These robots are novel to the robotics research field as well, since conventional robotic designs and techniques are not extendable to the cyclic, large inertia, and high power nature of lower-limb interaction.

This thesis presents and analyzes a promising design for a cyclic lower-limb robot. It discusses the incorporation of inertia, damping, and path actuation into the device, and the acceptability and implications of traveling repeatedly through singularities. Results from an in-depth simulation show that the device's clever design allows it to keep the user's foot pedal on the desired path with a reasonably sized damper and motor.

Acknowledgements

To Ed Colgate and Michael Peshkin, for advising me, teaching me, encouraging me, and challenging me

To Kevin Lynch and Kornel Ehmann, my other committee members, for their insights and help in this research.

To the members of LIMS, for their help, knowledge, and entertainment. Especially to Eric for his mentorship, Aaron for his partnership, Kyle for his encouragement, and David for his generosity.

To Emily for encouraging me, supporting me, pushing me, cheering me, celebrating with me, and, most importantly, humoring me.

"For the foolishness of God is wiser than man's wisdom, and the weakness of God is stronger than man's strength." — 1 Corinthians 1:25

Table of Contents

List of Tables

List of Figures

CHAPTER 1

Introduction

1.1. Overview

There is a need for haptic exercise robots that interact with users' lower limbs. In the exercise realm, such robots will provide complete customization of foot pedal paths and dynamics, giving users a flexibility that current exercise machines do not offer. In rehabilitation, these robots will improve patients' recoveries, allowing for targeted, asymmetrical exercise routines. In psychophysiology, lower-limb robots will help researchers find ways to reduce the perceived exertion within exercise, whether through changes in the kinematics or dynamics, or through haptic cues at the pedals. And in physiology, these robots will support the study of the human body and how it works.

Research on lower-limb exercise robots is also motivated by the fields of robotic design and control. Lower-limb haptic exercise robots are novel and they require untraditional design and control methods. Conventional robotic techniques, even those of the contemporary field of haptics, are not extendable to lower limb exercise.

For example, lower limb activity typically involves continuous, cyclic motions, such as walking, running, stair climbing, and skiing. There are many machines (exercise or otherwise) designed specifically for cyclic motions, but not so in robotics — in general, robots are designed for start-stop, even exploratory, motion. Furthermore, almost all machines designed for (non-circular) cyclic motion involve linkages that travel repeatedly through

singularities, such as internal combustion engines, windshield wipers, and, of course, elliptical exercise machines. Traditional robotics emphatically avoids singularities because of the resulting degradation of controller performance. Can lower-limb robots be designed such that they repeatedly, intentionally, and successfully travel through singularities?

Second, exercise users desire inertia in exercise machines, to help carry them around the pedals' paths. Existing exercise machines use flywheels to accomplish this. Traditional robotics wisdom, however, says to minimize inertia, so that actuators do not need to overcome it — a problem that the (one-degree-of-freedom) exercise machines do not have. How, then, should the inertia be incorporated into an (multi-degree-of-freedom) exercise robot? Can it be added such that the path actuators do not have to fight it?

Finally, lower-limb interaction involves large forces and powers to and from the user. Conventional haptic devices can't handle such interaction, while robots that can handle it are usually not safe for human interaction. In addition, exercise results in a large net flow of energy from user to device — the user wants a workout, after all. What can be done to reduce the power consumption and improve the safety of lower-limb robots? How should the devices be designed to be strong yet safe?

I began this research in an attempt to design and build an all-in-one exercise machine. But after countless struggles with designs' compromises, I realized that there is a more basic research question to be answered. Can a successful lower-limb haptic robot be designed, and if so, what are the generalizable lessons? This thesis attempts to answer that question.

In the next chapter, I present the need for lower-limb haptic robots, drawing motivation from various academic and commercial fields. Chapter 3 discusses the attributes

of this novel class of robots, using measurable quantities whenever possible. Chapter 4 presents my specific mechanism design for a robot, which I use in my analyses in the later chapters. Chapter 5 discusses the inclusion of inertia, damping, and actuation in the device. Chapter 6 analyzes the design's singularities and their implications for paths, mobility, apparent inertia, and the path controller. In Chapter 7, I show the results from an in-depth computer simulation of the device, a simulation that incorporates models for the human user, path, and masses of the mechanism. Chapter 8 details my conclusions.

1.2. Terminology

To begin, let me define some terminology.

This thesis is concerned with a class of *robots*, as opposed to a class of *machines* or *mechanisms*. A mechanism is an assembly of moving parts that performs one specific function [**86, 85**], and a machine is a device, possibly consisting of interrelated components or mechanisms with individual functions, that transfers or modifies energy [**81, 80**]. Robots are devices that sense qualities about their environment, and perform reprogrammable tasks based on those qualities [**113**]. The major distinction between robots and machines or mechanisms is the reprogrammability aspect.

A second required definition is that of a haptic device, often called a haptic display. The term *haptic* refers to the sense of touch [**51**]. Thus a haptic device is one that communicates with a human user via physical touch. Since all haptic interaction is bidirectional[1], the term "haptic display" is not entirely proper, as "display" implies one-way communication. Within this thesis, I restrict myself to the phrases "haptic device" and "haptic

---

[1]Both interacting entities are affected through their touching, as opposed to visual or auditory interaction, which is one way.

robot". An example of a haptic device is a robot that simulates virtual environments: the user holds onto and moves the robot as it simulates virtual objects with physically felt inertia, viscosity, and gravity.

Also, this thesis focuses on the rarely studied *lower-limb* haptic interaction. The class of robots described herein is meant to interact with a user via contact at the legs, most practically at the soles of the shoes. Robots that interact with a user's legs encounter much higher contact forces than those that interact with hands or fingertips. Leg interaction also means that the user has poorer motion and force control at the contact sites, since lower limbs are not as dextrous or sensitive as hands and fingers.

Although haptic interaction is both *kinesthetic* and *tactile*, I focus only on the kinesthetic sense. The tactile sense involves the contact-site sensations within the user's skin, such as stickiness, roughness, vibration, temperature, and edging. The kinesthetic sense, meanwhile, involves bodily position, movement, and forces. A haptic example involving both is the holding of an orange: the orange's skin feels rough and bumpy (using the tactile sense) and the orange feels soft, heavy, round, and inertial (using the kinesthetic sense).

Within this thesis, I restrict myself to the term *cardiovascular exercise*, although *aerobic exercise* may also be correct. While there is an important distinction with regard to physiology and medicine[2], these terms are often used interchangeably in the consumer exercise market, as devices for one type of exercise are useful for the other. Whenever I refer to the literature, I use the term used by the authors, to avoid any errors when the distinction is important.

----

[2]Cardiovascular relates to the heart and blood vessels, while aerobic involves oxygen consumption by the body.

Interaction with both legs requires the clarification of *dependent* and *independent* foot pedals (or physical interaction). With regard to exercise machines, the terms focus on the positional relationship between the pedals. Dependent pedals are those whose positions are related through a linkage or mechanism, such as the pedals of existing elliptical machines — moving one pedal moves the other. Independent pedals are not related positionally — they can be moved in separate motions by the user — such as with most two-pedaled stair climbers and ski machines. Yet even the positionally independent pedals are *indirectly* related through the dynamics of the machine, since they use the same inertial and damping elements.

Finally, I use the terms *passive* and *active* when describing machines and robots. Here, these terms refer to the net flow of energy between device and user[3]. A passive exercise machine or robot can store energy from, and return energy to, the user, such as with a flywheel or spring, but it cannot impart additional net energy to the user, such as from a motor. On the other hand, an active device can impart additional net energy to the user through its actuators.

---

[3]This is in contrast to the use of passive as "without actuators".

CHAPTER 2

The Need for Lower-Limb Haptic Exercise Robots

This chapter describes the motivation for lower-limb haptic exercise robots. I begin by discussing motivating applications, including exercise and rehabilitation. The later sections are devoted to presenting existing devices — exercise machines, exercise robots, and haptic devices — and their limitations for my particular needs. By the end of this chapter, the reader should have a clear understanding of the need for lower-limb haptic robots.

2.1. Motivating Applications

Motivation for this thesis and the presented class of robots comes from several applications, including cardiovascular exercise machines, rehabilitation, and psychophysical and physiology experiments. In general, the applications involve human users interacting with devices via their lower limbs, at non-trivial levels of exertion. Although the later motivations are more academic, I find it easier to begin with lower-limb exercise, as it is the most familiar. Chapter 3 gives a more thorough description of the application attributes that are fundamental to lower-limb haptic exercise robots.

2.1.1. Lower-Limb Exercise

The research into lower-limb haptic robots was born from a desire for an all-in-one lower-limb cardiovascular exercise machine. Today, gyms and exercise equipment stores are filled

with a variety of cardiovascular exercise machines, including ellipticals, stair climbers, ski machines, bicycles, treadmills, arc trainers, and more. See Figure 2.1 for a relatively small sampling of the assortment of exercise machines. Different machines have different foot pedal paths, from the circular bicycles to the linear stair climbers, to the individually unique and oddly shaped ellipticals. Manufacturers must run assembly lines for each type, and commercial gyms must purchase multiples of each type, so that gym users are able to find unoccupied machines of their choosing. If all of these machines can be combined into one machine, then manufacturing and purchasing is simplified. Gyms can purchase fewer machines, and users need not switch machines to vary their workout.

In addition, an all-in-one exercise machine can give more flexibility than just the type of machine or type of pedal path. If such a device has reprogrammable pedal paths (thus becoming by definition a robot), then users can customize the path to their preferences. If users want standard elliptical motion, they can choose it, but they can also modify the path shape as desired (such as increasing the stride length, rotating the shape, or flattening a specific section). This customizing of path shape can also be done by a personal trainer or by the device itself, and could be varied in time during the workout in a clever and beneficial way. With such modifications, the user, trainer, or device has potentially programmed the robot to have a pedal path that no previous exercise *machine* has had before.

Going even further, suppose the all-in-one cardiovascular exercise robot also has programmable simulated dynamics along the path, namely inertia and damping. (Existing exercise machines already have programmable damping, but it is not dynamically controlled: the damping coefficient is constant within cycles.) This new exercise robot allows

Figure 2.1. A sampling of the cardiovascular exercise equipment available. Pictures courtesy of the Life Fitness, Nautilus, NordicTrack, Matrix, Octane, Precor, Kettler, StarTrac, Cybex, and Tony Little websites.

users to determine how much the device carries them (inertia), how difficult it is to move the device (damping), and to fluctuate these amounts within a pedal cycle.

Or suppose the exercise robot has programmable stiffness perpendicular to the path. With lower stiffnesses, users have the ability to deviate from the nominal path by applying forces perpendicular to it. Such flexibility may be useful in some instances, since springiness and damping is common with real surfaces. In typical exercise, however, users want stiff path constraints. Users are rarely pushing directly tangent to the path (as shown

from the recorded forces in Section 3.4) and they are more comfortable using the path constraints to guide the pedals.

But what about the angle of the pedal relative to ground? There is anecdotal evidence that suggests, and ergonomic and physiological researchers agree, that pedal — and thus ankle — angle is very important. Because of this, existing exercise machines are designed to achieve ergonomic pedal angles at different parts of the cycle [44]. For example, ellipticals are designed so the front of the pedal is higher than its back during the front half of the cycle, and lower than its back during than back half of the cycle. Otherwise, the user's foot might be extended forward from the body and pointed downward (or backward and upward): an ergonomically poor position.

While I acknowledge that pedal angle is important, I do not address it in this thesis. I limit this discussion to the more interesting horizontal and vertical dimensions of the pedal path, and assume that proper pedal angle, whether kinematically enforced or dynamically controlled, can be added to the design at a later stage. At that time, implementing a dynamically controlled pedal angle will allow for analysis and optimization of the angle based on physiological criteria.

The aforementioned programmabilities combine to require a four-degree-of-freedom (the horizontal and vertical directions for each independent pedal) exercise robot. This robot will have the potential to revolutionize the consumer exercise market as a fully user-customizable exercise device. Not only will it replace many existing machines, but it also will give the user flexibility never seen before. The following sections discuss more academic, less market-driven, motivations.

2.1.2. Rehabilitation

A lower-limb haptic robot also has application in the rehabilitation field. Studies show that aerobic exercise during stroke rehabilitation improves strength and motor control of lower extremities [35], and greatly reduces the energy expended by, and cardiovascular demands of, the patient during a standardized walking test [82]. Furthermore, many stroke patients are physically unconditioned. Potempa and colleagues showed that stroke patients can improve their aerobic capacity and motor control with post-stroke exercise [109].

Recovering patients with high-functioning lower limbs can use lower-limb haptic robots for general exercise, but more importantly, for exercise that is customizable to their specific, even anisotropic or asymmetrical, needs. Rehabilitation patients, such as those from surgery or stroke, often train by repeating the same motion many times, preferably with resistance increasing as the patient regains strength. A haptic robot could provide the desired path with or without assistance (for motion rehabilitation), and with the desired resistance (for strength rehabilitation). It can interact with only one leg, both legs independently, or both legs dependently. Furthermore, it can isolate specific muscles for more efficient rehabilitation. As Brown suggests, "An ideal exercise would specifically target weaker muscles without exacerbating abnormal muscle activity...." [19]

2.1.3. Psychophysical and Physiological Research

Motivation for lower-limb haptic robots also comes from the psychophysical research field. For example, *perceived exertion*, or "the feeling of how heavy and strenuous a physical task is" [12], is a well-established measure of how hard a person feels they are physically

working. It is most often measured via the Ratings of Perceived Exertion (RPE), commonly called the Borg Scale [8]. For a detailed review of the perceived exertion literature, please see Appendix A.

Of significant interest is a study done by Zeni *et al.* Zeni and his colleagues tested users on various types of cardiovascular exercise machines (including stair climbing, treadmill, and cycling machines), and found that, for the same level of perceived exertion, subjects exercised at different levels of physiological and mechanical power depending on the machine [151]. Stated differently, for the same level of power output, some machines felt more difficult than others. The results from an experiment run by Glass and Chvala [48] (meant to test self-selected exercise) support these findings. Because of these and the aforementioned exercise-characteristics results, I modified a one-degree-of-freedom stair climber into a robotic device, and performed a preliminary, unpublished human experiment that suggests that increasing the device's (simulated) inertia can decrease the perceived level of workout by the user [31]. Please see Appendix B for a full description.

These studies, along with plenty of anecdotal evidence, suggest that exercise machines and robots can be designed to optimize users' workouts while reducing perceived exertion. Haptic exercise robots will allow researchers to study how various paths and dynamics affect perceived exertion, so that ideal trajectories, and simpler mechanisms that create them, can be selected to help users exercise more easily at a higher level.

Also within the psychophysical field is research into applying control and cuing techniques to help users maintain a certain level of exercise speed or intensity. Horowitz, Li, and Shields applied an adaptive damping controller to a modified stair climber to maintain users' step rates [129]. Similarly, Ferber ran human experiments on another robotic

stair climber, testing haptic cuing at the pedals [**43**]. Please see Appendix C for more information.

2.1.4. Other Areas of Motivation

Another area of motivation for lower-limb haptic exercise robots is physiological research: an exercise robot that can isolate a trajectory or muscle group in a leg can be used to study the human body and how it works. Please see Appendix C for a detailed review of the literature.

Finally, motivation comes from the robotics research field itself. Traditional robotics says to minimize inertia and avoid singularities — two guidelines inappropriate for lower-limb exercise. Can robots be designed that break these guidelines while still being successful? More information on this motivation is found throughout the remainder of this thesis.

2.2. Existing Cardiovascular Exercise Machines

Exercise machine consumers have a growing diversity of machines to choose from. In the last two decades, the consumer exercise market has seen significant growth in the array of lower-limb cardiovascular machines, with emerging and evolving machines such as bicycles, treadmills, stair climbers, ski machines, arc machines, and ellipticals. Bicycles and treadmills are relatively straightforward and I do not cover them in detail; instead I focus on the remaining four types in the following sections. Please see Appendix C for additional information.
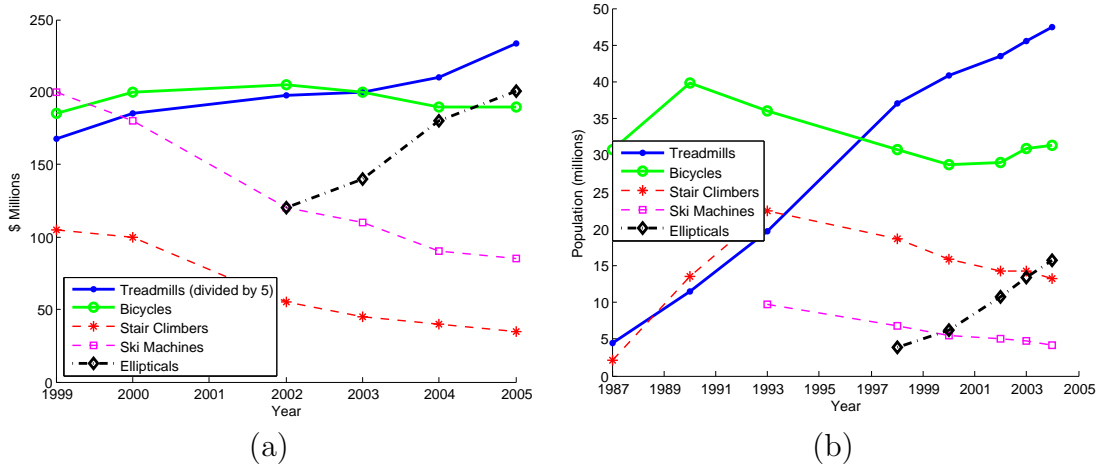
Figure 2.2. Cardiovascular equipment trends from the SGMA. (a) U.S. wholesale value of annual manufacturers shipments. (b) U.S. population, 6 years of age or older, who used a machine at least once per year. (Data taken from [**125, 126, 128, 127**]; not available for every year.)

In the last several years, ellipticals have increased dramatically in popularity, while stair climbers and ski machines have declined. Data from the Sporting Goods Manufacturers Association (SGMA) shows these trends in both monetary and participation terms; see Figure 2.2. Note that the monetary data does not directly convey quantity: for example, stair climbers generally cost less than treadmills. The data does imply, however, that users are choosing the (newer) ellipticals instead of (older) stair climbers and ski machines.

Exercise machines often have user-selectable damping levels achieved by an electronically controlled alternator. Alternators are electromechanical devices that take in a mechanical rotation and output a voltage, and can be found in many other applications, including automobiles. Exercise machines connect the pedals' cyclic motion to the rotation of the alternator, and by controlling the electrical resistance across the alternator,

they control the damping (*i.e.*, *resistance*) felt at the pedals. For a more detailed analysis of alternators with regard to exercise, see [**42**].

2.2.1. Stair Climbers

Stair climbers, also called steppers or stair steppers, are exercise machines that simulate climbing stairs. They are either passive two-pedaled devices or active escalator-like machines — an example of each type is shown in Figure 2.3. For the two-pedaled stair climbers, the pedals are usually positionally independent, and slide downward under the user's force or weight with some damping and a spring return.

When using stair climbers, users must keep exercising to stay off the ground. On two-pedaled stair climbers, they must continually step between the pedals to keep from sliding to the floor; on escalator versions, they must climb up the downward-moving stairs to avoid riding off the bottom of the machine. Treadmills use a similar motivation: to avoid falling off the back of the treadmill, users must keep running. While these techniques are effective, they are based on avoidance rather than enjoyment, like spurs on a horse rather than verbal encouragement. As such, they may be detrimental to the user's experience — users might enjoy the workout more if the motivation is positive.

2.2.2. Cross-Country Ski Machines

Cross-country ski machines (see Figure 2.4) are another class of exercise machine. They first entered homes and gyms in the 1980's, but have never gained the popularity of other machines because users feel awkward-looking when using them. Ski machines consist of passive and independent pedals or skis, as well as passive and dependent handles on either

Figure 2.3. Two examples of stair climber exercise machines. On the left, a two-pedal version from Life Fitness. On the right, an escalator version from StairMaster.

Figure 2.4. An example of an exercise ski machine, from NordicTrack.

swinging arms or cables. Both the sliding pedals and the moving handles have variable resistance in the aft direction (pulling for the handles, pushing for the pedals). Users push back on the pedals and pull on the handles as the primary efforts.

2.2.3. Arc Machines

Arc machines, also called arc trainers or swingers, are a rare type of exercise machine employing the swinging of the pedals in a simple arc. See Figure 2.5 for a few examples. They are a cross between one-dimensional stair climbers and three-dimensional-workspace ellipticals.

Figure 2.5. Examples of exercise arc machines, from Cybex (2x) and Tony Little.

2.2.4. Ellipticals

Elliptical exercise machines are named for the roughly elliptical shape of their pedal paths. Four examples of elliptical machines are shown in Figure 2.6, along with sketches of their mechanisms[1]. Ellipticals have a damped flywheel attached to the pedals via a linkage. Usually, the linkage extends to handles, allowing users to also exercise their upper bodies. The flywheel is located either in the back or the front of the device. Several designs (such as the one analyzed in Section 3.3) include secondary linkages that stretch or deform the shape of the pedal path from that of the simpler four-bar versions. Damping (thus workout) is controlled by an alternator attached to the flywheel. The main advantage of an elliptical over, say, a treadmill, is the low-impact pedals — the user's feet never fully leave the pedals.

The name "elliptical" is actually inaccurate and misleading. The actual shape of an elliptical's pedal path depends on the device's mechanism, and no two brands are alike. See Figure 2.6c for examples of approximate pedal paths. In fact, many of the path shapes are far from elliptical. Adding to the complexity is the choice of front- or rear-located

---

[1]The linkages and paths sketched in Figure 2.6 are estimated from pictures and familiarity with the devices. Exact mechanisms and dimensions are tightly guarded by manufacturers. Thus, the selected ellipticals are actually examples with relatively simple mechanisms.

(a)

(b)

(c)
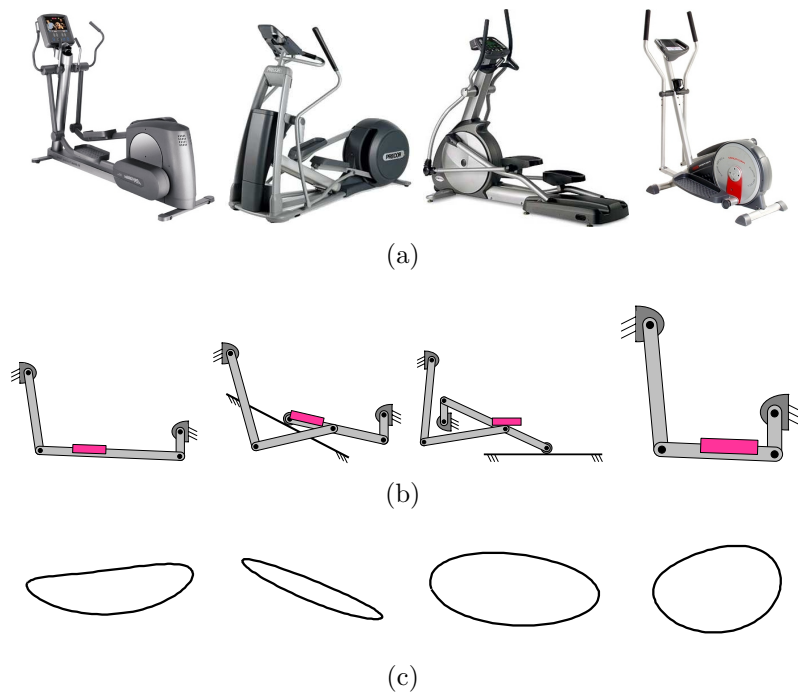
Figure 2.6. Four examples of elliptical exercise machines. From left to right, they are made by Life Fitness, Precor, Matrix, and ProForm. (a) Photos (courtesy of their websites). (b) Sketches of their linkages. (c) Approximate pedal paths.

flywheels, as the same linkage design has different (horizontally flipped) paths depending on which way it's oriented. Thus, actual path shapes range from warped and bent loops to teardrop shaped. For some ellipticals, the pedal path is strikingly similar to the path a runner's feet follow (as I will show in Figure 3.1); for others, it is far from it.

Ellipticals have always had user-selectable resistance levels, and recently have begun to incorporate limited programmability of their path shapes. Figure 2.7 shows examples of this programmability. Most of the flexibility affects the stride length. Initially, changes to the stride length were accomplished through manual adjustments made to the linkage before the user got on the machine (Figure 2.7a). Later designs allowed for adjustment

Figure 2.7. Types of path shape adjustments available on ellipticals. (a) Manual stride-length adjustment (*e.g.*, ProForm and Life Fitness). (b) Button or console stride-length adjustment (*e.g.*, Octane and SportsArt). (c) Automatic stride-length adjustment (*e.g.*, Life Fitness and Nautilus). (d) Path-tilt adjustment (*e.g.*, Precor), arm-leg direction toggling (*e.g.*, StarTrac), and flexible pedal angle (*e.g.*, Matrix).

via buttons on the console or handles (Figure 2.7b), and more recently as automatic adjustment based on a user's input — the stride slowly lengthens or shortens based on the force input at the pedal (Figure 2.7c). It is unclear whether this automatic adjustment is accomplished through a strong damper, or a sensor and actuator combination. Other examples of programmability (Figure 2.7d) are in the tilt of the pedal paths (by adjusting the slope of a linear rail), toggling the direction of arm motion with respect to leg motion (*i.e.*, moving in the same or opposite direction), and flexible pedal angles via compliant connections.

2.3. Existing Robots for Human Interaction

While the consumer exercise market contains a plethora of cardiovascular exercise machines, there are also many examples of robots that are designed for interaction with

human users. Of interest are robotic stair climbers, locomotion devices, robotic free weights, gait rehabilitation devices, and haptic devices. I include a brief review here; see Appendix C for a more information.

As previously mentioned in Section 2.1.3, there exist stair climbers modified to be reprogrammable [**129, 43**]. These devices are consumer stair climbers refitted with computers and possibly motors. That is, the pedal paths are still restricted to one-dimensional workspaces.

There are also several examples of locomotion devices in the literature, usually meant for use in virtual reality. These devices employ pedaling (*e.g.*, [**17**], [**23**]), programmable foot platforms (*e.g.*, [**58**], [**63**], [**3**]), or treadmills (*e.g.*, [**29**], [**97, 88**], [**61**], [**57, 56**]).

With regards to strength exercise, a few robotic devices have been designed to simulate free weights using motors or brakes [**68, 142, 84**]. None of these robots saw much investigation after being built, although some patents exist [**116, 131**].

In rehabilitation, researchers usually use exercise machines such as bicycle ergometers and treadmills. However, there are some robots commercially available for gait rehab (*e.g.*, [**120**], [**105**], [**27**], [**55**], [**132**]) but they typically focus on body weight support rather than foot paths.

Perhaps more pertinent to this discussion is the existing research into haptic devices[2]. Over the last few decades, many haptic robots have been designed and built. The vast majority of them — in fact, all of them mentioned here or in the appendix — are meant for interaction with the user's upper body. Their methods of contact range from fingertip

---

[2]Recall from Section 1.2 that I am concerned with devices that interact kinesthetically with the user.

thimbles to grasped handles, to full-arm exoskeletons. They all sense a user's motion or force, and impart forces or motions in response.

Haptic devices can be roughly categorized as either energetically active or passive. (Recall the terminology discussion in Section 1.2.) Of interest are the popular, active PHANTOM [**83, 123**], and the passive PTER [**4, 22, 7**], PADyCs [**140, 122, 121**], and Cobots [**25, 107**].

2.4. Summary

There is a definite need for novel lower-limb haptic exercise robots, motivated by the consumer exercise market, rehabilitation, psychophysical and physiological research, and robotics. Commercial exercise machines, although plentiful and of wide variety, are limited in their programmability. Likewise, existing exercise, locomotion, rehabilitation, and haptic robots are not feasible for the desired applications. In the following chapters, I describe the desired attributes of lower-limb haptic exercise robots, embodied and analyzed in one specific, promising design.

CHAPTER 3

Class Characteristics

In this chapter, I describe the major attributes of lower-limb haptic exercise robots. I intend this discussion to be a specification for this rarely studied class of devices, as it details what the robots must be able to achieve. Each application attribute, *i.e.*, class characteristic, is presented in depth with measured or estimated values whenever possible. The attributes that I discuss are

1. Programmability
2. High Quality Constraints
3. Cyclic Motion
4. High User Force
5. High User Power
6. User Workout
7. Energy Storage
8. Low Power Consumption
9. Safety

In later chapters, I present and analyze one specific instance of a lower-limb exercise robot that achieves these attributes.

3.1. Programmability

Lower-limb exercise robots will allow users to fully customize, *i.e.*, program, the device. Current exercise machines offer basic programmability, such as the damping level and more recently the stride length. Yet for the applications described in Chapter 2, much more programmability is desired: from tweaks of the path shape to tuning of the path dynamics. Furthermore, this programmability should be electronic or automatic (as

opposed to manual), so that the user can program the robot from the console, or the robot can sense the user's intent via the pedals and adjust accordingly. The idea of programmability is not novel — indeed, robotics and haptics rely on it — but the application of this high level of programmability to lower-limb exercise *is* novel.

Of course, some reasonable restrictions can be placed on this programmability. First, the workspace size can be limited to the range of human motion, and the pedal path can be assumed to be cyclic. I address these two restrictions in Section 3.3, as well as additional bounds on the shape of the path. Second, the path dynamics can be restricted in two ways. The damping programmability can be limited to the range of user forces seen in normal exercise; Section 3.4 discusses this range of forces. Similarly, the inertia can be limited to the order of magnitude discussed in Section 3.7; I do not get into the details here.

3.2. High Quality Constraints

For lower-limb exercise, haptic robots must impart constraints on the user's motion, guiding the user's feet along the path. The pedal is constrained to a programmable path in a multi-dimensional workspace — effectively an always-on *virtual constraint*, also called a virtual surface.

First introduced by Rosenberg in 1994 as virtual fixtures [**114, 115**], virtual constraints are computed but physically felt constraints on the user's input, such as when a robot simulates the abrupt stiffness of a wall that isn't really there. These constraints can be used for increasing immersion in virtual reality (*e.g.*, [**74**]), providing feedback

to teleoperation users (such as the feeling of inner organs of a telesurgery patient; *e.g.*, [**137**]), and guiding the user during motion tasks (similar to a straightedge; *e.g.*, [**79**]).

Virtual constraints imparted by haptic robots (lower-limb or otherwise) should be of high quality. But what does high quality entail? First, the constraints should be stiff perpendicular to the path — users should have difficulty moving off the path. Second, the constraints should be smooth tangent to the path — motion along the path should not be bumpy, sticky, or rough. Upper-limb haptic devices are generally concerned with a third attribute: suddenness — the switch between unconstrained and constrained motion (such as when encountering a virtual wall) should be instantaneous. For lower-limb exercise, however, suddenness is insignificant because the constraint is always on. Thus, lower-limb haptic exercise robots should exhibit stiff and smooth pedal paths.

Stiff and smooth paths can be easily achieved if a device's linkage is locked into a one-degree-of-freedom mechanism. Although the device may have a set of attainable pedal paths that exist in a multi-dimensional workspace, each individual path requires one degree of freedom. If the device's actuators are locked such that the resulting one-degree-of-freedom mechanism achieves the desired path, that path will be stiff and smooth.

Realistically, one or more actuators may need to be moving to achieve the desired path. In this case, the actuators must be attached so that the constraints are of high quality, such as via a non-backdriveable transmission.

3.3. Cyclic Motions

The first major distinction between robots for lower-limb exercise and other haptic applications is the cyclic nature of the pedal paths. Unlike upper-body motion, most

lower-limb motion is cyclic, whether running, walking, skiing, or climbing stairs. Figure 3.1d shows sample motions for running and walking.

To get a sense of an actual exercise path, I modeled an existing elliptical (a Life Fitness X5) by measuring the linkages and creating a simulation in software. I assumed that the flywheel had constant velocity, since it has the majority of the inertia within the device. While this is not exactly the case (the user actually slightly speeds up the flywheel during parts of the cycle, *i.e.*, power strokes, and slows it during other parts, as will be seen in Section 3.4), it is a sufficient approximation for this analysis. The elliptical, its mechanism, and sample exercise paths are shown in Figure 3.1.

The range of human motion limits the set of cyclic motions desired, as users can reach only so far with their legs, and current exercise machines are approaching these boundaries[1]. For example, the longest workspace available is on the Nautilus EV916 elliptical: a fore-aft reach of 81 cm. (Most ellipticals have 66 cm or less.) The tallest workspace available is on the Life Fitness 9500 stair climber: a vertical range of 56 cm, although the normal physical stair is between 12 and 20 cm high. Table 3.1 has a sampling of stride lengths for existing exercise machines. These ranges reflect the typical range of human running and stepping.

3.4. High User Force

Another result of interaction with lower-limbs is that the exercise device must be able to impart high forces. Users are able to push down on the pedals with forces greater than their weight, and the robot must withstand these forces to keep the pedal on its path.

---

[1]Pedal path restrictions are relevant only on machines that have individual pedals for each foot. Machines such as treadmills and the escalator-style stair climbers, which do not have separate pedals, cannot assume the foot travels in a prescribed path.
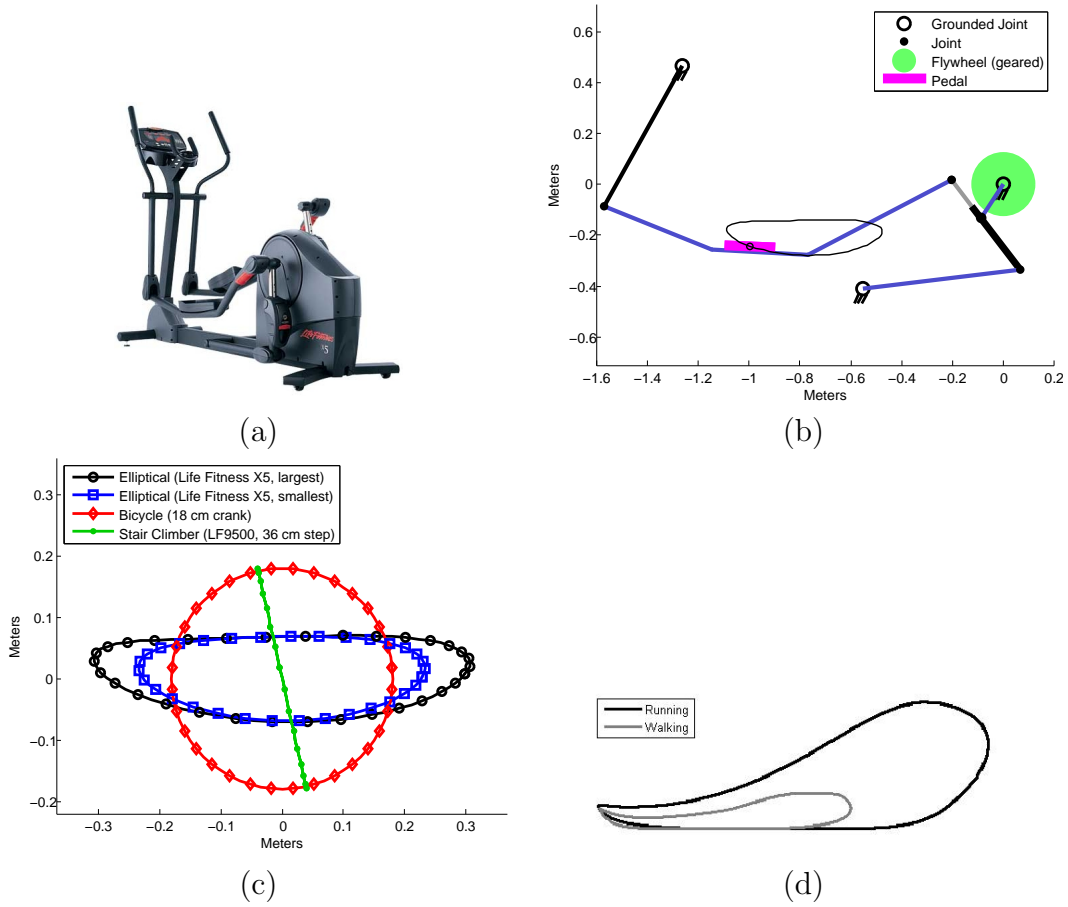
Figure 3.1. (a) Existing Life Fitness X5 elliptical, with manually adjustable stride length. (Photo courtesy of www.lifefitness.com). (b) Elliptical's mechanism. (c) Sample exercise paths, as modeled and centered at the origin. (User is facing to the left.) (d) Sample foot paths, for running and walking. (User is facing to the left.) Obtained by analyzing video available from www.ptiphoenix.com and by modifying a figure in [**60**].

To understand the forces involved in cardiovascular exercise, the aforementioned elliptical (Section 3.3) was fitted with a force sensor under one pedal and tested during normal, high rpm, high damping level, and other various workloads. Sample results showing the maximum force encountered are given in Figure 3.2a. These results are from a relatively normal style of operation by a 104 kg user. Vertical forces peaked around 1600 N, and

Table 3.1. A sampling of the stride lengths available (in centimeters; horizontal for ellipticals and ski machines, vertical for stair climbers). Data taken from the corresponding websites, unless otherwise noted.

Ellipticals		Stair Climbers	
NordicTrack 990	46	NordicTrack MTN740	N/A
NordicTrack 800	46	LifeFitness 9500 (measured)	56
NordicTrack 600	46	Life Fitness 95S	N/A
Life Fitness 95X	51	Precor C776	33
Life Fitness 93X	51	StarTrac Pro	41
Life Fitness 91X	46	SportsArt 7005	36
Life Fitness 90X	51	SportsArt 7100	36
Life Fitness X5 (measured)	61	SciFit TC1000	36
Precor EFX5.33	48	Nautilus StepMill7000PT	20
Precor EFX5.23	48		
Precor EFX5.21	48		
Precor EFX5.19	48	Ski Machines	
Precor EFX5.17	48		
Octane Pro35	50	NordicTrack ClassicPro	N/A
Octane Pro350	50		
Octane Pro350XL	61		
StarTrac Elite	N/A		
StarTrac Pro	N/A		
SportsArt 807	66		
SportsArt 805	66		
SportsArt 803	66		
SportsArt E82	66		
Matrix MX-E5x	66		
SciFit SXT7000	N/A		
Nautilus EV916	81		

fore-aft forces reached just under 200 N. These forces are scalable for the desired user. If, for example, it is arbitrarily decided that the device should be useable by a 113 kg (250 lbf) user, the scaled forces required by the device at the pedal are 1725 N vertically and 215 N horizontally. Examination of one pedal cycle (Figure 3.2b) shows that the maximum force occurred in the lower front of the stride, *i.e.*, when the user was planting his weight onto his forward foot. These forces are much greater than encountered during other haptic applications.
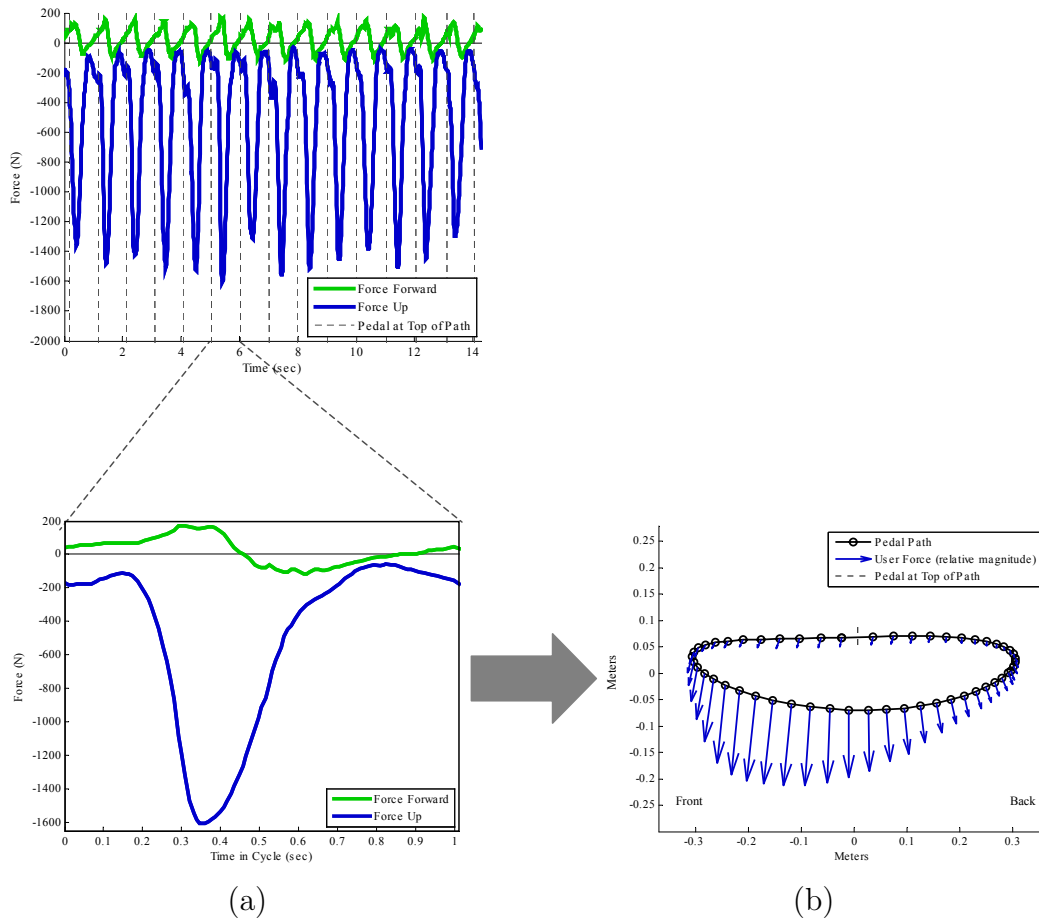
Figure 3.2. User forces measured on Life Fitness X5, for a 104 kg user, during normal operation, at approximately 60 rpm. (a) Forces versus time (b) Force direction within one cycle (path as modeled by simulation).

3.5. High User Power

Lower-limb haptic exercise robots also encounter high instantaneous power *to* and *from* the user. It is well known that humans can output many hundreds of watts of mechanical power during peak exertion loads. Even moderate exercise involves several hundred watts: the U.S. Department of Health and Human Services defines moderate exercise as exertion of around 250-500 watts [124]. Table 3.2 gives samples of mechanical power outputs[2]

[2]Power output for exercise is defined as energy flowing from user to device.

Table 3.2. A sampling from the literature of average power levels from users during exercise. Exertion levels are as stated by the corresponding authors.

Researchers	Exercise	Exertion Level	Power (W)
U.S. Dept. of Health [124]	Miscellaneous	Moderate	250–500
Johnson, *et al.* [66]	Climbing stairs	Moderate	250
Pearson, *et al.* [104]	Cycle	Moderate	450
Ulmer, *et al.* [141]	Cycle	Moderate	200
Zeni, *et al.* [151]	Treadmill	Moderate	650
	Stair climber	Moderate	575
	Ski machine	Moderate	575
	Cycle	Moderate	475
Ratel, *et al.* [111]	Treadmill	Sprint	500
	Treadmill	Sprint, fatigued	300
	Cycle	Sprint	900
	Cycle	Sprint, fatigued	600

in the literature, for various modes and levels of exercise (as defined by the respective authors). Granted, these values are for *average* net power to the machine, but because they are average and significant, they show that there is significant instantaneous power from the user during the exercise. While these power levels vary, they all involve several hundreds of watts. Similarly, the recorded force data in the previous section (Section 3.4) was taken during cyclic motions of around 60 rpm, and therefore involves equivalently high powers.

Conversely, during some parts of cyclic lower-limb exercise, there may be many watts of power from the device *to* the user. If users are non-ideal in their exercise — and they most certainly are — then they can be expected to do negative work on the exercise device, such as riding an elliptical's pedal around, or a stair climber's pedal up (if the pedals are coupled). This negative power output is on the order of hundreds of watts: *e.g.*, lifting the user's mass (*e.g.*, 100 kg) at a typical speed (*e.g.*, 1.0 m/s). While the energy flow from device to user occurs for only a fraction of the cycle, it certainly occurs and therefore must be achievable by the exercise device.

This high power ability is novel for haptic robots. Existing haptic robots are meant for upper-limb interaction and exploration, and therefore are not designed to impart or receive significant energy. Because of this, they are not easily scaled for lower-limb exercise applications. Thus, lower-limb exercise robots must be designed from scratch, and designed to interact with the user at high levels of power.

3.6. User Workout

Not only is the user imparting high instantaneous power to the exercise device, and *vice versa*, but also the net power is large and into the device. That is, users are putting much net energy into the machine or robot, because they want a workout. Typical average numbers for cardiovascular exercise are on the order of several hundred watts (again, see Table 3.2). Not only do lower-limb haptic exercise robots need to be able to receive this amount of energy, but they should be able to do something intelligent with it, such as shuffle it around and reuse it, rather than simply burning it off as heat. This is far different from other haptic applications, where little net energy flows from user to device.

Since the direction of net flow is from user to robot, the robot conceivably could be passive. An ideal exercise device would be able to receive energy from the user during one part of the cycle and return it during another, never requiring more energy than what the user has already given it.

3.7. Large Inertia

The field of haptics, and robotics in general, emphatically tries to eliminate inertia in robots. Robots are usually designed with lightweight components so that neither the device nor the user has to exert large forces to overcome inertia.

It is the opposite case in lower-limb exercise. Users want a large inertia to help carry them around the cyclic path, and most cardiovascular exercise machines are designed with large inertias. Many exercise machines have highly geared-up flywheels, while others, such as powered treadmills and escalator-type stair climbers have effectively infinite inertia.

For example, the previously measured Life Fitness elliptical has a flywheel geared at 9.33 to 1. The flywheel has a mass of around 9.1 kg, with an inertia of approximately $0.122 \, \text{kgm}^2$ — thus, its effective inertia after gearing is $10.6 \, \text{kgm}^2$. At 60-rpm pedal speed, it is storing over 200 joules.

3.8. Low Power Consumption

As with all haptic devices, lower-limb exercise robots should have low power consumption. This involves using the smallest motors possible as well as reusing the energy received from the user (Section 3.6). Ideally, the devices will require no additional power from a wall outlet — in fact, many existing bicycles, stair climbers, ski machines, and passive treadmills achieve this, even powering their simple consoles from the user's exertion. Realistically, exercise robots should be designed to be as low power consuming as possible, without limiting their functionality.

3.9. Safety

The most important attribute of haptic lower-limb exercise robots is that of user safety. While this is an obvious concern in the design of any device that interacts with a human, safety means that scaling existing active, haptic robots is not desired, as the resulting large motors are potentially unsafe in interaction with the user. Therefore, exercise robots should be as passive as possible, with several layers of safety checks implemented.

Table 3.3. Comparison of attributes between lower-limb exercise robots and existing devices.

	Lower-Limb Exercise Robots	Consumer Exercise Machines	Robotically Modified Exercise Machines	Haptic Devices
Programmability	High	**Low**	**Low**	High
Constraint Quality	High	High	High	High
Motions	Cyclic	Cyclic	**Various**	**Various**
User Force	High	High	High	**Low**
User Power	High	High	High	**Low**
User Workout	High	High	High	**Low**
Energy Storage	High	High	**Low**	**Low**
Power Consumption	Low	Low	Low	Low
Safety	High	High	High	High

The less obvious implication of safety is that the user should *feel* safe on the device, even if the device is inherently safe in the first place. This means that the pedals should feel solid and durable and the paths should feel smooth and secure. The user should feel confident when exercising with the device.

3.10. Comparisons to Existing Devices

These nine attributes help characterize lower-limb haptic exercise robots. But how do these robots compare to existing machines and robots, and what are the existing devices' limitations? Table 3.3 compares lower-limb exercise robots to existing commercial exercise machines, robotically modified exercise machines, and haptic devices. The following paragraphs discuss each in turn.

Because cardiovascular exercise machines are designed for lower-limbs, they have many of the attributes discussed here. They prescribe cyclic motions, achieve high forces and powers, handle large net power from the user, store energy, and typically consume little power. Yet they are rarely programmable dynamically, and if so, in a limited way (as discussed in the previous chapter). Therefore, they are unfortunately insufficient for the motivating applications.

As mentioned previously in Section 2.1.3, there exist examples of stair climbers that have been modified into robotic devices [**129, 31, 43**]. While these devices satisfy several of the application characteristics because of their design for exercise (such as high force, and high power), they do not fulfill all of them. They do not take advantage of the cyclic nature of exercise, nor the large net power from the user. Furthermore, they do not incorporate energy storage (although they simulate it via a motor). Finally, they do not have programmable foot paths in multiple dimensions — stair climbers are one-dimensional. Therefore, a new type of haptic exercise robot needs to be designed.

Upper-limb haptic applications have similar characteristics as the motivating applications, but with several important distinctions. Like exercise, conventional haptic applications require programmability, high-quality constraints, low power consumption, and safety. However, interaction with the hand and arm for virtual environments requires far less force and power than lower-limb cardiovascular exercise. In conventional haptics, users explore the space gently and at relatively slow speeds. They also explore in random directions, and so conventional haptic devices are designed with minimal inertia and cannot assume or take advantage of cyclic motions. Furthermore, conventional devices are meant for applications that have very little net energy flow from the user (the user does *not* want a workout), and so they must overcome or minimize friction to simulate low- or no-damping situations.

To help visualize the distinction between these device types, and other devices, consider Figure 3.3. The three variables selected are the device's programmability, its design for cyclic motions, and its ability to handle large user forces and powers. The visualization
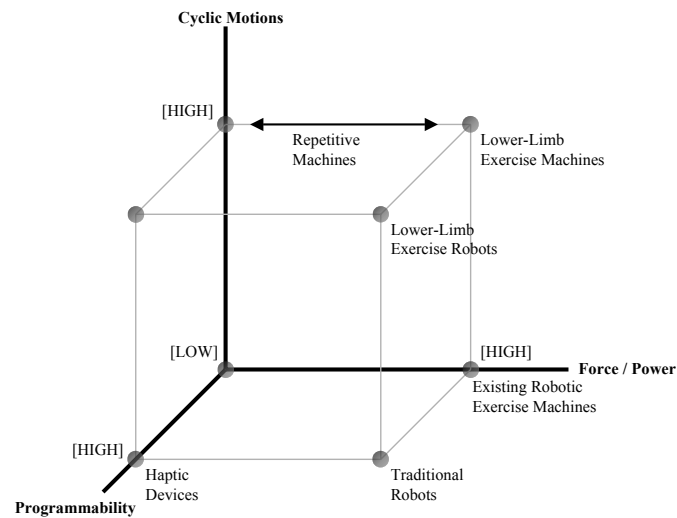
Figure 3.3. Visualization of the comparison between lower-limb haptic exercise robots, and existing devices.

shows that the class of lower-limb exercise robots discussed in this thesis is novel to both the exercise and robotics research fields.

3.11. Conclusion

From the class characteristics discussed in this chapter, it is clear that lower-limb exercise is a novel application for haptic robots. Existing haptic designs are neither readily applicable nor scalable to lower-limb exercise, and so new techniques and designs are needed. The high force and power nature of exercise, and the desire for energy storage, for example, lead to new haptic robots. In the next chapter, I take these attributes and embody them in one specific design.

CHAPTER 4

A Specific Design

This chapter presents the mechanism design of a lower-limb haptic exercise robot that travels through singularities and incorporates inertia. While the design may seem complex at first, the reasoning for each component is well founded, as I will show here.

The design focuses on only one leg, *i.e.*, one side, of the device. This is to simplify the problem, but also because the second leg can be identical to the first, and coupled through a mechanism such as that discussed at the end of this thesis, in Section 8.2. Unless stated otherwise (as in Section 8.2), the analysis here and in the following chapters is for one leg only.

In all of the figures, the user is facing to the left.

The design presented here is, of course, not the only possible design. There are many other designs that I rejected for various reasons, and there are surely designs that are improvements on this one. Nevertheless, the analysis performed here and in later chapters is analogous to many other designs. Appendix D shows many of the preliminary designs that I considered.

4.1. Overview

The design is shown in Figure 4.1a. On the upper-right is a pedal that travels in a path, such as the ellipse drawn. The mechanism consists of three subsystems, shown in Figure 4.1b: the pedal-supporting Modified Pantograph, the cyclic-motion-creating
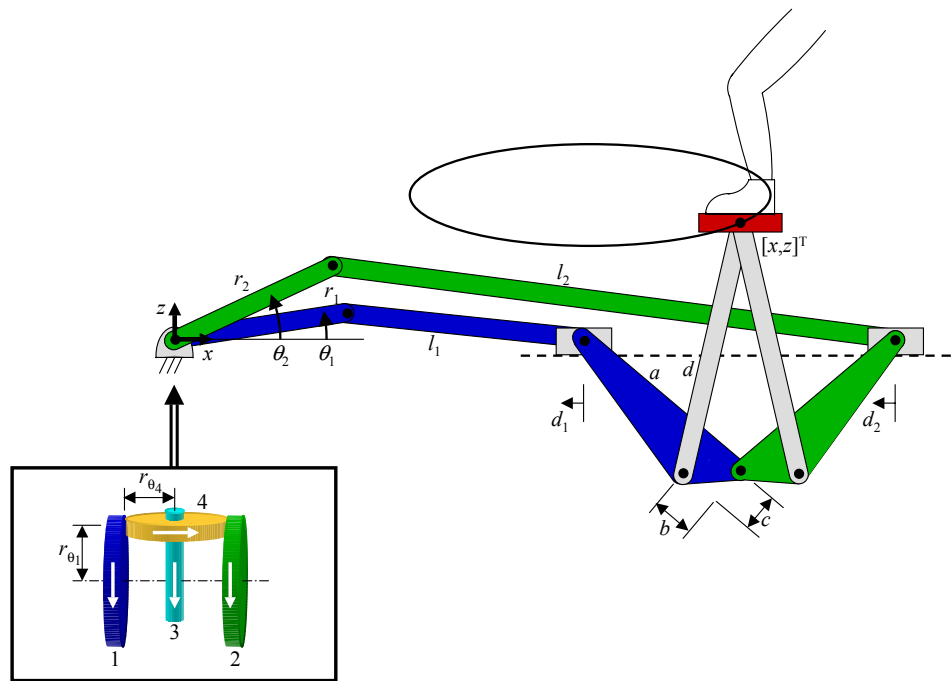
(a)
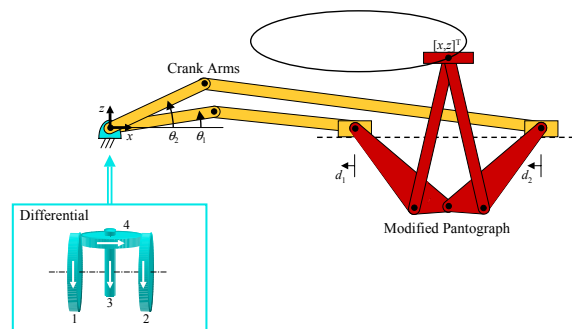
(b)

Figure 4.1. The specific design. (a) Colored for relative linkages. (b) Colored for the three subsystems.

Crank Arms, and the phase-isolating Differential. In the following sections, I discuss each of these subsystems in depth.

4.2. Modified Pantograph

The pedal is supported by the Modified Pantograph subsystem; see Figure 4.2a. The pedal's position, $[x, z]^T$, is related to the linear positions of the two sliders: d_1 and d_2. These sliders are constrained to the horizontal axis, such as by linear rails. By moving the sliders in unison, the device moves the pedal in the x direction, and by moving the sliders in equal and opposite direction, the device moves the pedal in the z directions. There exist kinematics and its derivative (Appendix E)

$$\boldsymbol{x} = \boldsymbol{f}_P(\boldsymbol{d}) \qquad \dot{\boldsymbol{x}} = \boldsymbol{J}_P(\boldsymbol{d}) \cdot \dot{\boldsymbol{d}},$$

where $\boldsymbol{x} = \begin{bmatrix} x \\ z \end{bmatrix}$, $\boldsymbol{d} = \begin{bmatrix} d_1 \\ d_2 \end{bmatrix}$, $\boldsymbol{J}_P$ is the Jacobian, and a dot over a variable represents differentiation with respect to time.

The Modified Pantograph design is complex, but it evolved from a much simpler design. I wanted the pedal support mechanism to be clear of the user's legs. So, my first design was a simple Triangle, as shown in Figure 4.2b. The Triangle works similarly to the Modified Pantograph: the average position of the sliders determines the pedal's x position, and their relative position determines the pedal's z-position.

The problem with the triangle support is that it is weakest when it needs to be strongest. Recall from Section 3.4 that the user is imparting the most force at the lower part of the pedal path, and in the downward direction. At the lower part of the path, the triangle is relatively flat, and thus a downward force at the pedal is amplified into larger, oppositely pointing, forces at the sliders. This means that actuators at the crank arms
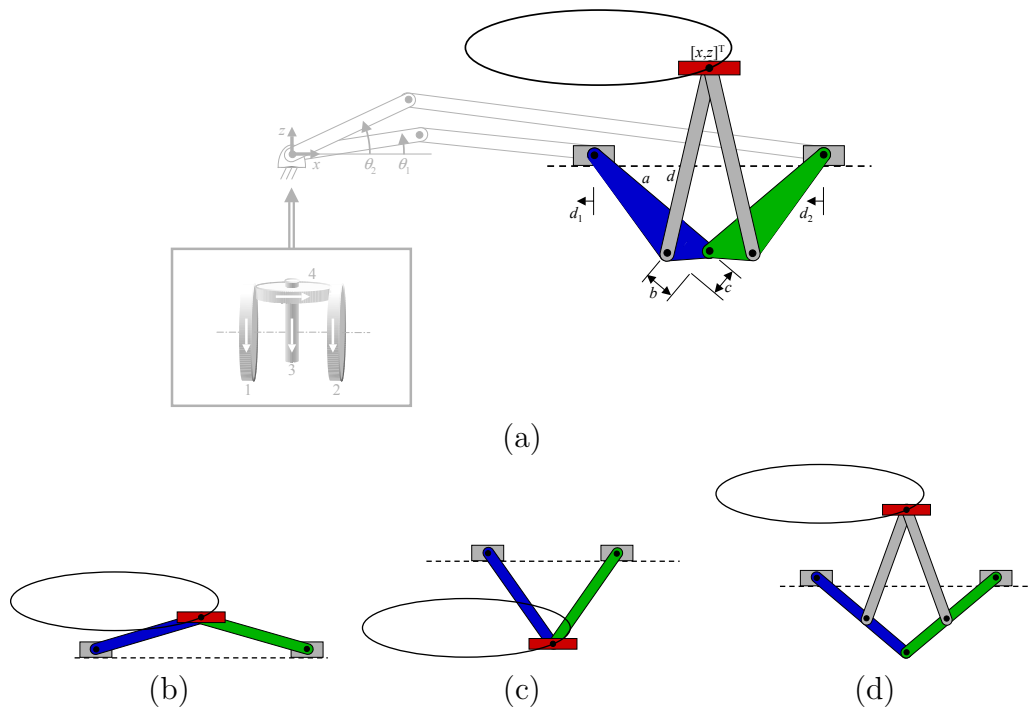
Figure 4.2. Designs for the pedal support subsystem. (a) The selected Modified Pantograph design. (b) The Triangle. (c) The Vee. (d) The Unmodified Pantograph.

must impart very large torques. Figure 4.3 shows a plot of this force amplification with respect to pedal height.

I desire a support mechanism that has the opposite effect: at the lower part of the cycle, it reduces the force required by the sliders (and thus puts more force vertically into the slider's rails). One way to do this would be to invert the triangle so that the pedal is lower than the sliders: the Vee design (sketch Figure 4.2c, force multiplier Figure 4.3). Then, when the pedal is lowest, the triangle is nearly vertically linear, and most of the user's force is applied to the rails. However, this means that the user's legs are lower than the mechanism, which is undesired. Therefore, a better design is needed.
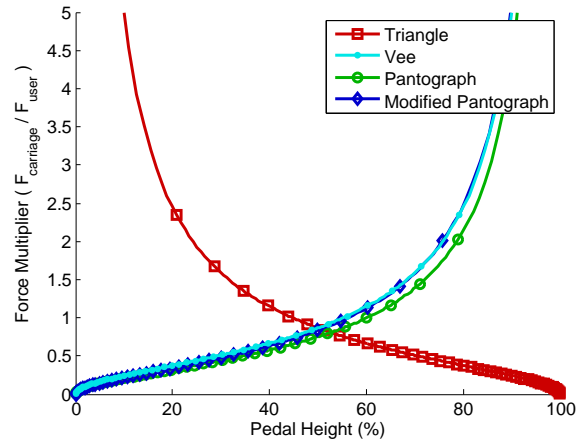
Figure 4.3. Force multiplier for pantograph designs.

I looked at several designs (see Appendix D), including the Unmodified Pantograph, as shown in Figure 4.2d. As the sliders move away from each other, the pedal is lifted vertically. This design has a good force multiplier (Figure 4.3), but it has a new concern: pedal stability. The triangular support (formed by the two links that are directly connected to the pedal) is quite thin, especially during the lower part of the path, when user forces are the highest. A thin support means that the torque on the support's base can be very high. Figure 4.4 shows the width of this support versus pedal height.

An improvement to the Unmodified Pantograph is the final Modified Pantograph design (Figure 4.2a). This design uses couplers to widen the base of the pedal's direct support. These couplers can be accomplished by a solid triangle (as in the figure), three links, a T-shaped link, or by bent links. The Modified Pantograph design has the proper force multiplier (Figure 4.3), and a much wider base for the pedal (Figure 4.4).

There is one final criterion to consider: the amount of slider motion relative to vertical pedal motion. That is, the Modified Pantograph's dimensions determine how much slider motion is required to move the pedal a certain height. For example, the higher the
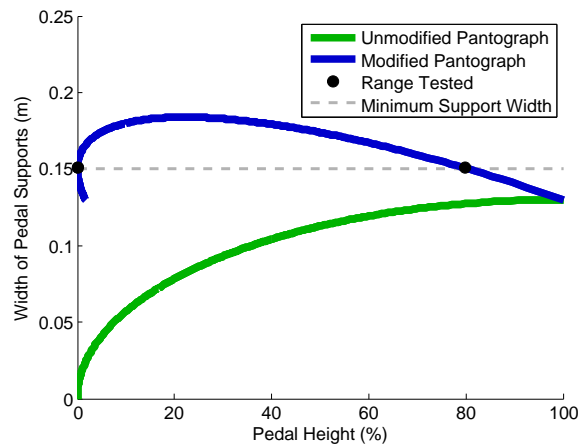
Figure 4.4. Width of the base of the pedal's direct supports, for two pantograph designs. Range Tested and Minimum Support Width are for the optimization routine.
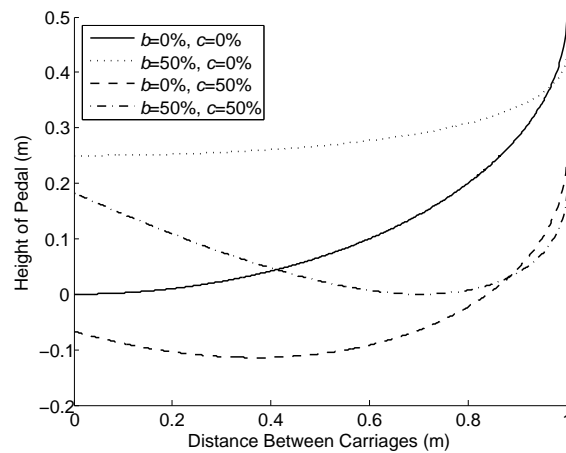
Figure 4.5. The dependence of pedal height on Modified Pantograph's parameters. Dimensions b and c are given as percentages of dimension a.

pedal's direct support is up the mechanism (*i.e.*, the greater b is in Figure 4.2a), the less the change in height of the pedal as the Modified Pantograph opens — see Figure 4.5.

I optimized the Pantograph's dimensions using my three criteria:

(1) Low force multiplication during bottom of path (satisfied by the Modified Pantograph design)
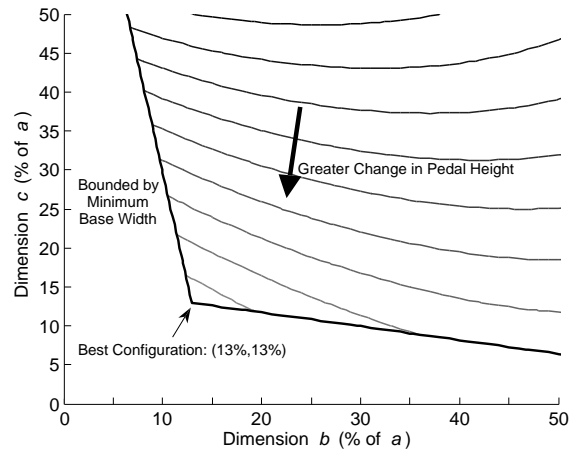
Figure 4.6. Optimization of two Modified Pantograph parameters.

(2) Support-base width greater than a given value (here, I use 0.15 meters)

(3) Maximum pedal motion relative to slider motion

To decrease the parameter space, I ignored the pedal support-arm dimension, d, and searched for the coupler dimensions b and c as percentages of the dimension a. I tested the design over a limited range of pedal height, to avoid maximum and minimum singularities of the mechanism. The optimization space is shown in Figure 4.6. From the graph, I see that the optimum dimensions are $b = 0.13 \cdot a$ and $c = 0.13 \cdot a$. Figure 4.7 shows the condition number of the Modified Pantograph's Jacobian, over the range tested.

4.3. Crank Arms

The second subsystem is the Crank Arms (see Figure 4.8). Since the pedal is to travel in cyclic paths, the sliders need to travel forward and backward along their rails, and this is accomplished by two rotating crank arms. The crank arms each have a rotation angle,
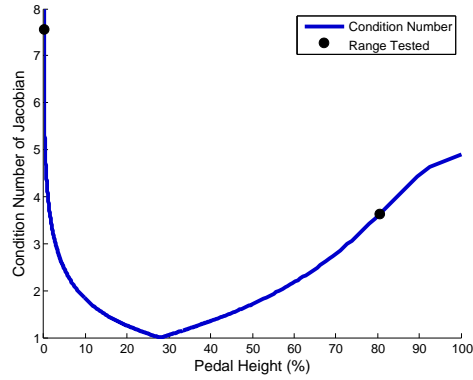
Figure 4.7. Condition number of the Modified Pantograph's Jacobian, over the range of optimized pedal heights.
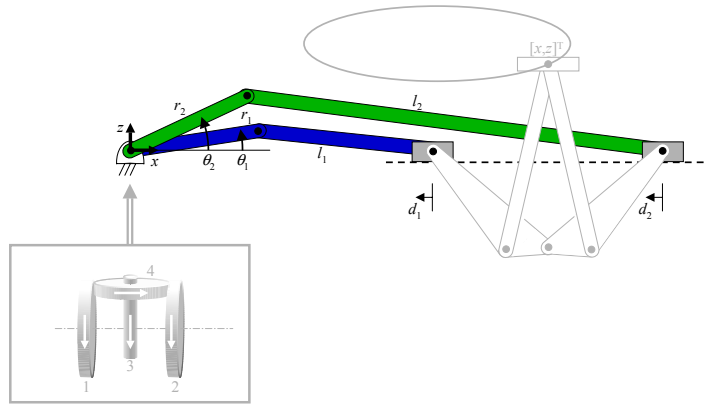
Figure 4.8. The Crank Arm subsystem.

θ_i, such that (Appendix E)

$$\boldsymbol{d} = \boldsymbol{f}_C(\boldsymbol{\theta}_{12}) \qquad \dot{\boldsymbol{d}} = \boldsymbol{J}_C(\boldsymbol{\theta}_{12}) \cdot \dot{\boldsymbol{\theta}}_{12},$$

where $\boldsymbol{\theta}_{12} = \begin{bmatrix} \theta_1 \\ \theta_2 \end{bmatrix}$. I assume that both crank arms rotate in the same direction. Also, as I will show in Section 5.2, the two crank arms rotate in near unison.
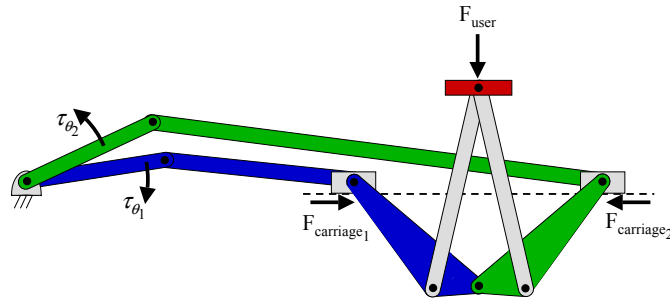
Figure 4.9. Effect of the user's vertical force. Assuming the crank arms are on the same side of the horizontal, a vertical user force results in opposite-acting torques on the crank arms.

4.4. Differential

The design is functional with just the Crank Arms and Modified Pantograph, however it has one major drawback. Suppose the mechanism is at the configuration shown in Figure 4.9. (This problems holds for any configuration where the two crank arms are on the same side of the horizontal axis.) The major component of the user's force is in the vertical direction, as drawn — such a force creates equal and opposite forces on the sliders, trying to pull them together. These forces are transmitted to the crank arms, resulting in torques trying to pull the crank arms apart. This means that any actuators on θ_1 and θ_2 must exert opposite (and large) torques to guide the pedal. Since the crank arms are almost always on the same side of the horizontal axis, the opposite torques are almost always occurring.

Adding the Differential subsystem improves the design. A differential consists of four main parts, as drawn in Figure 4.10 — the differential in the figure is drawn with friction contacts, although it could include gears instead[1]. Two wheels (or gears), labeled **1** and

---

[1]Differentials are commonly used in car transmissions, to allow one drive shaft to power two wheels at different speeds (such as when turning the car).
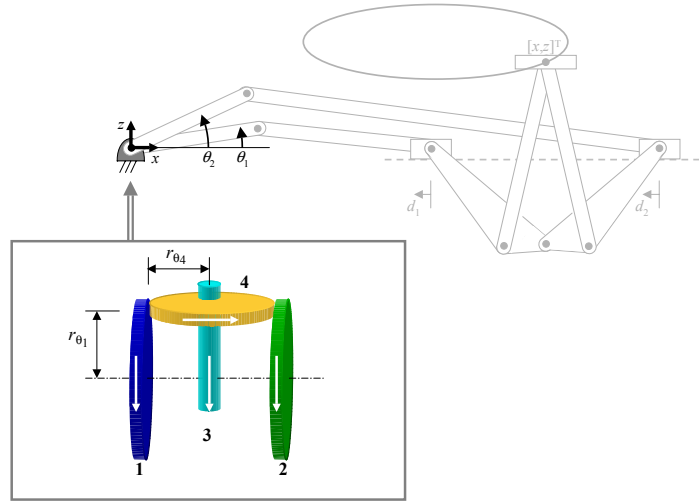
Figure 4.10. The Differential Subsystem.

2, and a shaft, labeled **3**, rotate about a common axis. Each wheel is in contact with a third wheel, labeled **4**, which rotates about shaft **3**. Shaft **3** does not rotate about its length. I assume that wheels **1** and **2**'s radii are the same length as the distance **4** is along shaft **3** (called r_{θ_1}), but that wheel **4** may have a different radius (called r_{θ_4}). The angular velocities of the four components are related by the Jacobian such that

$$\begin{bmatrix} \dot{\theta}_1 \\ \dot{\theta}_2 \end{bmatrix} = \begin{bmatrix} 1 & \frac{r_{\theta_4}}{r_{\theta_1}} \\ 1 & -\frac{r_{\theta_4}}{r_{\theta_1}} \end{bmatrix} \cdot \begin{bmatrix} \dot{\theta}_3 \\ \dot{\theta}_4 \end{bmatrix} \qquad \begin{bmatrix} \dot{\theta}_3 \\ \dot{\theta}_4 \end{bmatrix} = \begin{bmatrix} \frac{1}{2} & \frac{1}{2} \\ \frac{1}{2}\frac{r_{\theta_1}}{r_{\theta_4}} & -\frac{1}{2}\frac{r_{\theta_1}}{r_{\theta_4}} \end{bmatrix} \cdot \begin{bmatrix} \dot{\theta}_1 \\ \dot{\theta}_2 \end{bmatrix}.$$

The torques on the four components are related by the transpose of the Jacobian:

$$\begin{bmatrix} \tau_1 \\ \tau_2 \end{bmatrix} = \begin{bmatrix} \frac{1}{2} & \frac{1}{2}\frac{r_{\theta_1}}{r_{\theta_4}} \\ \frac{1}{2} & -\frac{1}{2}\frac{r_{\theta_1}}{r_{\theta_4}} \end{bmatrix} \cdot \begin{bmatrix} \tau_3 \\ \tau_4 \end{bmatrix} \qquad \begin{bmatrix} \tau_3 \\ \tau_4 \end{bmatrix} = \begin{bmatrix} 1 & 1 \\ \frac{r_{\theta_4}}{r_{\theta_1}} & -\frac{r_{\theta_4}}{r_{\theta_1}} \end{bmatrix} \cdot \begin{bmatrix} \tau_1 \\ \tau_2 \end{bmatrix}.$$

The velocities can be integrated to obtain the Differential's kinematics (Appendix E):

$$\boldsymbol{\theta}_{12} = \boldsymbol{f}_D(\boldsymbol{\theta}_{34}),$$

where $\boldsymbol{\theta}_{34} = \begin{bmatrix} \theta_3 \\ \theta_4 \end{bmatrix}$.

Ignoring the gear ratio between **1**-**2**-**3** and **4**, the equations show that the angular velocity of **3** is the average of the velocities of **1** and **2**, while the velocity of **4** is the difference. That is, $\dot{\theta}_3$ is the average motion of the device around its cyclic path, while $\dot{\theta}_4$ is the rate of change of the angle between **1** and **2**. Conversely, the torque on **3** is the difference of the torques of **1** and **2**, while the torque on **4** is the average. This means that for opposite torques on **1** and **2** (as caused by the user's vertical force), τ_3 is small while τ_4 is large.

The significance of the Differential will become clearer when I discuss the idea of phasing in Section 5.2, and from the simulation results in Section 7.3. The Differential allows me to put actuators on **3** and **4**.

4.5. Whole Device: Kinematics and Dynamics

The kinematics of the device relate the actuated angles of **3** and **4** to the resulting pedal position in $\boldsymbol{x}$. The subsystems kinematics are derived in Appendix E; their results

are

$$\boldsymbol{x} = \boldsymbol{f}_P(\boldsymbol{d}) = \begin{bmatrix} \frac{1}{2}d_1 + \frac{1}{2}d_2 \\ \sqrt{d^2 - (\frac{b}{a}e + \frac{c}{a}\sqrt{a^2 - e^2})^2} - (\frac{a-b}{a}\sqrt{a^2 - e^2} + \frac{c}{a}e) \end{bmatrix}$$

$$\boldsymbol{d} = \boldsymbol{f}_C(\boldsymbol{\theta}_{12}) = \begin{bmatrix} r_1 \cos \theta_1 + \sqrt{r_1^2 \cos^2 \theta_1 + l_1^2 - r_1^2} \\ r_2 \cos \theta_2 + \sqrt{r_2^2 \cos^2 \theta_2 + l_2^2 - r_2^2} \end{bmatrix}$$

$$\boldsymbol{\theta}_{12} = \boldsymbol{f}_D(\boldsymbol{\theta}_{34}) = \begin{bmatrix} \theta_3 + \frac{r_{\theta_4}}{r_{\theta_1}}\theta_4 + \theta_1|_{t=0} \\ \theta_3 - \frac{r_{\theta_4}}{r_{\theta_1}}\theta_4 + \theta_2|_{t=0} \end{bmatrix},$$

where $e = \frac{1}{2}d_2 - \frac{1}{2}d_1$. The full device has the kinematics

$$\boldsymbol{x} = \boldsymbol{f}_{Full}(\boldsymbol{\theta}_{34}) = \boldsymbol{f}_P(\boldsymbol{f}_C(\boldsymbol{f}_D(\boldsymbol{\theta}_{34}))).$$

The Jacobians are the derivatives with respect to time, and found to be

$$\dot{\boldsymbol{x}} = \boldsymbol{J}_P(\boldsymbol{d}) \cdot \dot{\boldsymbol{d}} = \begin{bmatrix} \frac{1}{2} & \frac{1}{2} \\ -k_P(d_1, d_2) & k_P(d_1, d_2) \end{bmatrix} \cdot \dot{\boldsymbol{d}}$$

$$\dot{\boldsymbol{d}} = \boldsymbol{J}_C(\boldsymbol{\theta}_{12}) \cdot \dot{\boldsymbol{\theta}}_{12} = \begin{bmatrix} k_{C_1}(\theta_1) & 0 \\ 0 & k_{C_2}(\theta_2) \end{bmatrix} \cdot \dot{\boldsymbol{\theta}}_{12}$$

$$\dot{\boldsymbol{\theta}}_{12} = \boldsymbol{J}_D(\boldsymbol{\theta}_{34}) \cdot \dot{\boldsymbol{\theta}}_{34} = \begin{bmatrix} 1 & \frac{r_{\theta_4}}{r_{\theta_1}} \\ 1 & -\frac{r_{\theta_4}}{r_{\theta_1}} \end{bmatrix} \cdot \dot{\boldsymbol{\theta}}_{34},$$
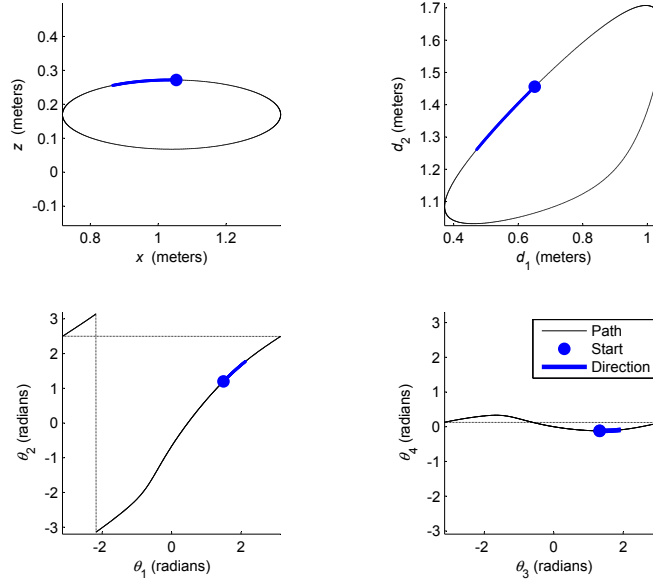
Figure 4.11. A sample pedal path in the four spaces.

where k_P, k_{C_1}, and k_{C_2} are given in the appendix. The full device has the equation

$$\dot{\boldsymbol{x}} = \boldsymbol{J}_{Full}(\boldsymbol{\theta}_{34}) \cdot \dot{\boldsymbol{\theta}}_{34}$$

$$= \begin{bmatrix} \frac{1}{2}(k_{C_1} + k_{C_2}) & \frac{1}{2}\frac{r_{\theta_4}}{r_{\theta_1}}(k_{C_1} - k_{C_2}) \\ -k_P(k_{C_1} - k_{C_2}) & -k_P\frac{r_{\theta_4}}{r_{\theta_1}}(k_{C_1} + k_{C_2}) \end{bmatrix} \cdot \dot{\boldsymbol{\theta}}_{34}.$$

Figure 4.11 shows a sample pedal path in the four different spaces.

4.6. Conclusion

The mechanism design is complicated but purposeful. The pedal's position in $\boldsymbol{x}$ is determined by the actuated angles $\boldsymbol{\theta}_{34}$, where θ_3 is the average position of the crank arms and θ_4 is related to the angle between them.

The following chapters discuss the inclusion of inertia, damping, and path actuation, and analyze this design and its capabilities.

CHAPTER 5

Inertia, Damping, and Actuators

5.1. Introduction

This chapter discusses the incorporation of inertia, damping, and path actuation into the device. The device consists of the subsystems discussed in the previous chapter, but as of yet in this discussion, it has no mass. Mass (inertia) is important for exercise, and separates exercise robots from traditional ones.

In all of the figures in this chapter, the user is facing to the left.

5.2. The Concept of Phase

One of the important ideas in the analysis of this device is the concept of phase. Recall the design, as shown in Figure 5.1. The crank arms are to continuously rotate, driving the pedal around its path in $[x, z]^T$. Suppose the crank arms are aligned (*i.e.*, $\theta_1 = \theta_2$) as shown in Figure 5.2a, and rotating at the same speed (*i.e.*, $\dot{\theta}_1 = \dot{\theta}_2$). The sliders travel forward and backward, nearly in unison, and thus the pedal travels in an almost horizontal path. (The path has some vertical motion because some of the links are not the same length, *i.e.*, $l_1 \neq l_2$.) Suppose instead that the crank arms are pointing in opposite directions (*i.e.*, $\theta_1 = \theta_2 + \pi$) as shown in Figure 5.2b, but still rotating at the same speed. Then, the sliders move in opposite directions, and the pedal travels in a nearly vertical path. Finally, suppose that the angle between the crank arms is neither 0 nor π, as in Figure 5.2c. In this case, the pedal travels in a loop in its space.
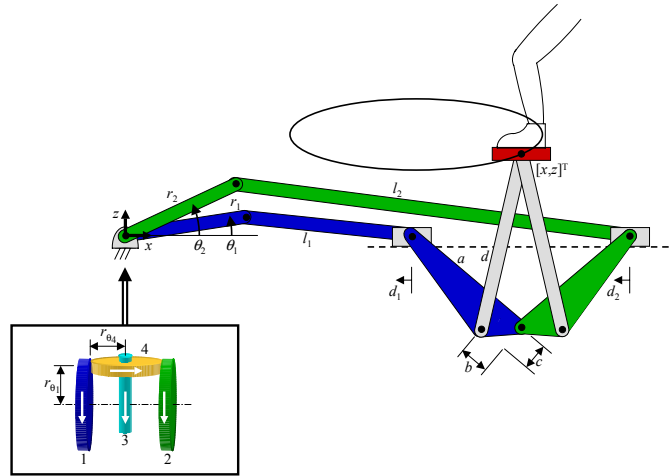
Figure 5.1. The mechanism design.

The angle, *i.e.*, *phase*, between the crank arms is important. The constant-phase paths shown in Figure 5.2 are very similar to paths created by existing exercise machines. The zero-phase path is very similar to a ski machine's path, the π-phase path is very similar to a stair climber's path, and the c-phase path is very close to an elliptical's path.

The set of constant-phase paths for the device is shown in Figure 5.3a, for phases from 0 to π. (Phases greater than π repeat the same shape paths.) As the phase increases from 0 to π, the loops gradually open vertically and close horizontally. (The flat top boundary of the set is the result of the maximum possible pedal height based on the Modified Pantograph dimensions.) By changing the phase within a cycle, the device can transition from one loop to another, achieving the desired path. For example, suppose the desired path is the ellipse shown in the Figure 5.3b. This path requires the phase values shown — the change in phase is relatively small throughout the cycle.

Therefore, let me define a two-dimensional **Phase**-space, where the phase is one dimension, and the other is the average position along the path. I define the phase, ϕ, and
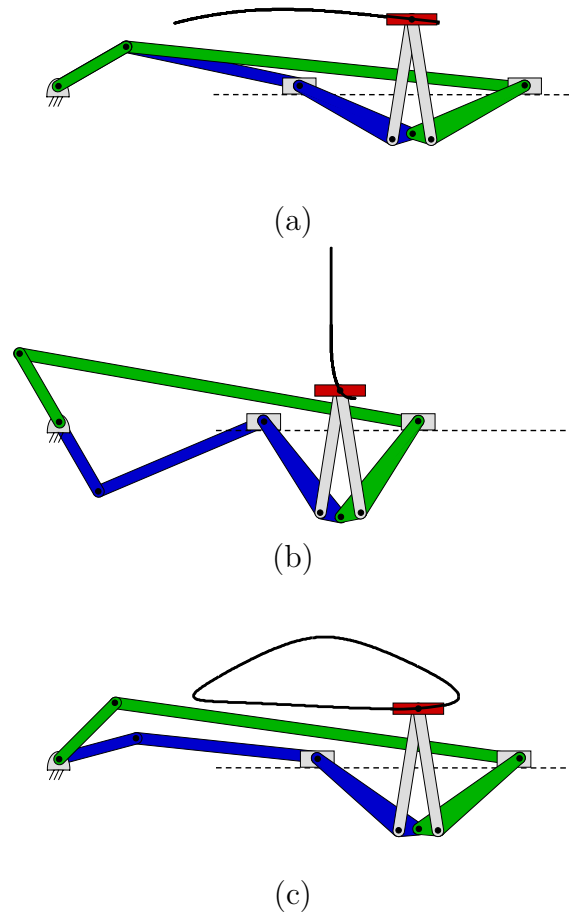
Figure 5.2. Sample paths resulting from constant phases (*i.e.*, the angles between the crank arms). (a) Phase = 0. (b) Phase = π. (c) Phase = $\frac{\pi}{6}$.

the position, ψ, as

$$\phi = \theta_1 - \theta_2 \qquad \psi = \frac{\theta_1 + \theta_2}{2}.$$

In the constant-phase curves in Figure 5.3a, $\dot{\psi}$ is velocity along those curves. Figure 5.4 shows constant-ψ curves for the pedal.
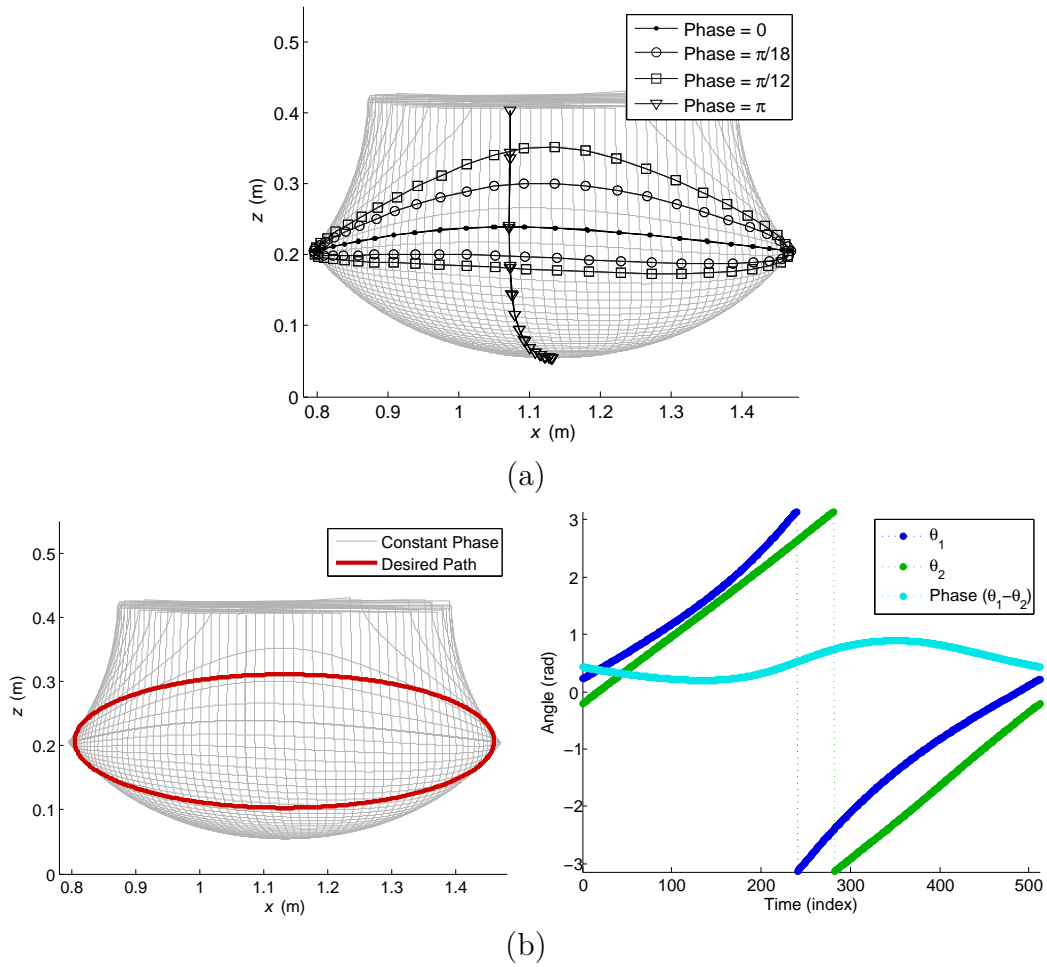
Figure 5.3. Phases for paths. (a) Set of constant-phase paths. (b) One desired path, with resulting phase values.

The differential helps the design because it isolates ϕ and ψ. Recall the differential's velocity equation

$$
\begin{bmatrix} \dot{\theta}_3 \\ \dot{\theta}_4 \end{bmatrix} = \begin{bmatrix} \frac{1}{2} & \frac{1}{2} \\ \frac{1}{2}\frac{r_{\theta_1}}{r_{\theta_4}} & -\frac{1}{2}\frac{r_{\theta_1}}{r_{\theta_4}} \end{bmatrix} \cdot \begin{bmatrix} \dot{\theta}_1 \\ \dot{\theta}_2 \end{bmatrix},
$$
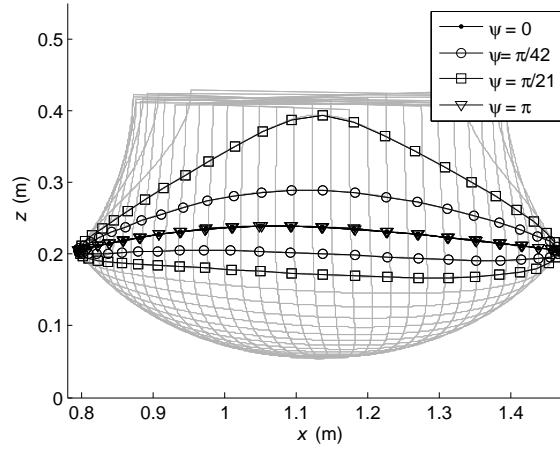
Figure 5.4. Set of constant-ψ paths.

This equation shows that $\dot{\theta}_3 = \dot{\psi}$ and $\dot{\theta}_4 = \frac{1}{2}\frac{r_{\theta_1}}{r_{\theta_4}} \cdot \dot{\phi}$. Thus, $\dot{\theta}_3$ is the *generic velocity* around the path, while $\dot{\theta}_4$ is (proportionally) the *change in phase*. The curves in Figures 5.3a and 5.4 are therefore also constant-θ_3 and -θ_4 curves.

These curves are not necessarily perpendicular to each other, because the Jacobian is a nonconformal transformation. This can be seen from the plots, but also by doing the appropriate math. If they are not perpendicular, then their dot product is nonzero:

$$\dot{\boldsymbol{x}}_{Constant\theta_4} = \boldsymbol{J}_{Full} \cdot \begin{bmatrix} \dot{\theta}_3 \\ 0 \end{bmatrix}$$

$$\dot{\boldsymbol{x}}_{Constant\theta_3} = \boldsymbol{J}_{Full} \cdot \begin{bmatrix} 0 \\ \dot{\theta}_4 \end{bmatrix}$$

$$\dot{\boldsymbol{x}}_{Constant\theta_3}^T \dot{\boldsymbol{x}}_{Constant\theta_4} = \begin{bmatrix} \dot{\theta}_3 & 0 \end{bmatrix} \cdot \boldsymbol{J}_{Full}^T \cdot \boldsymbol{J}_{Full} \cdot \begin{bmatrix} 0 \\ \dot{\theta}_4 \end{bmatrix}$$

$$= \begin{bmatrix} \dot{\theta}_3 & 0 \end{bmatrix} \begin{bmatrix} \dots & (\frac{1}{4} + k_P^2)\frac{r_{theta_4}}{r_{theta_1}}(k_{C_1} + k_{C_2})(k_{C_1} - k_{C_2}) \\ \dots & \dots \end{bmatrix} \cdot \begin{bmatrix} 0 \\ \dot{\theta}_4 \end{bmatrix}$$

$$= (\frac{1}{4} + k_P^2)\frac{r_{theta_4}}{r_{theta_1}}(k_{C_1} + k_{C_2})(k_{C_1} - k_{C_2})\dot{\theta}_3\dot{\theta}_4,$$

which is nonzero unless $k_{C_1} = \pm k_{C_2}$, $\dot{\theta}_3 = 0$, or $\dot{\theta}_4 = 0$.

Because I am concerned with closed-loop paths, I restrict myself to the class of pedal paths defined by a monotonically increasing θ_3 and bounded θ_4:

$$0 \le \dot{\theta}_3 \qquad \text{and} \qquad 0 \le \theta_4 \le \frac{1}{2}\frac{r_{\theta_1}}{r_{\theta_4}} \cdot \pi.$$

Thus, θ_4 is bounded by $0 \le \phi \le \pi$. In practice, these restrictions may be inverted, when the user is traveling backwards around the path.

Let me stress it again. θ_3 is the generic position around the path. θ_4 is proportional to the phase.

5.3. Adding Inertia

Given the concept of phase and generic motion, where should inertia be incorporated? To begin, I again plot the sample elliptical pedal path in the various spaces — see Figure 5.5. In $\boldsymbol{\theta}_{12}$-space, the path has a slope near to 1 — both θ_1 and θ_2 rotate continuously, at nearly the same speed. However, in $\boldsymbol{\theta}_{34}$-space, θ_3 continuously rotates while θ_4 oscillates around 0.
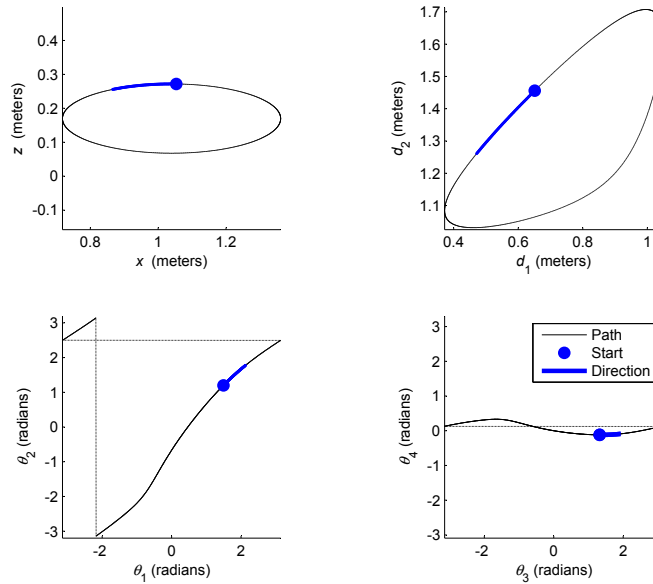
Figure 5.5. Goal path in the different spaces.

The inertia should be added to the device using two guidelines. First, it should be added so that it helps carry the user around the path. Second, it should be added such that its effect on the device's actuators is minimal. The logical place for it, therefore, is on θ_3 so that it affects the *generic motion* around the path. From here on, I assume that there is significant inertia added via a (possibly geared) flywheel on **3**.

5.4. Inertia's Effect on the Path

If the dominant inertia in the device is via a flywheel on θ_3, then $\dot{\theta}_3$ will stay relatively constant within a cycle. (In actuality, it will vary slightly within cycles because of the shuffling of energy to and from the links' masses, and to and from the user.) The constant-flywheel approximation is appropriate for many of the existing exercise machines as well, since they each have a highly geared flywheel. Figure 5.6 shows plots of constant $\dot{\theta}_3$ versus constant path length.
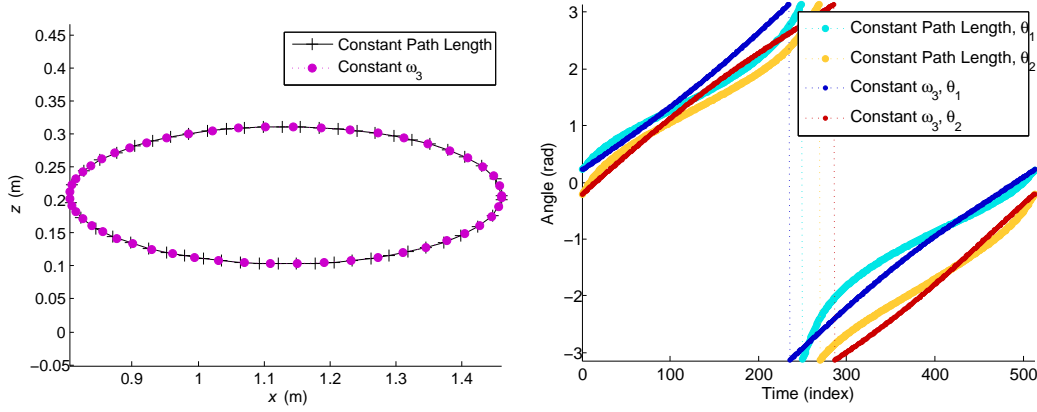
Figure 5.6. Comparison of constant-$\dot{\theta}_3$ and constant-path-length paths.

Clearly, constant flywheel speed does not correspond to constant path speed. In fact, the speed along the path varies due to the linkages separating the pedal from the flywheel[1]. This is common in existing exercise machines, and yet it is not unpleasant to the user. How does this device's pedal's velocity, acceleration, and jerk compare with that of other exercise machines? Figure 5.7 shows a comparison, assuming constant flywheel speed. Note that the path shape has a significant effect on the higher derivatives.

5.5. Adding Phase Actuation

Because the dominant inertia is on θ_3, and ignoring the user for now, the pedal will travel in constant θ_4, constant $\dot{\theta}_3$ paths. Figure 5.8 shows a sketch of the pedal on one of these paths. The velocity, $\dot{\boldsymbol{x}}_{InertiaOnly}$, is tangent to the path. I would like the phase actuator to create forces perpendicular to this path, such that the actuator guides the pedal without affecting its tangential velocity, *i.e.*, without changing speed. This means that I desire the force vector, $\boldsymbol{F}_{Constrain}$ to be normal to $\dot{\boldsymbol{x}}_{InertiaOnly}$, as drawn in the figure.

---

[1]The inertia felt by the user varies as well, as I discuss in Section 6.4
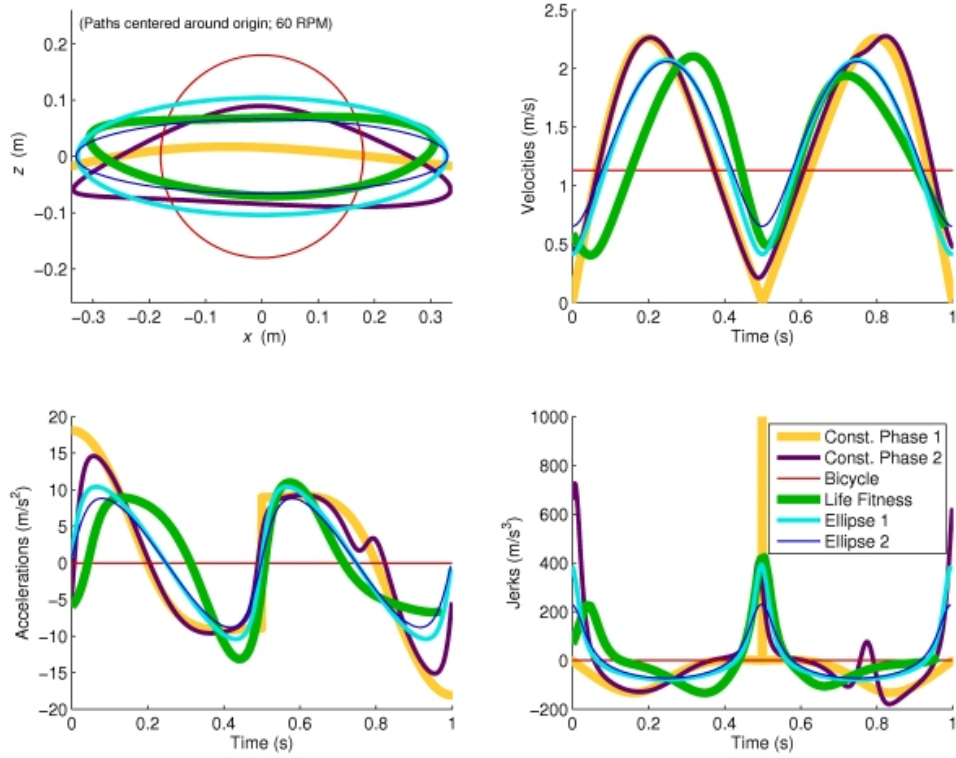
Figure 5.7. Comparison of various paths and their higher derivatives. The paths include two constant-phase paths, two possible desired paths, and two paths from existing exercise machines. Note that path shape has a significant effect on the higher derivatives.

Mathematically, this means I desire

$$0 = \boldsymbol{F}_{Constrain}^{T} \cdot \dot{\boldsymbol{x}}_{InertiaOnly}$$

$$= \left[\boldsymbol{J}_{Full}^{-T} \ \boldsymbol{\tau}_{34} \right]^{T} \cdot \boldsymbol{J}_{Full} \ \dot{\boldsymbol{\theta}}_{34}$$

$$= \boldsymbol{\tau}_{34}^{T} \cdot \boldsymbol{J}_{Full}^{-1} \ \boldsymbol{J}_{Full} \cdot \dot{\boldsymbol{\theta}}_{34}$$

$$= \boldsymbol{\tau}_{34}^{T} \cdot \dot{\boldsymbol{\theta}}_{34}.$$
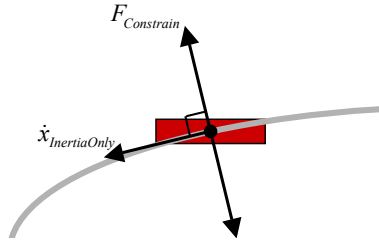
Figure 5.8. Path due to inertia at **3**, and the desired constraint direction.

I know $\dot{\boldsymbol{\theta}}_{34}$, so I desire $\boldsymbol{\tau}_{34}$ to be:

$$\dot{\boldsymbol{\theta}}_{34} = \begin{bmatrix} \dot{\theta}_3 \\ 0 \end{bmatrix} \qquad \boldsymbol{\tau}_{34} = \begin{bmatrix} 0 \\ \tau_4 \end{bmatrix}.$$

Therefore, an actuator on **4** provides the restoring force without affecting the speed.

If the flywheel on **3** is the only inertia in the device (or if the inertias of the links are negligible compared to it), then a steering actuator on θ_4 does not see it — the inertia affects the average velocity of **1** and **2**, but not their difference from the average (and thus the phase).

5.6. Adding Damping

Following the logic in the last section, I want to create damping along the path, so that the user has to exert energy to move the device. That is, the damping force should be parallel to the velocity vector in Figure 5.8. Therefore, the damping is determined by τ_3. The damper does not see the actuator on θ_4, or *vice versa*.

This damping can be created by a motor instead of a damper. However, the damping should never add energy to the system, so using a simple damper is sufficient.

5.7. Conclusion

This chapter discussed the inclusion of inertia, actuators, and damping into the device. The logic led to

- Inertia and damping on **3**

- Phase actuation on **4**

Assuming the only mass is on **3**, the actuator on **4** feels neither the inertia nor the damping, and *vice versa*. The actuator on **4** can impart energy to the user, but it cannot affect the speed of the inertia on **3**.

CHAPTER 6

Singularities

Interestingly, this device design readily travels travels through multiple singularities each cycle. Each crank arm encounters two singularities per revolution: when their links are fully folded and fully extended. Singularities are common in machines that generate repetitive motion (*e.g.*, internal combustion engines, windshield wipers, and even existing ellipticals), but traditional robotics wisdom says to avoid singularities at all costs. This is because the controller keeping the robot on its desired path often behaves poorly near singularities, even going unstable.

This chapter looks at the singularities found in the presented design, and their effect on motion and the path controller. Can I design a robot that purposely and successfully travels through singularities? How does inertia affect the analysis? What are the effects on mobility?

6.1. Path Boundaries

Recall Figure 5.3a showing constant-phase pedal paths, but also included here as Figure 6.1. The set of paths has an odd-shaped boundary to it, highlighted in the figure. This boundary is caused by the devices singularities.

Because the crank arms rotate in complete revolutions, they must travel through their fully folded and fully extended singularities. Suppose the device is in the configuration shown in Figure 6.2, with $\theta_1 = \pi$, and $\theta_2 \neq 0$ or π. θ_1 *must* be in this position at least
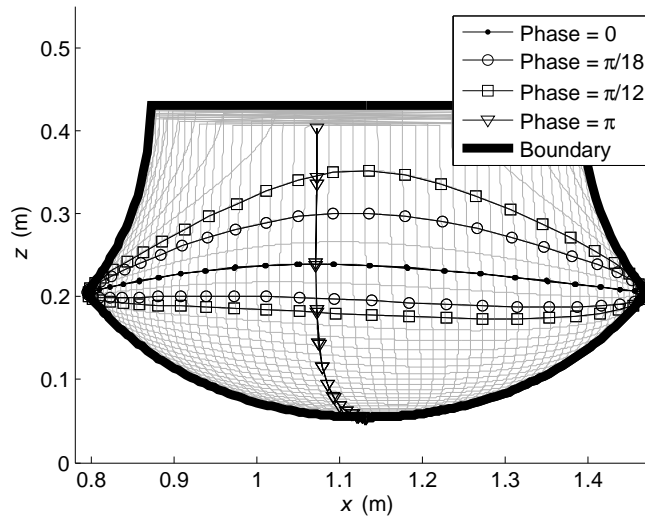
Figure 6.1. Set of constant-phase pedal paths, and its unique boundary.
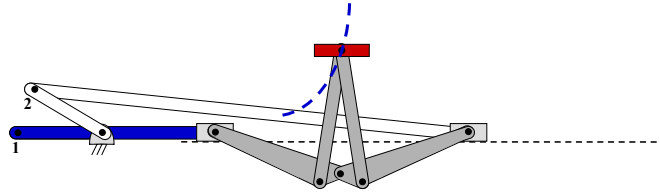
Figure 6.2. Path boundary due to singularity at $\theta_1 = \pi$.

once per cycle. In this configuration, slider **1** must be at the given location, which means that the pedal must lie on the one-degree-of-freedom arc defined by θ_2. Thus, the two-dimensional pedal space is flattened to a one-dimensional curve, a curve that forms one boundary on the pedal's workspace. Furthermore, the pedal *must* touch (and not cross) this boundary every cycle.

The second singular configuration for **1** is at $\theta_1 = 0$ — see Figure 6.3. Here, crank arm **1** is fully extended, and the pedal is once again constrained to a one-degree-of-freedom path. As with the other boundary, the pedal must touch this boundary every cycle, for **1** to rotate in complete revolutions.
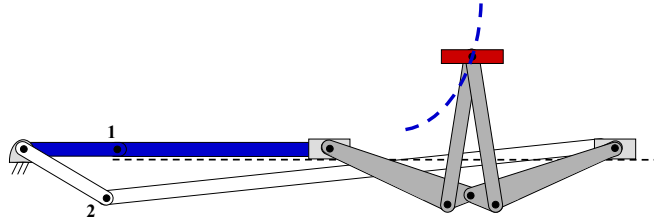
Figure 6.3. Path boundary due to singularity at $\theta_1 = 0$.

Similar to crank arm **1**, crank arm **2** has two singularities forming boundaries on the pedal's workspace. In addition, there is a maximum and minimum pedal height defined by the pantograph's geometry, although these boundaries need not be encountered every cycle.

The four singularity boundaries and two height boundaries form the perimeter of the pedal's workspace. All pedal paths must touch each of the four singularity boundaries — sample paths that do so are shown in Figure 6.4.

6.2. Path Restrictions

The singularities restrict the set of (monotonically-increasing) paths that the device can achieve without further actuation. Because the path must touch the four boundaries, paths such as those in Figure 6.5 are invalid. However, these paths can be achieved by actuating the lengths of three of the crank arm links, as I show here.

Which of the Crank Arm subsystem's dimensions should be actuated? Assuming the global position of the path is not important, the dimensions have the following effects on these boundaries (see Figure 6.6):

- r_i describes the horizontal distance between i's boundaries. Changing both r_i's by the same factor changes the width of the path, without changing the height of
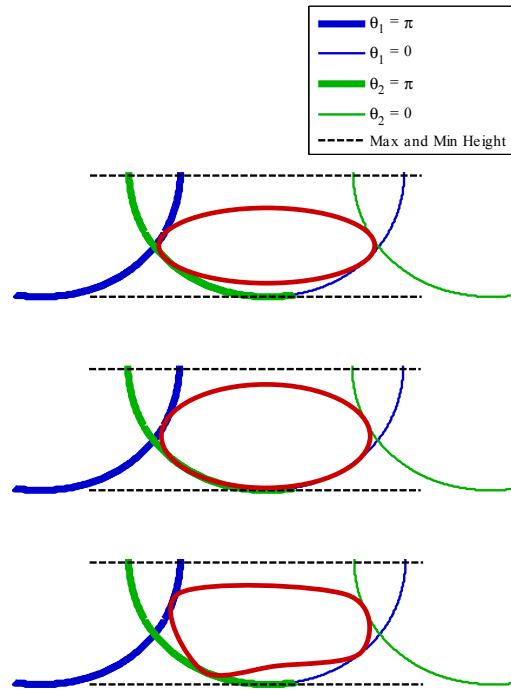
Figure 6.4. Sample valid paths that touch all four boundaries.

the left and right boundary intersections. Changing one r_i relative to the other affects both intersections of the boundaries. Because the boundaries are curves, multiplying r_1 by a constant does not have the same result as dividing r_2 by that same constant. Therefore, actuation of both r_i's is needed.

- l_i determines how far along the x-axis slider i is. Thus, changing l_i moves i's boundaries left or right, without moving them closer or farther apart[1]. Note, though, that shifting **1**'s boundaries to the right by some constant has the same effect as shifting **2**'s boundaries to the left by that same constant. Thus, actuation of only one l_i is needed.

---

[1]It also affects how x changes with θ_i.
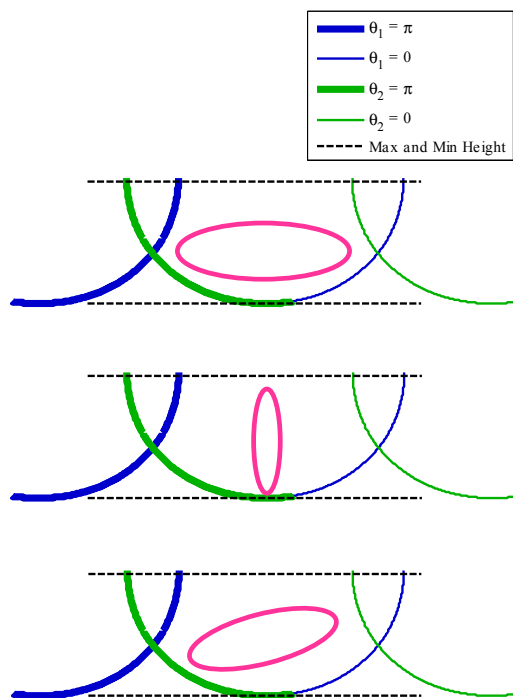
Figure 6.5. Sample invalid paths that do not touch all four boundaries.
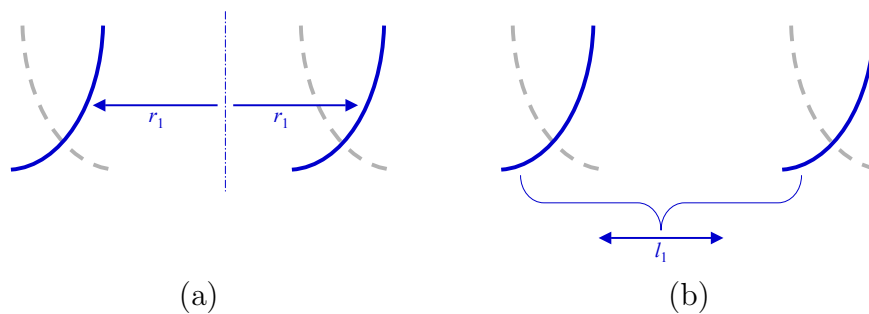
Figure 6.6. Effect of Crank Arms' dimensions. (a) r_i. (b) l_i.

Figure 6.7 shows the once invalid paths as now valid paths for other r_i's and l_i. Therefore, the Crank Arm subsystem needs three offline actuators: on r_1, r_2, and l_1 or l_2.
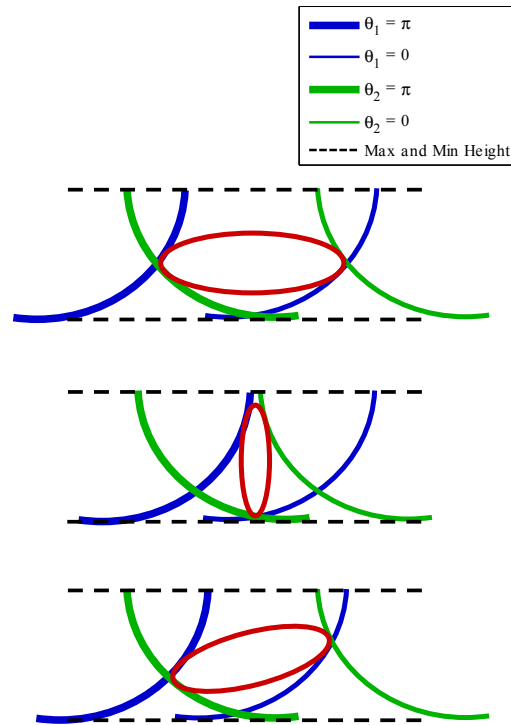
Figure 6.7. The invalid paths become valid with changes in the Crank Arms dimensions.

6.3. Mobility Issues

As in traditional robotics, the singularities result in a loss of mobility, as the two-dimensional pedal workspace flattens to one dimension at the singularities. With regard to users, the loss of mobility actually helps maintain high quality constraints — users' inputs have less effect perpendicular to the path near the singularities. Users' influences tangent to the path also decrease (but not to zero), which means they can't as easily speed up or slow down the mechanism.

Thus, it is important that the device is never at more than one singularity at a time. If θ_1 or θ_2 is at a singularity but the other isn't, then the user is still able to move in one dimension. However, if the device is at rest and both θ_1 and θ_2 are at singularities,

then the user cannot move the device at all (at least, without using the other leg if they two pedals are dependent). This restriction means that "$\theta_1 = \theta_2 = 0$ or π" should never occur, *i.e.*, the path should never touch the intersection of two singularity boundaries.

6.4. Apparent Inertia

As discussed in Section 5.3, there is a large inertia attached to **3** that is assumed to be the dominant inertia in the device. Because this inertia is on the opposite side of the crank arms' singularities from the user, the user sees a significant change in the inertia at the pedal as it travels along its path. Yet, this inertia fluctuation is not unpleasant to users, as similar variations exist with existing exercise machines.

The actuators constrain the pedal to a one-dimensional path, but there are still dynamics along that path, namely damping and inertia. I would like to know how much inertia is seen at the pedal along its path. This inertia is called the *apparent inertia* of the device.

To calculate the apparent inertia, m_{App}, I use the equation for kinetic energy (KE), assuming the only inertia is on **3**:

$$KE = \frac{1}{2}\ \dot{\boldsymbol{\theta}}_{34}^T\ \boldsymbol{I}_{34}\ \dot{\boldsymbol{\theta}}_{34} = \frac{1}{2}\ I_3\ \dot{\theta}_3^2$$

$$= \frac{1}{2}\ \dot{\boldsymbol{x}}^T\ \boldsymbol{M}_x\ \dot{\boldsymbol{x}} = \frac{1}{2}\ m_{App}\ v^2$$

$$m_{App} = \frac{1}{v^2}\ I_3\ \dot{\theta}_3^2,$$

where $\boldsymbol{I}_{34}$ and $\boldsymbol{M}_x$ are inertia matrices, I_3 is the inertia on **3**, and v is the tangential velocity of the pedal. Figure 6.8 shows a plot of m_{App} per unit of mass on I_3, for one cycle. Thus, the user sees from 8 to 136 times the inertia on **3**, for an average of around 32
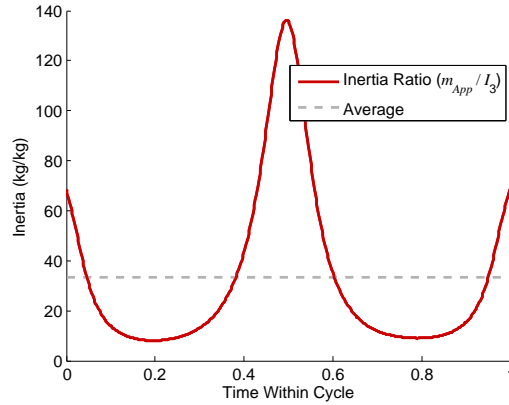
Figure 6.8. Apparent inertia (as a ratio of flywheel inertia) along the path.

times. That is, the kinematics act as a cyclic gear ratio, providing an average reduction of around 5.7. Further reduction (and thus scaling in inertia) can be accomplished by adding additional gearing at the flywheel on **3**.

6.5. Controller Design

In robotics, controllers commonly behave poorly near robots' singularities. This would surely be the case for this device, if the controllers attempted to follow a path in $\boldsymbol{x}$-space using actuators in $\boldsymbol{\theta}_{34}$-space — if the controller and path are separated by the singularity-causing Crank Arms. As the device approached a singularity, the controller would lose influence, over compensate, and probably cause instability. I saw such behavior when doing initial simulations of the mechanism.

However, the singularity issue for the controller can be avoided by transforming the desired path into the $\boldsymbol{\theta}_{12}$ or $\boldsymbol{\theta}_{34}$ space. Now the controller does not encounter any singularities in its path, and the pedal successfully follows the desired path in the controller's space.
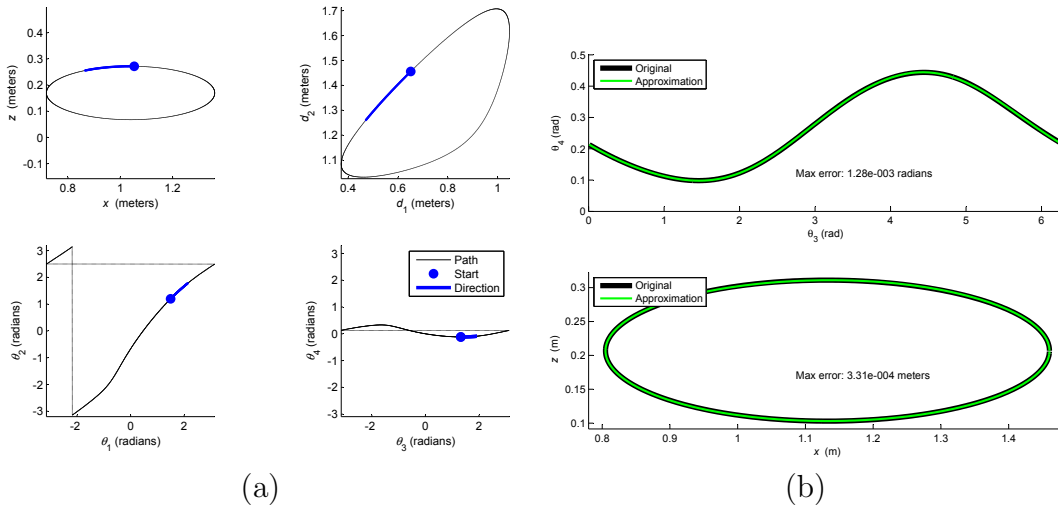
Figure 6.9. Fourier approximation of path in $\boldsymbol{\theta}_{34}$-space. (a) Path in various spaces. (b) Three-term Fourier approximation, with maximum errors.

To aid in the control, I would like the desired path to be defined simply and analytically. The inverse kinematics of the crank arms are double-valued, and thus the path in $\boldsymbol{\theta}_{12}$-space is not analytically computable.

I can simplify things greatly by approximating the path with an analytical one. See the sample path in $\boldsymbol{\theta}_{12}$-space in Figure 6.9a. This path can be easily approximated by a polynomial fit, but when doing so, the controller must have additional logic to handle the wrapping of the θ's. If the path is transformed to the $\boldsymbol{\theta}_{34}$-space, then the path appears near sinusoidal. I can approximate this path with a few-term Fourier summation, which automatically handles the cyclicality (see Figure 6.9b). For the sample path, a three-term Fourier series approximates the path with a maximum error in $\boldsymbol{x}$ of under a third of a millimeter:

$$\text{Max Error in } \boldsymbol{\theta}_{34} : 1.28 \cdot 10^{-3} \text{ radians} \qquad \text{Max Error in } \boldsymbol{x} : 3.31 \cdot 10^{-4} \text{ meters}$$

The path controller for the device is similar to ones used in cobotic devices [**38**]. At each timestep, the controller calculates the position and velocity errors ($\triangle\boldsymbol{\theta}_{34}$ and $\triangle\dot{\boldsymbol{\theta}}_{34}$) based on a reference point (that is tracked by the controller), and calculates a torque based on its gains:

$$\boldsymbol{\tau}_{feedback_{34}} = K \cdot \triangle\boldsymbol{\theta}_{34} + B \cdot \triangle\dot{\boldsymbol{\theta}}_{34},$$

where K and B are the gains. The torque is then projected onto the path's current normal ($\boldsymbol{N}$) to guarantee no effect on motion along the path:

$$\boldsymbol{\tau}_{normal_{34}} = \boldsymbol{N}\boldsymbol{\tau}_{feedback_{34}}^{T}\boldsymbol{N}.$$

The controller is successful even in the midst of human disturbance, as I will show from simulation results in Section 7.3. Since the controller is run in $\boldsymbol{\theta}_{34}$-space, the singularities actually help, since user influence is decreased.

6.6. Path Algorithm

The path and the device dimensions must be intelligently chosen such that the path touches all four of the singularity boundaries. This section describes the current algorithm for defining valid paths.

This algorithm is complex. Although it takes around 30 seconds using Matlab on a Pentium 4, 1.5 GHz processor, it will be significantly faster on the device's computer. Furthermore, this algorithm is only run when the pedal path is first defined, not during operation.
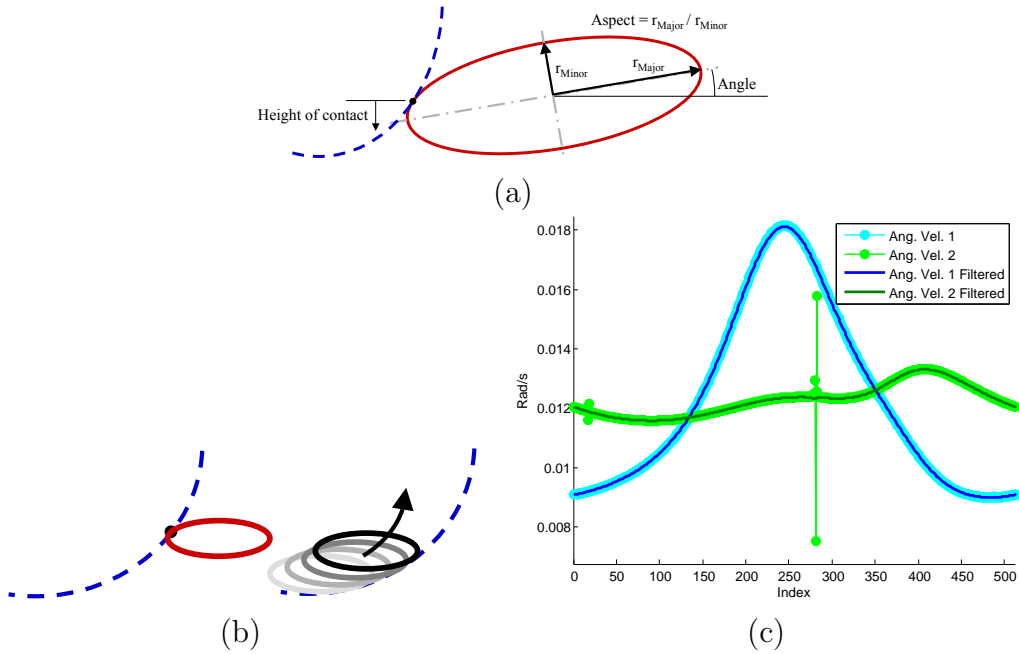
Figure 6.10. Path algorithm. (a) Path parameters given to path-search algorithm. (b) Algorithm routine of traveling up the right-side boundary to search for the closest that the (identical) given-sized ellipses' are to each other. (c) The resulting angular velocities before and after filtering.

The current algorithm to define a path (coded for the simulation in Chapter 7) assumes that the path is elliptical. In practice, this is too restrictive, but for this thesis, it is a reasonable assumption. The algorithm has the following steps:

(1) Given the following parameters:

    (a) Mechanism dimensions: Modified Pantograph and Differential dimensions, r_1 and l_1 (assuming l_1 is fixed but l_2 is actuated).

    (b) Path parameters (see Figure 6.10a): aspect ratio, angle from horizontal, and height of where to touch path.

(2) Find the major axis length that touches both r_1 boundaries. This involves growing the major axis (and thus the constant-aspect ellipse), over several loops of increasing fine searches. For each search (see Figure 6.10b):

    (a) Find the correspondingly sized ellipse tangent to the left boundary at the given point. This requires the contact point and its slope.

    (b) Travel up the right boundary and find the correspondingly sized ellipse tangent to the right boundary. Record the distance between the centers of the ellipse.

    (c) Determine the closest the centers got for this size of ellipse, and at what size and position. Refine the search.

(3) Once the ellipse has been found within some tolerance, use the inverse kinematics of the Modified Pantograph to determine the d_1 and d_2 values. These are used to calculate the variable linkage dimensions r_2 and l_2:

$$r_2 = \frac{1}{2}\left(\max(d_2) - \min(d_2)\right) \qquad L_2 = \max(d_2) - r_2.$$

(4) Use the crank arm's inverse kinematics to get the path in $\boldsymbol{\theta}_{12}$-space. This involves stepping through the path and determining the correct handedness of the crank arms, based on their positions and velocities.

(5) Because the path was searched for in $\boldsymbol{x}$-space, the resulting $\boldsymbol{\theta}_{12}$-space path (which is on the other side of the Crank Arms' singularities) needs to be filtered. Do so on the velocities. This is accomplished by unwrapping $\boldsymbol{\theta}_{12}$, differentiating, performing a zero-phase forward and reverse digital filtering, re-integrating, and re-wrapping. Figure 6.10c shows the path before and after filtering.

(6) Use the differential's inverse kinematics to get the path in $\boldsymbol{\theta}_{34}$-space.

(7) Approximate the path as a Fourier summation, for the controller. See Section 6.5 for more details.

6.7. Conclusion

It is clear that the device can readily and purposely travel through singularities. These singularities, however, restrict the set of achievable paths without the addition of three offline actuators. The singularities also increase the apparent inertia at the pedal, but finitely and without detriment to the user's experience. Most importantly, the singularities do not adversely affect the controller if the controller is run in $\boldsymbol{\theta}_{34}$-space. Results from the simulation in the following chapter will confirm this analysis.

CHAPTER 7

Simulation

This chapter presents an in-depth simulation of the device. The simulation takes into account the masses of the individual links, flywheel inertia and damper torque on **3**, a phase actuator torque on **4**, and a model of the human's input. Results from the simulation show that this design is a promising lower-limb exercise robot.

Throughout this chapter, the user is facing to the left in the figures.

7.1. Human Model

For this simulation, I defined a rough model of the human's input based on the forces measured on the existing Life Fitness elliptical (see Section 3.4). The forces measured within a cycle are shown again in Figure 7.1. Note that the user pushes mainly in the downward direction, and at the lower-front part of the path.
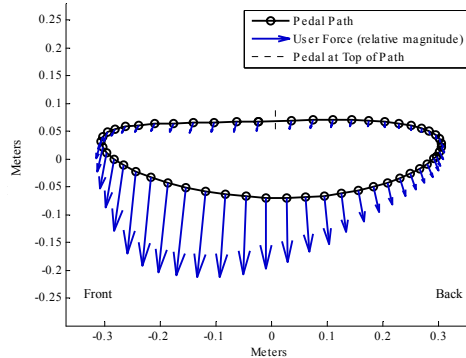
Figure 7.1. User forces measured on Life Fitness X5 during normal operation, shown as force direction within one cycle (path as modeled by simulation).

To model the user's force, I assume perfectly repetitive users: users push in the same direction at the same part of every cycle. While this is an adequate assumption for my purposes, it is obviously not the case in practice, as users have variation in their exertion and timing.

Furthermore, I assume that the user's force is a function of the generic angle within the cycle. The Life Fitness path shown in Figure 7.1 is close to the sample elliptical path that I will use for the simulation, and so I first parameterize the user's force, $\boldsymbol{F}_{user} = \begin{bmatrix} F_x \\ F_z \end{bmatrix}$, with regard to the angle within the cycle, β:

$$x_{Center} = \frac{1}{2}\left(\max(x) + \min(x)\right)$$

$$z_{Center} = \frac{1}{2}\left(\max(z) + \min(z)\right)$$

$$\beta = \arctan(\frac{z - z_{Center}}{x - x_{Center}}).$$

Thus, β is monotonically increasing.

I then parameterize my elliptical desired path in terms of this same β:

$$x = x_{Center} + r_{major}\cos(\beta)$$

$$z = z_{Center} + r_{minor}\sin(\beta),$$

where r_{major} and r_{minor} are the lengths of the major and minor axes. I transform these points to $\boldsymbol{\theta}_{34}$-space, and thus can plot the user's force versus θ_3. I use θ_3 because it is the same space as parameterization of the path — see Section 6.5.
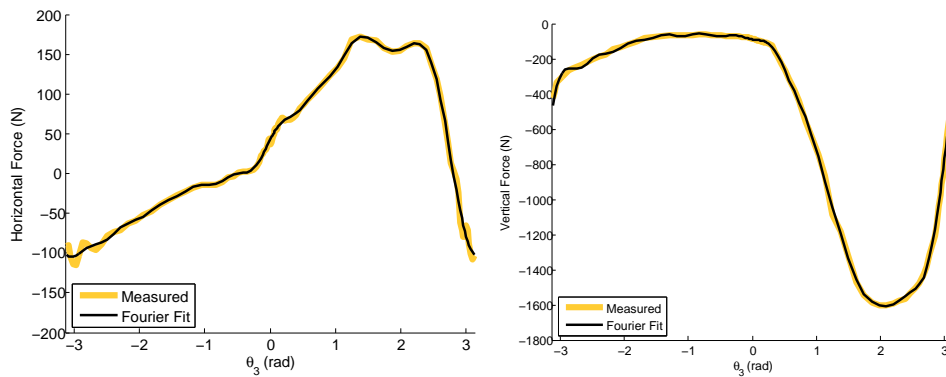
Figure 7.2. Fourier fit for user's forces.

Finally, I approximate the forces as a Fourier Summation, as I did with the path. With 11 terms, the average errors are below 2%:

$$\text{Max Error for } F_x : 15 \text{ N} \qquad \text{Avg Error for } F_x : 4 \text{ N}$$

$$\text{Max Error for } F_z : 43 \text{ N} \qquad \text{Avg Error for } F_z : 9 \text{ N}$$

Figure 7.2 shows the Fourier fit to the forces. Given a θ_3, the Fourier model calculates a F_x and F_z.

This model may be overly specific. I am modeling human input based on one specific recorded cycle. I probably could have more loosely approximated the user's input without much loss of accuracy. For example, I could have filtered the measured data to remove the higher frequencies, and then Fourier approximated the path. Nevertheless, as is, the model is sufficient for the simulation.

7.2. Algorithm and Equations

To analyze the device, I created a simulation in Matlab that takes into account the mass of each link, the flywheel, actuator torques, and forces from the user. The dynamic equations for the system are derived in Appendix E, with the results shown here.

Let $\boldsymbol{J}_i$, $\boldsymbol{m}_i$, and $\boldsymbol{w}_i$ be Jacobian, mass matrix, and weight matrix for link i. The change of energy of the total device is equal to the power flow into the device:

$$\boldsymbol{\tau}_{34} = \boldsymbol{M}(\boldsymbol{\theta}_{34})\ddot{\boldsymbol{\theta}}_{34} + \boldsymbol{C}(\boldsymbol{\theta}_{34}, \dot{\boldsymbol{\theta}}_{34})\dot{\boldsymbol{\theta}}_{34} + \boldsymbol{N}(\boldsymbol{\theta}_{34}),$$

where

$$\boldsymbol{M}(\boldsymbol{\theta}_{34}) = \sum \boldsymbol{J}_i^T \boldsymbol{m}_i \boldsymbol{J}_i$$

$$\boldsymbol{C}(\boldsymbol{\theta}_{34}, \dot{\boldsymbol{\theta}}_{34}) = \sum \boldsymbol{J}_i^T \boldsymbol{m}_i \left(\begin{bmatrix} \frac{\partial \boldsymbol{J}_i}{\partial \theta_3} & \frac{\partial \boldsymbol{J}_i}{\partial \theta_4} \end{bmatrix} \dot{\boldsymbol{\theta}}_{34} \right)$$

$$\boldsymbol{N}(\boldsymbol{\theta}_{34}) = \left(\sum \boldsymbol{J}_i^T \boldsymbol{w}_i \right) - \boldsymbol{J}_{Full}^T \boldsymbol{F}_{user}.$$

The simulation has the following algorithm:

(1) Given all masses, dimensions, and other parameters, and the path in $\boldsymbol{\theta}_{34}$-space

(2) Parameterize path as a Fourier series, as discussed in Section 6.5.

(3) Parameterize user's input as a Fourier series, as discussed in Section 7.1.

(4) Simulate time. At each timestep:

    (a) Calculate the $\boldsymbol{\theta}_{34}$ error from the reference point on the path.

    (b) Calculate the torques on the device. This includes the user's torque, the controller torque as discussed in Section 6.5, and the damping torque as a

function of the velocity:

$$\boldsymbol{\tau}_{Damping} = -B_{damp} \cdot \dot{\boldsymbol{\theta}}_{34}$$

    (c) Calculate the inertia of the device by calculating the mass matrices of each link, from the equations above.

    (d) Calculate $\ddot{\boldsymbol{\theta}}_{34}$ from the dynamics equations, and increment the actual and reference $\boldsymbol{\theta}_{34}$'s

  (5) Analyze the results, including calculating derivatives and powers.

The masses of the links are assumed to be small compared with the flywheel. To determine the amount of damping, the simulation was run with the user input and the damping was increased until the power received from the human was 300 W. Then, the user was removed, and the inertia was increased until the device took 2 seconds to slow down from normal speed (the same time it takes the existing Life Fitness elliptical to do so). Thus, the simulation requires the same amount of energy from the user, while providing the same amount of inertia. The resulting inertia and damping are 10.0 kgm² and 3.5 Nms. This inertia corresponds roughly to a 10 kg flywheel of 0.2 m radius with a gear ratio of 7. In fact, it is nearly identical to the 10.6 kgm² inertia of the flywheel in the existing elliptical (Section 3.7).

7.3. Results

The simulation was run for 90-RPM cycles of 300 W user input, with 10.0 kg·m² inertia of the flywheel.
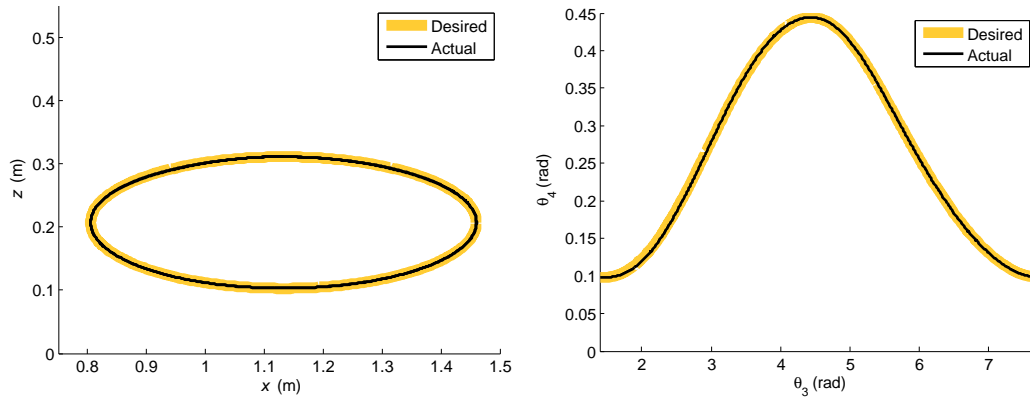
Figure 7.3. Ability of the controller (in $\boldsymbol{\theta}_{34}$-space) to keep the pedal on the desired path.

The controller in the simulation successfully kept the pedal on the desired path. The resulting path from the simulation is shown in Figure 7.3, in both the $\boldsymbol{x}$ and $\boldsymbol{\theta}_{34}$ spaces. Maximum error in the $\boldsymbol{x}$ space was less than 2 millimeters, an error that is well below human detection at the legs. The controller overcame forces from the user that were almost normal to the path, as can be seen in Figure 7.4. This figure shows the torques on the device at the timestep when the user's torque was at its maximum; note that at this timestep, $\boldsymbol{\tau}_{user}$ is near perpendicular to the path.

Of significant interest is the power required of the actuators to achieve this path at this damping. From the Differential equations in Section 4.4, it can be shown that the
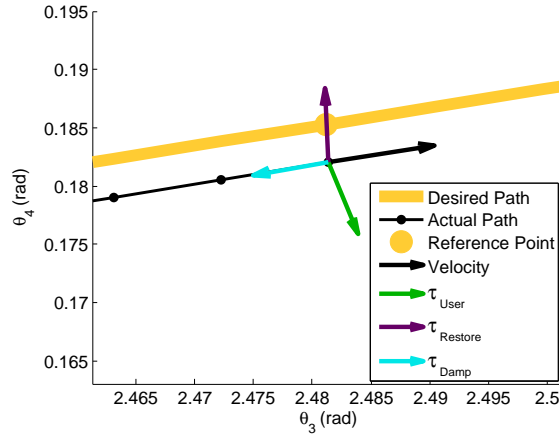
Figure 7.4. Torques on the device at one timestep, when the user's torque was maximum.

powers at **1**, **2**, **3**, and **4** are

$$P_1 = \tau_1 \dot{\theta}_1$$

$$P_2 = \tau_2 \dot{\theta}_2$$

$$P_3 = \tau_3 \dot{\theta}_3 = (\tau_1 + \tau_2)\frac{1}{2}(\dot{\theta}_1 + \dot{\theta}_2) = \frac{1}{2}(\tau_1\dot{\theta}_1 + \tau_1\dot{\theta}_2 + \tau_2\dot{\theta}_1 + \tau_2\dot{\theta}_2)$$

$$P_4 = \tau_4 \dot{\theta}_4 = \frac{r_{\theta_4}}{r_{\theta_1}}(\tau_1 - \tau_2)\frac{1}{2}\frac{r_{\theta_1}}{r_{\theta_4}}(\dot{\theta}_1 - \dot{\theta}_2) = \frac{1}{2}(\tau_1\dot{\theta}_1 - \tau_1\dot{\theta}_2 - \tau_2\dot{\theta}_1 + \tau_2\dot{\theta}_2).$$

Since the design needs little phase change (*i.e.*, $\dot{\theta}_4$ is small, so $\dot{\theta}_1 \approx \dot{\theta}_2 = \dot{\theta}$), the powers become

$$P_1 \approx \tau_1\dot{\theta} \qquad\qquad P_2 \approx \tau_2\dot{\theta}$$

$$P_3 \approx (\tau_1 + \tau_2)\dot{\theta} \qquad P_4 = \tau_4\dot{\theta}_4.$$

Furthermore, as discussed in Section 4.4, a vertical force on the pedal (the major direction of the user's input) creates forces in opposite directions on the sliders, and thus
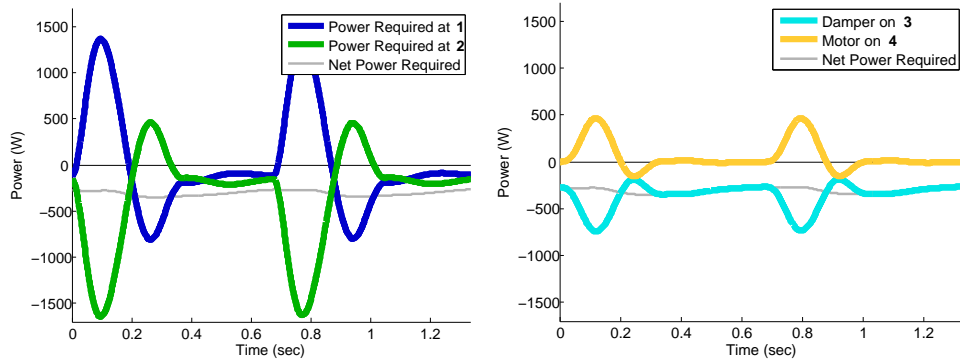
Figure 7.5. Power requirements of actuators at **1-2** *or* **3-4**, for two cycles of the path.

torques that are in opposite directions on **1** and **2**. That is, for most positions of the pedal, τ_1 has the opposite sign of τ_2, and therefore, P_1 and P_2 have opposite signs while P_3 is lower. This means that actuators on **1** and **2** must be large to handle significant torques at speeds around 1-2 Hz, but actuators on **3** and **4** can be much smaller.

Figure 7.5 compares the power requirements for two cycles of the device, at **1-2** versus **3-4**. (This power is required at either **1-2** or **3-4**, but not both.) Here, positive power means energy flowing from actuator to device and user. First, note that the net power at each location is the same, and always negative — the device is always receiving significant net power from the user. Second, note that the powers at **1** and **2** are nearly opposite and equal — this is as expected because of the user's force on the Modified Pantograph. Finally, note that the power required at **3** is always negative — the damper is always drawing power from the system. This was not enforced by the simulation; it is a result of choosing **3-4** over **1-2**.

These plots show the benefit of applying those actuators to **3** and **4** instead of **1** and **2**. By using the differential, the large and opposite powers on **1** and **2** are added and
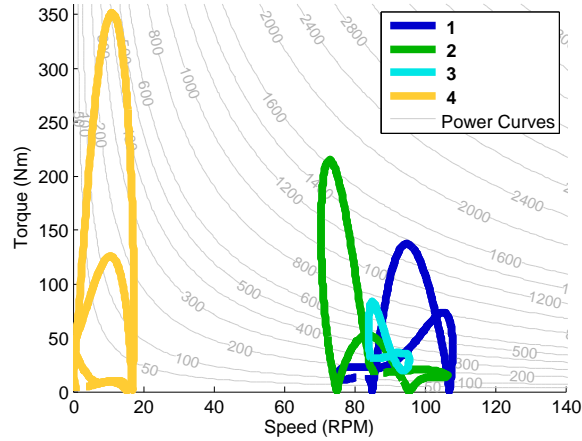
Figure 7.6. Speed-torque curves for actuators on **1**-**2** versus **3**-**4**.

subtracted, resulting in two smaller powers on **3** and **4**. Figure 7.6 shows these powers on a speed-torque plot. Note that **1** and **2** require 1400 and 1650 W motors, but **3** and **4** only require 750 and 470 W actuators. Thus, the actuators needed are an 750 W damper on **3** and a 470 W motor on **4**.

7.4. Passivity

The results from the simulation suggest that a purely passive device is feasible for lower-limb robots. Since the net energy flow is always from user to device, an ideal (frictionless) device would be able store that energy and return it when needed. This ideal device would use passive actuators, making it safer and non-energy-consuming. Furthermore, because the user is putting multiple hundreds of watts into the device, it seems reasonable that even a non-ideal (friction-containing) device would have enough net power input to overcome inefficiencies while still being passive.

7.5. Conclusion

Assuming the models are valid, the in-depth simulation shows that this design is a successful lower-limb exercise robot. The power requirements are promising, as the device requires a relatively small motor and damper to maintain the desired path. This is the result of using an intelligently designed Modified Pantograph, the cyclic Crank Arms, and the phase-isolating Differential.

CHAPTER 8

Conclusion

8.1. General

Analysis of applications and the literature shows that there is a need for cyclic robots for the lower limbs. Current designs, devices, and robotic techniques are not extendable to the cyclic, large inertia, and high power nature of lower limb interaction, especially for exercise and rehabilitation.

The design presented in this thesis is of a promising lower-limb exercise robot. It uses the optimized Modified Pantograph subsystem to support the pedal, the Crank Arms subsystem to create cyclic motion, and the Differential subsystem to isolate phase (*i.e.*, shape of pedal path) from speed along the path. Because the Differential is used, the inertia, damping, and path actuation can be added to the system such that the phase actuator does not feel the inertia or damping, or *vice versa*.

Going against conventional robotics wisdom, this device repeatedly, intentionally, and successfully travels through multiple singularities each cycle. The robot is well-behaved because the inertia, path definition, and controller are all on the cyclic side of the singularities. In fact, the singularities help the controller because they reduce the user's influence on the actuators. Unfortunately, these singularities also restrict the set of possible pedal paths achievable by the device without further (offline) actuation.

Finally, an in-depth simulation of the design shows that the device will require reasonably sized motors and dampers. This simulation takes into account the components' masses, a model of the user's input, and the torques from the actuators. It also suggests that, with further designing, the device may be able to use purely passive actuators.

8.2. Connecting the Pedals

Before now, I have focused on only one pedal, *i.e.*, leg, of the device, assuming that the opposite pedal is identical. One way to couple the two pedals is to add only one degree of freedom: a phasing between the two pedals. Thus the pedals would be dependent except for their relative phase. This would be useful because an unanswered question about ellipticals is how the two pedals should be phased: spatially, temporally, or not at all. Existing ellipticals have the pedals spatially and temporally 180-degrees out of phase at the flywheel, but not necessarily at the pedals. Unfortunately, if the two pedals are at all coupled, the device loses the ability to interact with each foot independently (something that might be useful for rehabilitation[1]), and so a second option is to add two degrees of freedom: the independent translation of the second pedal. Therefore, the two-pedaled device can have a taskspace of either three or four degrees of freedom: the two translations of one pedal, and either the phasing between pedals or a completely independent second pedal. Appendix D shows some designs for coupling the two legs.

---

[1]That is, it may be useful to be able to have different paths or dynamics at each leg for patients with one-sided or asymmetrical injuries.

References

[1] F. Alton, L. Baldey, S. Caplan, and M. C. Morrissey. A kinematic comparison of overground and treadmill walking. *Clinical Biomechanics*, 13:434–440, 1998.

[2] O. Bock. Early stages of load compensation in human aimed arm movements. *Behavioral Brain Research*, 55:61–68, 1993.

[3] R. F. Boian, M. Bouzit, G. C. Burdea, J. Leswis, and J. E. Deutsch. Dual stewart platform mobility simulator. In *9th International Conference on Rehabilitation Robotics*, pages 550–555, Chicago, IL, 2005.

[4] Wayne Book, Robert Charles, Hurley Davis, and Mario Gomes. The concept and implementation of a passive trajectory enhancing robot. In *ASME Dynamic Systems Control Division*, pages 633–638, Atlanta, GA, 1996.

[5] Wayne Book and David Ruis. A microprocessor controlled robotic exercise machine for athletics and rehabilitation. In *Joint Automatic Control Conference*, pages 771–775, 1979.

[6] Wayne Book and David Ruis. Control of a robotic exercise machine. In *Joint Automatic Control Conference*, 1981.

[7] Wayne J. Book and Davin K. Swanson. Reach out and touch someone: controlling haptic manipulators near and far. In *Seventh IFAC Symposium on Robot Control*, pages 87–95, Wroclaw, Poland, 2003.

[8] Gunnar Borg. Perceived exertion as an indicator of somatic stress. *Scandanavian Journal of Rehabilitation Medicine*, 2(3):92–98, 1970.

[9] Gunnar Borg. Simple rating methods for estimation of perceived exertion. In Gunnar Borg, editor, *Physical Work and Effort*, pages 39–45. Pergamon Press, Oxford; New York, 1975.

[10] Gunnar Borg. General discussion. In Gunnar Borg, editor, *Physical Work and Effort*, pages 417–439. Pergamon Press, Oxford; New York, 1977.

[11] Gunnar Borg. Psychophysical studies of effort and exertion: Some historical, theoretical and empirical aspects. In G. Borg and D. Ottoson, editors, *The Perception of Exertion in Physical Work*, pages 3–12. Macmillan Press, London, 1986.

[12] Gunnar Borg. *Borg's Perceived Exertion and Pain Scales*. Human Kinetics, Champaign, IL, 1998.

[13] Gunnar Borg, Peter Hassmen, and Monica Lagerstrom. Perceived exertion related to heart rate and blood lactate during arm and leg exercise. *European Journal of Applied Physiology and Occupational Physiology*, 65:679–685, 1987.

[14] Gunnar A. V. Borg. Psychophysical bases of perceived exertion. *Medicine and Science in Sports and Exercise*, 14(5):377–381, 1982.

[15] Paul Bosscher and Eric LaFay. Haptic cobot exoskeleton: Concepts and mechanism design. In *ASME 2006 International Design Engineering Technical Conferences and Computer and Information in Engineering Conference*, Philadelphia, Pennsylvania, 2006.

[16] E.S. Boy, C.L. Teo, and E. Burdet. Collaborative wheelchair assistant. In *IEEE/RSJ International Conference on Intelligent Robots and System*, volume 2, pages 1511–1516, 2002.

[17] David C. Brogan, Ronald A. Metoyer, and Jessica K. Hodgins. Dynamically simulated characters in virtual environments. *IEEE Computer Graphics and Applications*, 15(5):58–69, 1998.

[18] M. E. Brokowski, Songho Kim, J. Edward Colgate, R. Brent Gillespie, and Michael Peshkin. Toward improved CVTs: Theoretical and experimental results. In *ASME International Mechanical Engineering Congress and Exposition*, New Orleans, LA, 2002.

[19] D. A. Brown and S. A. Kautz. Increased workload enhances force output during pedaling exercise in persons with poststroke hemiplegia. *Stroke*, 29:598–606, 1998.

[20] Enzo Cafarelli. Peripheral contributions to the perception of effort. *Medicine and Science in Sports and Exercise*, 14(5):382–389, 1982.

[21] Matthieu Kevin Pierre Chardon. *Design and Control of the Vertical Planar Cobot*. MS, Northwestern University, 2006.

[22] Robert Andrew Charles. *The Development of the Passive Trajectory Enhancing Robot*. MS, Georgia Institute of Technology, 1994.

[23] Robert R. Christensen, John M. Hollerbach, Yangming Xu, and Sanford G. Meek. Inertial-force feedback for the treadport locomotion interface. *Presence*, 9(1):1–14, 2000.

[24] Jason Yap Chua. *Design of a Wearable Cobot*. PhD, Florida State University, 2006.

[25] J. Edward Colgate, Michael A. Peshkin, and Witaya Wannasuphoprasit. Nonholonomic haptic display. In *IEEE International Conference on Robotics and Automation*, pages 539–544, Minneapolis, Minnesota, 1996.

[26] J. Edward Colgate, Witaya Wannasuphroprasit, and Michael A. Peshkin. Cobots: Robots for collaboration with human operators. In *International Mechanical Engineering Congress and Exhibition*, volume 58, pages 433–439, Atlanta, 1996.

[27] G. Colombo, M. Joerg, R. Schreier, and V. Dietz. Treadmill training of paraplegic patients using a robotic orthosis. *Journal of Rehabilitation Research and Development*, 37:693–700, 2000.

[28] Consumer Reports. Treadmills and ellipticals - indoor exercise. Technical report, Consumer Reports, January, 2005.

[29] Rudoplh P. Darken, William R. Cockayne, and David Carmein. The omni-directional treadmill: A locomotion device for virtual worlds. In *ACM Syposium on User Interface Software and Technology*, pages 213–221, Banff, Canada, 1997.

[30] Hurley Davis and Wayne Book. Torque control of a redundantly actuated passive manipulator. In *American Control Conference*, pages 959–963, Albuquerque, New Mexico, 1997.

[31] Brian P. DeJong. Stair climber, April 28, 2005.

[32] Brian P. DeJong, Eric L. Fauling, J. Edward Colgate, and Michael A. Peshkin. Lessons learned from a novel teleoperation testbed. *Industrial Robot*, 33(3):187–193, 2006.

[33] V. Dietz, W. Zijlstra, and J. Duysens. Human neuronal interlimb coordination during split-belt locomotion. *Experimental Brain Research*, 101:513–520, 1994.

[34] Christopher C. Dunbar, Robert J. Robertson, Randy Baun, Michelle F. Blandin, Kenneth Metz, Ray Burdett, and Fredric L. Goss. The validity of regulating exercise

intensity by ratings for perceived exertion. *Medicine and Science in Sports and Exercise*, 24(1):94–99, 1992.

[35] Pamela Duncan, Lorie Richards, Dennis Wallace, Joni Stoker-Yates, Patricia Phol, Carl Luchies, Abna Ogle, and Stephanie Studenski. A randomized, controlled pilot study of a home-based exercise program for individuals with mild and moderate stroke. *Stroke*, 29:2055–2060, 1998.

[36] R. H. T. Edwards, A. Melcher, C. M. Hesser, O. Wigertz, and L.-G. Ekelund. Physiological correlates of perceived exertion in continuous and intermittent exercise with the same average power output. *European Journal of Clinical Investigation*, 2:108–114, 1972.

[37] R. Emrich and A. Hodgson. A translational-to-rotational continuously variable transmission element for a parallel cobot. In *ASEM IMECE DSC*, volume 69, pages 1285–1292, 2000.

[38] Eric L. Fauling, J. Edward Colgate, and Michael A. Peshkin. A high performance 6-DOF haptic cobot. In *IEEE International Conference on Robotics and Automation*, pages 1980–1985, New Orleans, 2004.

[39] Eric L. Fauling, J. Edward Colgate, and Michael A. Peshkin. High performance cobotics. In *International Conference on Rehabilitation Robotics*, pages 143–148, 2005.

[40] Eric L. Fauling, J. Edward Colgate, and Michael A. Peshkin. Control and performance of the rotational-to-linear cobotic transmission. In *Symposium on Haptic Interfaces for Virtual Environment and Teleoperator Systems*, pages 103—107, Alexandria, Virginia, 2006.

[41] Eric L. Faulring, Kevin M. Lynch, J. Edward Colgate, and Michael A. Peshkin. Haptic interaction with constrained dynamic systems. In *IEEE International Conference on Robotics and Automation*, Barcelona, 2005.

[42] Aaron Ferber. Stair climber alternator analysis summary. Technical report, 2005.

[43] Aaron R. Ferber. *Affecting Exercise Intensity Through Haptic Communications*. MS, Northwestern University, 2007.

[44] Octane Fitness. Body-mapping ergonomics: The science behind an ideal elliptical cross trainer.

[45] Force Dimension. DELTA haptic device: 6-DOF force feedback interface, July 2004.

[46] R. Brent Gillespie, J. Edward Colgate, and Michael A. Peshkin. A general framework for cobot control. *IEEE Transactions on Robotics and Automation*, 17(4):391–401, 2001.

[47] R. Brent Gillespie, Carl A. Moore, Michael Peshkin, and J. Edward Colgate. Kinematic creep in a continuously variable transmission: Traction drive mechanics for cobots. *Journal of Mechanical Design*, 124:713–722, 2002.

[48] Stephen C. Glass and Angela M. Chvala. Preferred exertion across three common modes of exercise training. *Journal of Strength and Conditioning Research*, 15(4):474–479, 2001.

[49] Mario Waldorff Gomes and Wayne J. Book. Control approaches for a dissipative passive trajectory enhancing robot. In *IEEE/ASME International Conference on Advanced Intelligent Mechatronics*, pages 92–97, 1997.

[50] G. S. Guthart and J. K. Salisbury. The intuitive telesurgery system: overview and application. In *IEEE International Conference on Robotics and Automation*, pages 618–622, San Francisco, 2000.

[51] Haptic. *The American Heritage Dictionary of the English Language*. Houghton Mifflin Company, fourth edition, 2004.

[52] Haption. Virtual touch, July 2004.

[53] Ryan C. Hayward and John M. Hollerbach. Implementing virtual stairs on treadmills using torso force feedback. In *International Conference on Robotics and Automation*, pages 586–591, Washington, D.C., 2002.

[54] V. Hayward, P. Gregorio, O. Astley, S. Greenish, M. Doyon, L. Lessard, J. McDougall, I. Sinclair, S. Boelen, X. Chen, J.-P. Demers, J. Poulin, I. Benguigui, N. Almey, B. Makuc, and X. Zhang. Freedom-7: A high fidelity seven axis haptic device with application to surgical training. In A.Casals and A. T. deAlmeida, editors, *Experimental Robotics V*, pages 445–456. Springer-Verlag, 1998.

[55] Stefan Hesse and Dietmar Uhlenbrock. A mechanized gait trainer for restoration of gait. *Journal of Rehabilitation Research and Development*, 37(6):701–708, 2000.

[56] John Hollerbach, David Grow, and Craig Parker. Developments in locomotion interfaces. In *9th International Conference on Rehabilitation Robotics*, pages 522–525, Chicago, IL, 2005.

[57] John M. Hollerbach. Locomotion and haptic interfaces to virtual environments. In *International Conference on Field and Service Robotics*, Pittsburgh, 1999.

[58] John M. Hollerbach, Yangming Xu, Robert R. Christensen, and Stephen C. Jacobsen. Design specifications for the second generation SARCOS Treadport locomotion interface. In *Haptics Symposium, Proceedings of the ASME Dynamic Systems and Control Division*, volume 69, pages 1293–1298, Orlando, 2000.

[59] R. Horowitz, P. Y. Li, and J. Shields. Control of self-optimizing exercise machines. *Annual Reviews in Control*, 24:201–213, 2000.

[60] Y. P. Ivanenko, R. Grasso, V. Macellari, and F. Lacquaniti. Control of foot trajectory in human locomotion: Role of ground contact forces in simulated reduced gravity. *Journal of Neurophysiology*, 87:3070–3089, 2002.

[61] Hiroo Iwata. The torus treadmill: Realizing locomotion in VEs. *IEEE Computer Graphics and Applications*, 19(6):30–35, 1999.

[62] Hiroo Iwata and Takashi Fuji. Virtual perambulator: A novel interface device for locomotion in virtual environments. In *Virtual Reality Annual International Symposium*, pages 60–65, 1996.

[63] Hiroo Iwata, Hiroaki Yano, and Fumitaka Nakaizumi. Gait master: A versatile locomotion interface for uneven virtual terrain. In *Virtual Reality 2001 Conference*, 2001.

[64] Laurent Jabre, Rebecca McGrew, R. Brent Gillespie, and Patrick Goleski. An assistive cobot for aid in self-care activities. In *IFAC Conference on Mechatronic Systems*, Berkeley, CA, 2002.

[65] L. Jensen, T. Prokop, and V. Dietz. Adaptional effects during human split-belt walking: Influence of afferent input. *Experimental Brain Research*, 118:126–130, 1998.

[66] A. N. Johnson, D. F. Cooper, and R. H. T. Edwards. Exertion of stairclimbing in normal subjects and in patients with chronic obstructive bronchitis. *Thorax*, 32:711–716, 1977.

[67] S. A. Kautz, D. A. Brown, H. F. M. Van Der Loos, and F. E. Zajac. Mutability of bifunctional thigh muscle activity in pedaling due to contralateral leg force generation. *Neurophysiology*, 88:1308–1317, 2002.

[68] H. Kazerooni and M. G. Her. A virtual exercise machine. In *IEEE International Conference on Robotics and Automation*, pages 232–238, 1993.

[69] Keehoon Kim, Wan Kyun Chung, and Y. Youm. Design and analysis of a new 7-dof parallel type haptic devide: PATHOS-II. In *IEEE/RSJ International Conference on Intelligent Robots and Systems*, Las Vegas, 2003.

[70] J. W. Krakauer, M. F. Ghilardi, and C. Ghez. Independent learning of internal models for kinematic and dynamic control of reaching. *Nature Neuroscience*, 2:1026–1031, 1999.

[71] Heikki Kyrolainen, Alain Belli, and Paavo V. Komi. Biomechanical factors affecting running economy. *Medicine and Science in Sports and Exercise*, 33(8):1330–1337, 2001.

[72] K. L. Lamb, R. G. Eston, and D. Corns. Reliability of ratings of perceived exertion during progressive treadmill exercise. *British Journal of Sports Medicine*, 33:336–339, 1999.

[73] S. D. Laycock and A. M. Day. Recent developments and applications of haptic devices. *Computer Graphics Forum*, 22(2):117–132, 2003.

[74] A. Lecuyer, C. Megard, J. M. Burkhardt, T. Lim, S. Coquillart, P. Coiffet, and L. Graux. The effect of haptic, visual, and auditory feedback on an insertion task on a 2-screen workbench. In *IPT 2002 Symposium*, Orlando, 2002.

[75] J. H. Lee, K. S. Eom, B.-J. Yi, and I. H. Suh. Design of a new 6-dof parallel haptic device. In *IEEE International Conference on Robotics and Automation*, pages 886–891, Seoul, Korea, 2001.

[76] Perry Li and Roberto Horowitz. Intelligent control of an exercise machine. In *International Workshop on Advanced Motion Control*, pages 271–276, 1996.

[77] Perry Y. Li and Roberto Horowitz. Control of smart exercise machines – part I: Problem formulation and nonadaptive control. *IEEE/ASME Transactions on Mechatronics*, 2(4):237–247, 1997.

[78] Perry Y. Li and Roberto Horowitz. Control of smart exercise machines – part II: Self-optimizing control. *IEEE/ASME Transactions on Mechatronics*, 2(4):248–258, 1997.

[79] Kevin M. Lynch, Caizhen Liu, Allan Sorensen, Songho Kim, Michael Peshkin, J. Edward Colgate, Tanya Tickel, David Hannon, and Kerry Shiels. Motion guides for assisted manipulation. *International Journal of Robotics Research*, 21(1):27–43, 2002.

[80] Machine. *The American Heritage Dictionary of the English Language*. Houghton Mifflin Company, fourth edition, 2004.

[81] Machine. Dictionary.com unabridged, 2007.

[82] R. F. Macko, C. A. DeSouza, L. D. Tretter, K. H. Silver, G. V. Smith, P. A. Anderson, N. Tomoyasu, P. Gorman, and D.R. Dengel. Treadmill aerobic exercise training reduces the energy expenditure and cardiovascular demands of hemiparetic gait in chronic stroke patients. *Stroke*, 28:326–330, 1997.

[83] Thomas H. Massie and J. K. Salisbury. The phantom haptic interface: A device for probing virtual objects. In *ASME Winter Annual Meeting, Symposium on Haptic Interfaces for Virtual Environment and Teleoperator Systems*, Chicago, IL, 1994.

[84] Yoky Matsuoka and Larry C. Miller. Domestic rehabilitation and learning of task-specific movements. In *International Conference on Rehabilitation Robotics*, Stanford, CA, 1999.

[85] Mechanism. *The American Heritage Dictionary of the English Language*. Houghton Mifflin Company, fourth edition, 2004.

[86] Mechanism. Dictionary.com unabridged, 2007.

[87] Patricia M. Mihevic. Sensory cues for perceived exertion: A review. *Medicine and Science in Sports and exercise*, 13(3):150–163, 1981.

[88] Tsutomu Miyasato. Tele-nursing system with realistic sensations using virtual locomotion interface. In *6th ERCIM Workshop on 'User Interfaces for All'*, Florence, Italy, 2000.

[89] Carl A. Moore, Michael A. Peshkin, and J. Edward Colgate. Design of a 3R cobot using continuously variable transmissions. In *IEEE International Conference on Robotics and Automation*, pages 3249–3254, Detroit, 1999.

[90] Jr. Carl A. Moore, Michael A. Peshkin, and J. Edward Colgate. Cobot implementation of virtual paths and 3-D virtual surfaces. *IEEE Transactions of Robotics and Automation*, 19(2):347–351, 2003.

[91] S. Munir, L. Tognetti, and W. J. Book. Experimental evaluation of a new braking system for use in passive haptic displays. In *American Control Conference*, San Diego, CA, 1999.

[92] F. A. Mussa-Ivaldi and J. L. Patton. Robots can teach people how to move their arm. In *IEEE International Conference on Robotics and Automation*, San Francisco, CA, 2000.

[93] Yoshihiko Nakamura, Woojin Chung, and Ole Jacob Sordalen. Design and control of the nonholonomic manipulator. *IEEE Transactions on Robotics and Automation*, 17(1):48–59, 2001.

[94] Bruce J. Noble. Clinical applications of perceived exertion. *Medicine and Science in Sports and Exercise*, 14(5):406–411, 1982.

[95] Bruce J. Noble. Preface to the symposium on recent advances in the study and clinical use of perceive exertion. *Medicine and Science in Sports and Exercise*, 14(5):376, 1982.

[96] Bruce J. Noble, Gunnar A. V. Borg, Ira Jacobs, Ruggero Ceci, and Peter Kaiser. A category-ratio perceived exertion scale: Relationship to blood and muscle lactates and heart rate. *Medicine and Science in Sports and Exercise*, 15(6):523–528, 1983.

[97] H. Noma and T. Miyasato. Design for locomotion interface in a large scale virtual environment, ATLAS: ATR locomotion interfaces for active self motion. In *ASME Dynamic Systems and Control Division*, volume 64, pages 111–118, 1998.

[98] R. Osu, E. Burdet, D. W. Franklin, T. E. Milner, and M. Kawato. Different mechanisms involved in adaption to stable and unstable dynamics. *Journal of Neurophysiology*, 90:3255–3269, 2003.

[99] Tammy M. Owings and Mark D. Grabiner. Step width variability, but not step length variability or step time variability, discriminates gait of healthy young and older adults during treadmill locomotion. *Journal of Biomechanics*, 37:935–938, 2004.

[100] Peng Pan, Kevin M. Lynch, Michael A. Peshkin, and J. Edward Colgate. Human interaction with passive assistive robots. In *International Conference on Rehabilitation Robotics*, pages 264–268, Chicago, IL, 2005.

[101] Peng Pan, Michael A. Peshkin, J. Edward Colgate, and Kevin M. Lynch. Static single-arm force generation with kinematic constraints. *Journal of Neurophysiology*, 93:2752–2765, 2004.

[102] Kent B. Pandolf. Differentiated ratings of perceived exertion during physical exercise. *Medicine and Science in Sports and Exercise*, 14(5):397–405, 1982.

[103] J. L. Patton and F. A. Mussa-Ivaldi. Robot-assisted adaptive training: Custom force fields for teaching movement patterns. *IEEE Transactions on Biomedical Engineering*, 51:636–646, 2004.

[104] S. J. Pearson, M. Cobbold, and S. D. R. Harridge. Power output of the lower limb during variable inertial loading: A comparison between methods using single and repeated contractions. *European Journal of Applied Physiology and Occupational Physiology*, 92:176–181, 2004.

[105] Michael Peshkin, David A. Brown, Julio J. Santos-Munne, Alex Makhlin, Ela Lewis, J. Edward Colgate, James Patton, and Doug Schwandt. Kineassist: A robotic overground gait and balance training device. In *International Conference on Rehabilitation Robotics*, pages 241–246, Chicago, IL, 2005.

[106] Michael A. Peshkin, J. E. Colgate, W. Wannasuphoprasit, C. A. Moore, R. B. Gillespie, and P. Akella. Cobot architecture. *IEEE Transactions on Robotics and Automation*, 17:377–390, 2001.

[107] Michael A. Peshkin, J. Edward Colgate, and Carl Moore. Passive robots and haptic displays based on nonholonomic elements. In *IEEE International Conference on Robotics and Automation*, pages 551–556, Minneapolis, Minnesota, 1996.

[108] Michael L. Pollock, Andrew S. Jackson, and Carl Foster. The use of the perception scale for exercise prescription. In G. Borg and D. Ottoson, editors, *The Perception of Exertion in Physical Work*, pages 161–176. Macmillan Press, London, 1986.

[109] Kathleen Potempa, Martita Lopez, Lynne T. Braun, J. Peter Szidon, Louis Fogg, and Tyler Tincknell. Physiological outcomes of aerobic exercise training in hemiparetic stroke patients. *Stroke*, 26:101–105, 1995.

[110] Christine C. Raasch and Felix E. Zajac. Locomotor strategy for pedaling: Muscle groups and biomechanical functions. *Journal of Neurophysiology*, 82:515–525, 1999.

[111] Sebastien Ratel, Craig A. Williams, and Jonathan Oliver. Effects of age and mode of exercise on power output profiles during repeated sprints. *European Journal of Applied Physiology and Occupational Physiology*, 92:204–210, 2004.

[112] Robert J. Robertson. Central signals of perceived exertion during dynamic exercise. *Medicine and Science in Sports and Exercise*, 14(5):390–396, 1982.

[113] Robot. Wikipedia, The Free Encyclopedia, 2007.

[114] L. B. Rosenberg. *Virtual Fixtures: Perceptual Overlays enhance operator performance in telepresence tasks*. PhD thesis, Stanford University, 1994.

[115] Luis B. Rosenberg and Bernard D. Adelstein. Perceptual decomposition of virtual haptic surfaces. In *IEEE Syposium on Research Frontiers in Virtual Reality*, pages 46–53, San Jose, CA, 1993.

[116] David A. Ruis, Russell W. Polhemus, and Wayne J. Book. Robotic exercise machine and method, 1980.

[117] William D. Russell. On the current status of rated perceived exertion. *Perceptual and Motor Skills*, 84:799–808, 1997.

[118] R. L. Sainburg, C. Ghez, and D. Kalakanis. Intersegmental dynamics are controlled by sequential anticipatory, error correction, and postural mechanisms. *Journal of Neurophysiology*, 81:1045–1056, 1999.

[119] Julio J. Santos-Munne. Extreme joystick: A cobot with stored energy, September 28, 1998.

[120] Henning Schmidt, Cordula Werner, Rolf Bernhardt, Stefan Hesse, and Jorg Kruger. Gait rehabilitation machines based on programmable footplates. *Journal of Neuro-Engineering and Rehabilitation*, 4(2), 2007.

[121] O. Schneider, J. Troccaz, O. Chavanon, and D. Blin. PADyC: a synergistic robot for cardiac puncturing. In *International Conference on Robotics and Automation*, pages 2883–2888, San Francisco, CA, 2000.

[122] Olivier Schneider and Jocelyne Troccaz. A six-degree-of-freedom passive arm with dynamic constraints (PADyC) for cardiac surgery application: Preliminary experiments. *Computer Aided Surgery*, 6(6):340–351, 2001.

[123] SensAble Technologies. Phantom premium haptic device, 2004.

[124] U.S. Department of Health Services and Human. Promoting physical activity: A guide for community action. Technical report, Human Kinetics, 1999.

[125] SGMA. Recreation market report 2000. Technical report, Sporting Goods Manufacturers Association, 2000.

[126] SGMA. Recreation market report: 2004 edition. Technical report, Sporting Goods Manufacturers Association, 2004.

[127] SGMA. Sports participation topline report: 2005 edition. Technical report, Sporting Goods Manufacturers Association, 2005.

[128] SGMA. Recreation market report: 2006 edition. Technical report, Sporting Goods Manufacturers Association, 2006.

[129] Joel Shields and Roberto Horowitz. Adaptive step rate control of a stair stepper exercise machine. In *American Control Conference*, pages 1058–1062, Philadelphia, Pennsylvania, 1998.

[130] Michael A. Smutok, Gary S. Skrinar, and Kent B. Pandolf. Exercise intensity: Subjective regulation by perceived exertion. *Archives of Physical Medicine and Rehabilitation*, 61:569–574, 1980.

[131] Michael W. III Stima. Microprocessor controlled electro-hydraulic exercise system, July 11, 1989.

[132] Dragoljub Surdilovic and Rolf Bernhardt. String-man: A new wire robot for gait rehabilitation. In *IEEE International Conference on Robotics and Automation*, pages 2031–2036, New Orleans, 2004.

[133] Davin K. Swanson and Wayne J. Book. Torque feedback control of dry friction clutches for a dissipative passive haptic interface. In *International Conference on Control Applications*, pages 736–741, Anchorage, Alaska, 2000.

[134] Davin K. Swanson and Wayne J. Book. Obstacle avoidance methods for a passive haptic display. In *IEEE/ASME International Conference on Advanced Mechatronics*, pages 1187–1192, Como, Italy, 2001.

[135] Davin K. Swanson and Wayne J. Book. Path-following control for dissipative passive haptic displays. In *11th Symposium on Haptic Interfaces for Virtual Environment and Teleoperator Systems*, 2003.

[136] Davin K. Swanson, Eric Romagna, Wayne J. Book, and Andre Barraco. Influence of actuator dynamics on passive haptic interface performance. In *IEEE/ASME International Conference on Advanced Intelligent Mechatronics*, pages 440–445, Atlanta, 1999.

[137] M. Tavakoli, R. V. Patel, and M. Moallem. Design issues in a haptics-based master-slave system for minimally invasive surgery. In *IEEE International Conference on Robotics and Automation*, pages 371–376, New Orleans, 2004.

[138] K. A. Thoroughman and R. Shadmehr. Electromyographic correlates of learning an internal model of reaching moevments. *Journal of Neuroscience*, 19:8573–8588, 1999.

[139] Lena H. Ting, Steven A. Kautz, David A. Brown, and Felix E. Zajac. Contralateral movement and extensor force generation alter flexion phase muscle coordination in pedaling. *Neurophysiology*, 83:3351–3365, 2000.

[140] Jocelyne Troccaz, Stephane Lavallee, and Emmanuelle Hellion. A passive arm with dynamic constraints: A solution to safety problems in medical robotics? In *Systems, Man and Cybernetics*, volume 3, pages 166–171, 1993.

[141] H.-V. Ulmer, U. Janz, and H. Lollgen. Aspects of the validity of Borg's Scale. is it measuring stress or strain? In Gunnar Borg, editor, *Physical Work and Effort*, pages 181–196. Pergamon Press, Oxford; New York, 1977.

[142] Midn. A. VanReet and M. G. Feemster. Development of an electrically actuated exercise system. In *Thirty-Sixth Southeastern Symposium on System Theory*, pages 246–250, 2004.

[143] Witaya Wannasuphoprasit, Prasad Akella, Michael Peshkin, and J. Edward Colgate. Cobots: A novel material handling technology. In *IMECE*, 1998.

[144] Witaya Wannasuphoprasit, R. Brent Gillespie, J. Edward Colgate, and Michael A. Peshkin. Cobot control. In *IEEE International Conference on Robotics and Automation*, pages 3571–3576, Albuquerque, NM, 1997.

[145] Witaya Wannasuphoprasit and Sirisak Sirikasemsuk. Kinematics of three dimensional serial link cobot. In *The 17th Conference of Mechanical Engineering Network of Thailand*, Thailand, 2003.

[146] Witaya Wannasuphroprasit and Thanachote Cheepsumol. Parallel CVT mechanisms. In *JSAE Annual Congress*, pages 15–18, 2004.

[147] Mitchell H. Whaley, Peter H. Brubaker, Leonard A. Kaminsky, and Christopher R. Miller. Validity of rating of perceived exertion during graded exercise testing in apparently healthy adults and cardiac patients. *Journal of Cardiopulmonary Rehabilitation*, 17(4):26–267, 1997.

[148] Tom Worsnopp, Michael Peshkin, Kevin Lynch, and J. Edward Colgate. Controlling the apparent inertia of passive human-interactive robots. *Journal of Dynamic Systems, Measurement, and Control*, 128(1):44–52, 2006.

[149] Marcelo Yamil Yambay Valiente. *Design of a Unicycle Cobot*. MS, Northwestern University, 2001.

[150] Jungwon Yoon, Jeha Ryu, and Kil-Byung Lim. Reconfigurable ankle rehabilitation robot for various exercises. *Journal of Robotic Systems*, 22:S15–S33, 2006.

[151] Anne I. Zeni, Martin D. Hoffman, and Philip S. Clifford. Energy expenditure with indoor exercise machines. *Journal of the American Medical Association*, 275(18):1424–1427, 1996.

APPENDIX A

Perceived Exertion Literature Review

1. Introduction

"First, it has become obvious that the proliferation of Borg Scale use [*i.e.*, perceived exertion], in both scientific and clinical environments, has not been accompanied with sufficient training in psychophysics by its users." - Noble [**95**], 1982

There has been much research on perceived exertion. Most of the literature is from the 1970s and 1980s, although it is still being studied today. While several different authors have suggested subjective scales for perceived exertion, the scale that is most often used is the Borg scale.

The first batch of research into the Borg scale was focused primarily on validating the scale, for multiple modes of exertion (*e.g.*, treadmill or cycle ergometer). Most experiments looked at the scale's relationship to heart rate, oxygen intake, and other psychophysical parameters. Once the Borg scale was validated, the research focus shifted to determining the perceptual cues that cause perceived exertion. Tests attempted to isolate cues to determine their influence. After some time and the general conclusion that any cue, when elevated, focused on, or given high value, can dominate perceived exertion, attention again changed, this time to whether the Borg scale can prescribe exercise. This is where the literature seems to be at today.

There are countless reviews on the perceived exertion literature. Two that I have obtained are the ones by Mihevic in 1981 [**87**] and Russell in 1997 [**117**]. Other reviews include ones by Borg and Noble (1974), Morgan (1981), Pandolf (1983), Carton and Rhodes (1985), Williams and Eston (1989), Watts and Grove (1993), and Noble and Robertson (1996). Borg [**11**] has also authored a historical review of the creation of the Borg scale.

2. The Borg Scale(s)

Scales for perceived exertion tend to be either *ratio* or *category*. A ratio scale involves an absolute zero and values spaced at equal distances with respect to one another (*e.g.,* a percentage scale). The main disadvantage of such a scale is the lack of individual assessment of intensity. For example, two subjects may deem one weight twice as heavy as another, but this doesn't tell whether they thought the weights were light or heavy. On the other hand, a category scale gives a subject's individual intensity level, but doesn't take into account individual differences. For example, one subject may rate a weight as "Somewhat Heavy", while another rates the same weight as "Light".

Perceived exertion was originally rated using a ratio scale. Then, in his dissertation in 1962, Borg presented a new category rating scale for a user's perceived exertion. This scale consists of 21 levels and is adverb symmetric about its center. See Table A.1. This scale is not linear with heart rate (HR).

Also in his dissertation, Borg presents results using a cycle ergometer showing that perceived exertion increases with physical workload (power) by a power function with exponent equal to 1.6. I assume from subsequent citations and discussions that this was

Table A.1. The original, symmetric perceived exertion scale created by Borg.

1	Nothing	12	
2		13	Fairly laborious
3	Very, very light	14	
4		15	Laborious
5	Very light	16	
6		17	Very laborious
7	Light	18	
8		19	Very, very laborious
9	Fairly light	20	
10		21	Maximum exertion
11	Neither light nor laborious		

Table A.2. The Borg Scale, or Ratings of Perceived Exertion (RPE).

6		14	
7	Very, very light	15	Hard
8		16	
9	Very light	17	Very hard
10		18	
11	Fairly light	19	Very, very hard
12		20	
13	Somewhat hard		

accomplished by asking subjects to subjectively double or half a presented workload. Other studies have shown the exponent for walking is around 3.0 [9]. I wasn't able to find exponent numbers for stair climbing or other exercise.

A few years later, Borg [8] introduced an improved scale, now commonly referred to as the "Borg Scale" or "Ratings of Perceived Exertion" (RPE; see Table A.2). This newer scale has 15 levels from 6 to 20, with 6 being resting and 20 being maximum exertion. Furthermore, this new scale is adverb asymmetric, such that it is approximately linear with HR (6 RPE $\approx$ 60 beats/min; 20 RPE $\approx$ 200 beats/min). Many, many studies since then have shown that RPE is linear with *relative* HR, oxygen consumption (VO_2), ventilation (VE) and respiratory rate (RR), and curve linear with blood lactate (BL).

Borg [8] states that the Borg scale is "fairly linear" with workload. Edwards, *et al.* [36] found that RPE correlated significantly with average power output for a cycle ergometer

Table A.3. Borg's category-ratio scale for perceived exertion.

0	Nothing at all	5	Strong
0.5	Very, very weak	6	
1	Very weak	7	Very strong
2	Weak	8	
3	Moderate	9	
4	Somewhat strong	10	Very, very strong

($r = 0.97$ for continuous workload, $r = 0.94$ for intermittent). Ulmer [141] also found RPE to be linear with workload (simple corr. $= 0.933$, partial corr. $= 0.693$). Note that this is discussing RPE, *not* perceived exertion.

In an attempt to gain the benefits of both category scales (*i.e.*, absolute ratings) and ratio scales (*i.e.*, better inter- and intra- subject consistency), Borg [14] introduced a newer ratio-category scale (CR; see Table A.3). Testing of CR by Noble, *et al.* [96] (the authors include Borg) shows similar exponents in the power relationships. Further testing of CR by Borg, *et al.* [13] shows similar physiological correlations as with RPE, however the plots of CR and RPE versus power and HR visibly curve in opposite directions! While this scale is not publicly rejected by researchers, it seems to be publicly ignored. Almost all research still uses the 15-pt RPE scale.

3. Studies Related to the Effect of Inertia

In one study cited by Ulmer [141], the moment of inertia of a cycle ergometer flywheel was increased by factor of 2.2, with very little (insignificant) change in RPE. Visually, the change, if it exists, is increased RPE with lighter flywheel. Says Ulmer in a conference discussion [10], "Therefore, I believe that [moment of inertia] is not an essential aspect [of perceived exertion]." See Figure A.1.
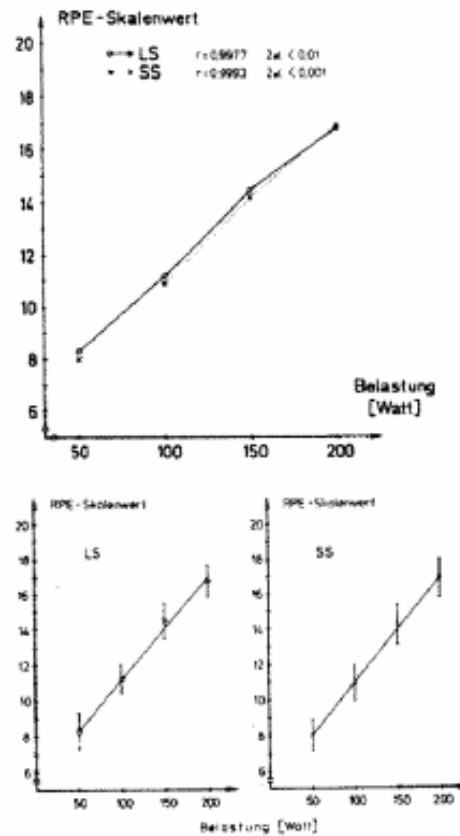
Figure A.1. Results for perceived exertion with respect to moment of inertia, as cited by (taken from) Ulmer [**141**]. LS = normal inertia. SS = 2.2 times normal inertia.

Johnson [**66**], *et al.* had subjects climb 12 flight of stairs and recorded RPE, HR, BL, and VE. The subjects consisted of 3 groups: young and healthy, middle-aged and healthy, and middle-aged with bronchitis problems. Johnson and his colleagues found that

- Subjects' climbing speed was remarkably constant for the entire climb.

- RPE correlates with HR ($r = 0.78$) and BL (also $r = 0.78$) for stair climbing.

- While power output (height per time) was significantly different between groups, RPE and relative HR were only slightly different. However, VE correlates with power ($r = 0.91$).

In 1996, Zeni *et al.* [**151**] tested energy expenditure (VO_2), HR, and BL at three RPE values for several different types of exercise machines. The machines used were a treadmill, stair climber, rowing ergometer, cross-country ski machine, cycle ergometer, and an Airdyne. They found that for all machines energy expenditure and HR were linear with RPE, and that BL was curve linear with RPE. Furthermore, they found that for the same RPE values, the treadmill had the highest energy expenditure and HR, with the stair climber a close second, and the stair climber had the highest BL.

4. Perceptual Cues for Perceived Exertion

There have also been many studies on what perceptual cues are important for perceived exertion. Unless otherwise cited, the following is from the summary by Mihevic [**87**] in 1981.

The exercise variables that affect perceived exertion include intensity, type, steady state versus intermittent, and duration. The perceptual cues can be categorized into two groups: Central Factors (*i.e.*, within the chest) and Local Factors (*i.e.*, at the site of physical activity, *e.g.*, the legs).

4.1. Central Factors

Central factor effects occur 30-180 seconds after the start of exercise [**112**]. Thus, most RPE experiments involve at least 5 minutes at a given power level.

The first of the central factors is HR. While RPE often correlates with absolute HR, studies that alter HR such as by hot environments or chemicals show that HR is not a major input for perceived exertion. For example, even when a subject's HR is elevated

by chemicals, his or her RPE does not change. In addition, several studies have shown that when pedaling rate is increased for same power output, RPE decreases while HR increases.

Meanwhile, *relative* VO_2 has been shown to be independent of exercise variables, but there is no evidence that VO_2 is monitored by the individual. For example, Robertson [112] found in his experiments that relative VO_2 correlated more closely to RPE than VE, RR or HR.

On the other hand, VE and RR can be consciously monitored. Furthermore, an experiment where the power intensity was sinusoidally varied on a cycle ergometer found that the peak of perceived exertion corresponded to peak VE rather than to the time of highest power.

Results from several studies suggest that training has little influence on RPE. Experiments where subjects were tested pre- and post-training show a decrease in RPE, however one-time cross-sectional comparisons of individuals show absolutely no training effect on RPE. Therefore, while training may decrease an individual's RPE, an individual's training history cannot predict his or her RPE.

4.2. Local Factors

One local factor believed to effect perceived exertion is blood lactate concentration. Research shows that at high exercise intensities, the lactate-RPE relationship is robust.

Other local factors include prioperception and muscle sensations. Studies using various pedaling speeds suggest that prioperception is an important factor for perceived exertion. There are some researchers, however, who disagree with this hypothesis.

4.3. Additional Discussion

Additional things to note regarding perceived exertion are skin and core temperature, and duration. Research is inconclusive about the effect of temperature but shows that duration is more critical to perceived exertion than the amount of work. Furthermore, in a 30-minute test, while VO_2 and VE remained steady after 10 minutes, perceived exertion continued to increase.

Cafarelli [20] looked at how perceived exertion cues are processed and found support for both feedforward and feedback processing.

There appears to have been little closure with regards to this avenue of research. Authors seem to come to the conclusion that any cue can be important. As Pandolf [102] states, "When a particular physiological cue is markedly altered over others during exercise [such as by chemicals or mental concentration], it appears that the resultant sensation can easily dominate the overall RPE."

5. Prescribing RPE

In general, experiments on RPE can be broken into two types: "Estimation" and "Production". The estimation technique involves presenting subjects with a workload and asking them to rate their perceived exertion. In contrast, the production technique involves asking subjects to achieve a RPE and then recording the actual physical and physiological levels. The vast amount of research on RPE was initially estimation, *i.e.*, to validate the scale. In the 1980's production experiments began to emerge, primarily to test whether RPE could be used to regulate exercise. For example, instead of telling

people to workout at a percentage of maximum heart rate, one could prescribe an RPE as the target intensity.

Smutok, *et al.* [130] ran one of the first of such experiments in 1980. They tested RPE production on a treadmill and found that it was valid and safe above 80% HR_{max} and 9.0 kph. Below these limits, RPE production was deemed inaccurate. They also found that at the same RPE, HR was higher for production trials than for an estimation trial.

Noble [94] also tested the use of RPE to prescribe exercise intensity. He states that while RPE is inappropriate for studying a production problem (training control), it is effective for regulating personal exercise.

In 1986, Pollock *et al.* [108] claimed significant validity in using RPE to prescribe exercise. They found that RPE correlated extremely well with Percent Heart Rate Reserve (*i.e.*, percentage of the (HR_{max} - HR_{rest}) reserve used). According to their results, 50-90% $HR_{maxReserve}$ = 12-16 RPE.

Furthermore, Dunbar *et al.* [34] found that RPE was significantly effective in producing levels of relative VO_2. However, visually the %VO_2 is lower for the produced trials than for the estimated trials.

Conversely, Whaley *et al.* [147] claim that RPE is inaccurate in prescribing HR, especially for cardiac subjects. They appear to not fully understand RPE, though, as they seem to support their discussion by misusing a quote from Borg that actually is discussing the opposite effect.

While they use estimation methods rather than production methods, Lamb *et al.* [72] claim that RPE, while good at showing one-time relative intensities, is not repeatable

from day to day. Retests of the same exercise showed variations in the subject's reported RPE levels.

APPENDIX B

Stair Climber Modifications and Exertion Experiment

1. As Received

The stair climber that I modified is a Life Fitness 9500 HR. As received, it was missing the plastic housing around the belts, alternator, and electronics, as well as the plastic foot pedals that attach to the metal supports. However, it was still fully functional. As received, the stair climber needed no external power supply, except to power the optional LCD monitor (for displaying television). See Figure B.1 for pictures of the unmodified stair climber.

A schematic of the mechanical components is shown in Figure B.2. The stair climber provided resistance to the user's motion by using a geared down alternator. The two foot pedals were positionally independent of each other, with individual spring returns to pull them to the top of the device. The pedals drove sprockets via timing belts, which in turn were connected to an axle via clutched bearings. These clutches allowed the pedals to move independent of the axle in the upward position and possibly downward, if the pedals were moving downward slow enough that the sprockets were spinning slower than the axle. Mathematically, foot pedal i was engaged with the axle when

$$\omega_{sprocket_i} = \frac{v_{pedal_i}}{r_{sprocket}} \geq \omega_{axle}.$$
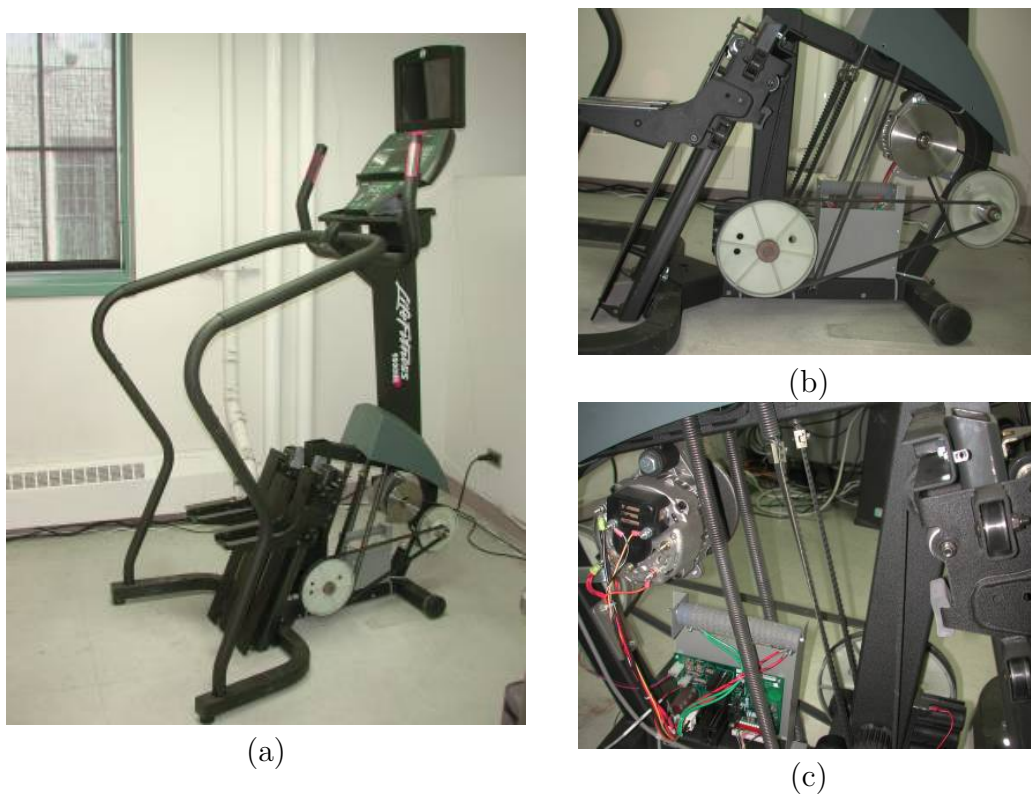
Figure B.1. The unmodified stair climber. (a) Overview. (b) Gearing. (c) Electronics.
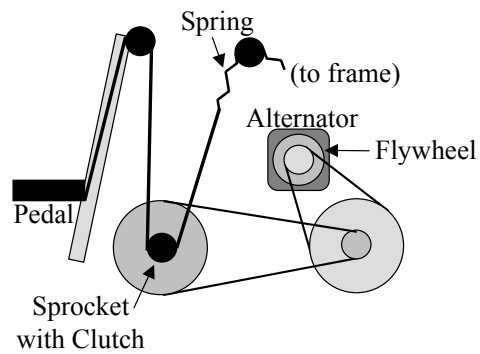
Figure B.2. A schematic of the mechanical parts of the unmodified stair climber.

This primary axle was connected to the alternator's axle through a two-part gear-belt, with a gear increase of approximately 28 to 1. Also on the alternator's shaft was a flywheel with a 0.1524m radius and an unmeasured mass. The alternator was connected

to the main electronics board so its damping could be controlled. In addition, a hall-effect sensor kept track of the central pulley in the gearing, which had a magnet attached near its outer edge.

Using the stair climber for exercise was dissatisfying. First, the pedals were independent of each other, so if the user stopped stepping, both pedals quickly slid to the floor. While this offered some motivation to continue moving, it did so more out of fear or avoidance of having to restart the stepping, than out of anything positive. Second, the machine supplied little feeling of inertia or sense of accomplishment. If a user worked hard one step and got the machine spinning fast, the following step was actually harder, since the clutch was less likely to engage, and therefore the pedals dropped downward until they got going fast enough. This feeling is unlike climbing real stairs — when climbing actual stairs, pushing harder off one stair makes the following one easier.

The damping versus exertion relationship for the unmodified stair climber is of interest. Increasing the level of workout via the stair climber's interface resulted in a decrease in the damping of the alternator (and thus the pedals). When the damping was decreased, the user dropped more quickly and so was forced to increase his or her step height or step rate. Thus, the user was doing more "stairs", or the vertical distance climbed, per time (a.k.a. power). This is opposite the effect you see in other exercise machines such as bicycles or ellipticals, where decreasing the damping results in a decrease of power.

2. Modifications

2.1. Theory

The goal of modifying the stair climber is to be able to influence and control the dynamics felt by users. One modification over the original stair climber would be to dynamically change the alternator's damping within step cycles. Unfortunately, this would be a purely passive system and thus not able to put energy back into users (*e.g.*, to lift them up), so the device's abilities would be limited. If I instead replace the alternator with a motor, then I can alter what users feel (*e.g.*, damping, stiffness, inertia) at the pedals by controlling the motor's torque or current.

There are countless things that I can do if I am able to dynamically (and actively) change what the user feels. Some of the possibilities are:

- Adjust the damping to keep the user's step rate constant, as done by Shields and Horowitz [129].

- Change the foot-trajectory profile, from sinusoidal to triangular to some other shape. Perhaps the shape of the path can improve users' experiences or decrease their perceived workout.

- Allow the user to affect the step rate and/or height in an arbitrary way. Techniques involve both how to measure the user's intent and how to apply it to the motion.

- Simulate various linkages or mechanical systems. For example, is a virtual damped flywheel preferred over a virtual spring-mass-damper system?

- Adjust the inertia-damping time constant. For the same damping, additional inertia may improve the user's experience.

- Keep the inertia-damping time constant when changing damping. That is, when the damping is increased, I can increase the inertia as well. How does this affect the user's perceived exertion?

- Cue the user when I want them to step. This may keep the user from riding a pedal back up (*i.e.*, merely shifting their weight from pedal to pedal) and force them to take a more aerobic step.

2.2. Physical Modifications

In light of these possibilities, I modified the stair climber so that a motor replaces the alternator. To allow one motor to affect both pedals, the two pedals are positionally linked via one timing belt over an added pulley. (Note that having the pedals positionally dependent unfortunately makes it easier for users to cheat during stepping by merely shifting their weight.) The clutched bearings have been removed so that one sprocket is free spinning on the axle while the other is rigidly fixed. A padded frame protects the user from falling into the mechanism, and proper plastic foot pedals were purchased and installed.

The motor used is an already owned Kollmorgen Goldline Brushless ME-207-B motor. It has continuous and peak torques of 6.6 Nm and 19.9 Nm, respectively, and is rated for 1.8 kW. Torque calculations (discussed later) show that this motor is sufficient for this application if geared down by the second stage of the existing gearing (about 5:1), so I attached it to the axle via the existing second stage pulleys and a gearing belt. See Figure
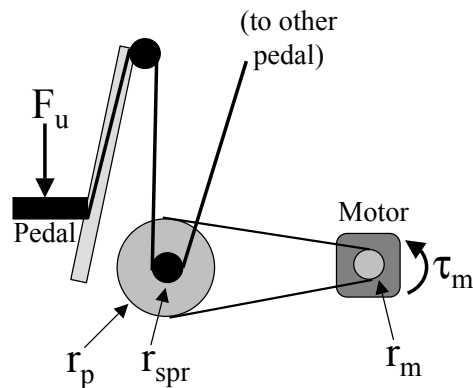
Figure B.3. Physical system.

B.3 for a model of the physical system. The motor is mounted on a frame that allows for manual adjustment of the horizontal position via a lead screw, thus the gearing belt can easily be tightened or loosened. For my application, the motor is torque-controlled via its amplifier.

I disconnected the preexisting electronics for the stair climber and installed different sensors and wiring. I installed an emergency-stop button next to the front console and attached limit switches at the bottom of each pedal's linear guide. These switches break contact to an enable input for the amplifier and thus engage the motor's internal (defaultly engaged) brake. Pedal position is obtained from the motor's internal encoder and a linear potentiometer attached to one of the pedal supports.

The wiring schematic for the modified stepper is shown in Figure B.4. A box with LED readout allows for powering and resetting (if a limit or e-stop switch is triggered) of the system. A Servo-To-Go board connected to a QNX computer reads the potentiometer and encoder signals, powers the potentiometer, and sends the motor torque command to the motor's amplifier.
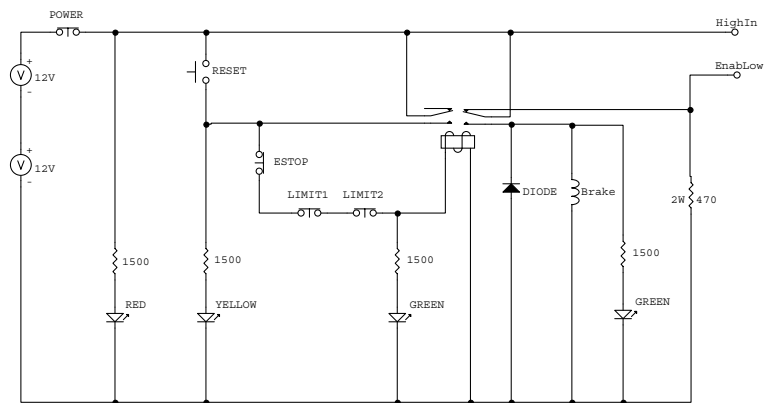
Figure B.4. Circuit schematic for the modified stair climber.

2.3. Gearing

The user's input is read as the torque at the motor. From the gearing, I know

$$\tau_m = F \cdot r_{sprocket} \cdot \frac{r_{motor}}{r_{pulley}}$$

$$= F \cdot {}^{\tau_m}_{F} K$$

$$\dot{\theta}_m = \frac{\dot{x}}{r_{sprocket}} \cdot \frac{r_{pulley}}{r_{motor}}$$

$$= \dot{x} \cdot {}^{\dot{\theta}_m}_{\dot{x}} K$$

$$= \dot{x} \cdot {}^{F}_{\tau_m} K$$

since

$$ {}^{\dot{\theta}_m}_{\dot{x}} K = \frac{1}{\frac{\tau_m}{F} K} = {}^{F}_{\tau_m} K.$$

For the stair climber, $\frac{\dot{\theta}_m}{\dot{x}} K \approx 233.3\frac{1}{m}$. (Any errors in this calculation result from inaccurate measurement of the gearing pulleys and the toothed sprocket diameters, as well as from slip of the gearing belt).

The motor has a $\tau_{cont} = 6.62$ Nm and a $\tau_{peak} = 19.9$ Nm, so the static values for achievable forces are

$$F_{cont} = \tau_{cont} \cdot \frac{F}{\tau_m} K = 1544 \text{ N}$$

$$F_{peak} = \tau_{peak} \cdot \frac{F}{\tau_m} K = 4643 \text{ N}.$$

These static values are sufficient.

2.4. Dynamics

So what dynamic situations can the motor handle? Stated differently, how fast can I vertically accelerate (*i.e.*, lift) a human of given mass? From the free-body diagram (Figure B.5),

$$m\ddot{x} = F - mg$$

$$\ddot{x} = \frac{1}{m}F - g$$

$$= \frac{1}{m}(\tau_m \cdot \frac{F}{\tau_m} K) - g.$$

Thus, for a human of 110 kg (243 lbs), and a constant torque available of 6.62 Nm, the maximum vertical acceleration continuously possible is

$$\ddot{x} = \frac{1}{110} \cdot 6.62 \cdot 233.3 - 9.81 = 4.23 \text{ m/s}^2.$$
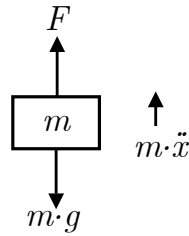
Figure B.5. Free-body diagram of human being lifted.

Suppose I wanted to move the human in a sinewave of a typical stair height (say 18 cm, or about 7 inches). How quickly can I do this? The human's position, velocity, and acceleration are given by the equations

$$x = A \cdot \sin(2\pi f t)$$

$$\dot{x} = 2\pi f A \cdot \cos(2\pi f t)$$

$$\ddot{x} = -4\pi^2 f^2 A \cdot \sin(2\pi f t).$$

Returning to the free-body diagram,

$$F = m(\ddot{x} + g)$$

$$= m(-4\pi^2 f^2 A \cdot \sin(2\pi f t) + g)$$

$$F_{max} = m(4\pi^2 f^2 A + g)$$

$$F_{rms} = m(\frac{\sqrt{2}}{2} \cdot 4\pi^2 f^2 A + g).$$

Since the motor can run above continuous torque for short periods of time, a good rule of thumb is to keep $\tau_{rms} \leq \tau_{cont}$. For a human of 110kg and an amplitude of a typical stair,

$$\tau_{rms} = F_{rms} \cdot \frac{\tau_m}{F} K$$

$$= 110(\frac{\sqrt{2}}{2} \cdot 4\pi^2 f^2 \cdot \frac{0.18}{2} + 9.81) \cdot \frac{1}{233.3}$$

$$\leq 6.62$$

$$f \leq f_{rms} = 1.30 \text{ Hz.}$$

The maximum torque the motor will see with at this frequency is

$$\tau_{max} = F_{max} \cdot \frac{\tau_m}{F} K$$

$$= 110(4\pi^2 1.30^2 \cdot \frac{0.18}{2} + 9.81) \cdot \frac{1}{233.3}$$

$$= 7.456 \text{ Nm}$$

$$\ll \tau_{peak}.$$

2.5. Friction Analysis

In order to explore changes in virtual damping, I need to know the effect of physical friction (*i.e.*, physical damping) on the system. For example, if I double the virtual damping, the damping felt by the user (*i.e.*, the physical plus virtual damping) does not exactly double. Thus, I need to know an approximation of the magnitude of force due to friction. This force is dependent on the load and is always resisting motion. In the stair climber, friction is primarily caused by the rollers holding the pedals onto the vertical tracks and the bearings in the various pulleys.

To calculate the effect of friction, I chose to lower a known weight at a given velocity. The weight on the stair climber is that of a human, although recall that the amount of the user's weight on each pedal varies during the step cycle. To approximate this, I used a human of average, known mass (75 kg) for the load. Similar to the weight, the velocity changes throughout the stair climber's cycle, thus I used the RMS velocity for the experiment (discussed in a following section). This velocity is 0.30 m/s at the pedals (0.75 Hz stepping).

The free-body diagram for this analysis is shown in Figure B.6, where m_H is the mass of the human, F_m is the force from the motor, and F_f is the force due to friction. (The mass of the pedals is assumed negligible.) From the diagram (remember velocity is assumed constant) come the equations:

$$m_H \cdot a = F_m + F_f - m_H g$$

$$m_H \cdot 0 = F_m + F_f - m_H g$$

$$F_f = m_H g - F_m = 75 \cdot 9.81 - F_m.$$

The human was lowered several times. Averages of the recorded values for F_m during the middle of the drops (*i.e.*, after start-up effects and before stopping) were used to calculate F_f as around the order of magnitude of 200 N. For the 736 N (75 kg) human and given speed, this meant that friction was between $\frac{1}{4}$ and $\frac{1}{3}$ the weight of the human.

3. Sample Virtual Models

I have implemented several virtual models on the modified stair climber.

$$F_m \quad F_f$$

$$m_H$$

$$m_H{\cdot}g \qquad m_H{\cdot}\ddot{x}$$
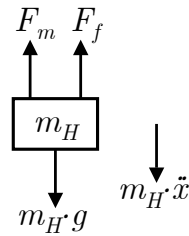
Figure B.6. Free-body diagram for friction analysis.

- Self-moving sinewave: The pedals move automatically in a constant-amplitude constant-frequency trajectory whose position is a sinewave in time. This is used to demonstrate the ability to control the pedal's trajectory.

- Self-moving triangle wave: The same as the self-moving sinewave except the pedal position is a cosine-approximated triangle wave in time. When compared to the sinewave, the triangle wave demonstrates the effect of trajectory and cuing on the haptic sensation felt by the user.

- Frequency-dependent sinewave: The pedals move in a constant-amplitude sinewave whose frequency is arbitrarily dependent on the user's input. Thus, when the user pushes with the direction of motion, the sinewave's frequency increases; when the user resists motion, the frequency decreases.

- Amplitude-dependent sinewave: The pedals move in a constant-frequency sinewave whose amplitude is arbitrarily dependent on the user's input. Thus, when the user pushes with the direction of motion, the sinewave's amplitude increases; when the user resists motion, the amplitude decreases.

- Frequency- and amplitude-dependent sinewave: A combination of the previous two models.

- Spring-mass-damper: The pedals behave as a spring-mass-damper system with the center of the vertical workspace as the zero-input-force equilibrium point. The spring tries to return the user to the center, the mass resists change in motion, and the damper resists any velocity.

- Flywheel: The pedals behave as if attached to a flywheel with a given inertia and rotational damping. See the Experiment section for more information.

4. Exertion Experiment

To test the usability of the modified stair climber and to begin research with it, I ran a simple experiment. In the unmodified stair stepper, there is no transfer of inertia from one step to the next. Thus, if users reduce exertion momentarily, they slide toward the ground, which many users find frustrating. In climbing real stairs, the energy in the body's inertia gained by exertion on one step persists and assists on the next step. I hypothesize that providing apparent inertia will contribute to a more satisfying experience and lower perceived exertion, even if actual muscular output power is held constant. The following section discusses my experiment.

4.1. Virtual Flywheel

The experiment uses the virtual flywheel model, ignoring the horizontal motion of the pedals in the model. See Figure B.7 for a diagram of the flywheel. Assume no friction
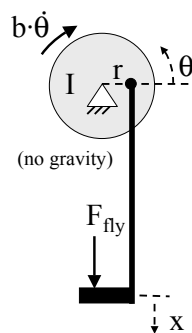
Figure B.7. Virtual flywheel model.

and no gravity. I know that

$$x = -r \cdot \sin \theta$$

$$\dot{x} = -r \cdot \cos \dot{\theta}.$$

The sum of the moments around the flywheel is:

$$\sum M = I \cdot \ddot{\theta} = -F_{fly} \cdot r \cdot \cos \theta - b \cdot \dot{\theta}.$$

Note that for the same F_{fly}, the larger the I, the smaller the fluctuation of $\ddot{\theta}$ (and hence $\dot{\theta}$).

The energy in the system is:

$$E = KE + PE = \frac{1}{2} \cdot I \cdot \dot{\theta}^2.$$

Thus the power is:

$$P = \frac{\partial E}{\partial t} = I \cdot \dot\theta \cdot \ddot\theta$$

$$= (-F_{fly} \cdot r \cdot \cos\theta - b \cdot \dot\theta) \cdot \dot\theta$$

$$= -F_{fly} \cdot r \cdot \cos\theta \cdot \dot\theta - b \cdot \dot\theta^2$$

$$= P_u - P_b,$$

where P_u is the power from the user and P_b is the power lost to damping.

For the experiment, the user attempts to keep $\dot\theta$ constant at a given non-zero value. In the ideal case,

$$\dot\theta = \dot\theta_{desired}$$

Then,

$$\ddot\theta = 0$$

$$P = I \cdot \dot\theta \cdot \ddot\theta = I \cdot \dot\theta_{desired} \cdot 0 = 0$$

$$P_u = P_b = -b \cdot \dot\theta^2_{desired}$$

In this case (*i.e.*, if the user is perfect at keeping $\dot\theta$ constant) P_u scales linearly with b and is independent of I.

The user, however, is not perfect. I approximate the user's fluctuation around $\dot{\theta}_{desired}$ as a sinewave (and the data — not shown — reflects this):

$$\dot{\theta} \approx \dot{\theta}_{desired} + A \cdot \sin \omega_0 t$$

$$\ddot{\theta} \approx A \cdot \omega_0 \cdot cos\omega_0 t$$

$$P_u = I \cdot \dot{\theta} \cdot \ddot{\theta} + b \cdot \dot{\theta}^2$$

$$= I \cdot (\dot{\theta}_{desired} + A \cdot \sin \omega_0 t) \cdot (A \cdot \omega_0 \cdot \cos \omega_0 t)$$

$$+ b \cdot (\dot{\theta}_{desired} + A \cdot \sin \omega_0 t)^2$$

$$= I\dot{\theta}_{desired} A\omega_0 \cdot \cos \omega_0 t + IA^2\omega_0 \cdot \sin \omega_0 t \cdot \cos \omega_0 t$$

$$+ b\dot{\theta}^2_{desired} + 2b\dot{\theta}_{desired} A \cdot \sin \omega_0 t + bA^2 \cdot \sin \omega_0 t^2.$$

While the RMS value of P_u is dependent on I, the RMS value is misleading since it depends on the square of the value. Thus stepping at a speed of 1.0 Hz is unfortunately interpreted as four times worse than stepping at 0.5 Hz. If the average of the power is used as a measure, I lose some information due to "negative" power cancelling "positive" power, so I focus on the user's output power, or power loss to the virtual damping. The average P_u is still independent of I.

4.2. Technique

To test the effect of inertia on perceived exertion, eight subjects were presented with 21 comparison pairs of inertia-damping values (m, b), in random inter-pair and intra-pair order. Subjects were asked which of each pair required less effort. Figure B.8 shows the
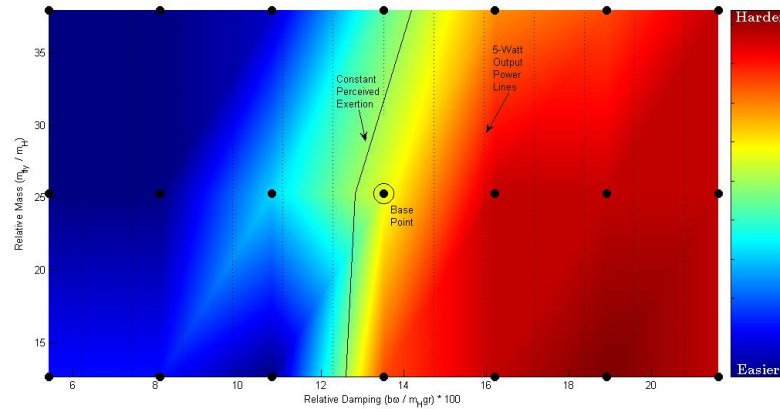
Figure B.8. Results from the experiment.

(m, b) points tested as well as results, plotted in a color scale representing the percentage of people who found a (m, b) point harder/easier than a comparison point, with a line representing interpolated points of equal exertion. Points of equal output power form vertical lines on this graph.

4.3. Results and Discussion

The results show that tripling the simulated inertia allowed a 5% increase in damping (approximately 8 W) without an increase in perceived exertion. The extent of my control over perceived exertion demonstrated here is modest, but it is a meaningful amount in the context of exercise physiology. I have so far explored only one dynamic effect (inertia), and not cuing, speed variation, or step length variations. Path shape variation, which is not possible with the stair stepper but will be possible with the proposed lower-limb haptic exercise robot, will add greatly to the diversity of user experiences that can be explored.

APPENDIX C

Additional Background

This appendix discusses further background that was not included in the main body of the thesis, for space consideration. It involves additional motivation (psychophysiology and physiology), consumer exercise machines, existing exercise and lower-limb robots, and haptic devices.

1. Additional Motivation

In the psychophysical realm, Horowitz, Li, and Shields have developed a control paradigm for an adaptive controller that optimizes a user's power output, based on a simultaneously estimated biomechanical model of the user [**76, 77, 78, 59**]. They successfully applied this technique to a stair climber by dynamically controlling the damping to maintain a user's step rate [**129**]. Similarly, Ferber further modified the previously mentioned robotic stair climber, and ran human experiments to test if haptic cuing at the pedals helps users maintain step rate [**43**] (see Figure C.1). Cues tested range from going-too-slow alerts like vibration or bumps, to subconscious aids like boosts in simulated energy. With haptic exercise robots having programmable footpaths, researchers can further explore control paradigms and conscious or subconscious cuing, in higher dimensions, to find techniques for making consistent exercise easier.

In physiology, lower-limb haptic robots can help the study of the human body and how it works. For example, there exists research into which biomechanical factors are

Figure C.1. The haptic robotic stair climber created by me, Ferber, and our colleagues at Northwestern University. [**43**]

important to running economy [**71**], and what step cycle characteristics are descriptive of locomotion control [**99**]. Similarly, there has been research into how humans interact with kinematic constraints [**79, 101, 100**]. There has also been research into the inaccuracy of using treadmill walking to study overground walking (*e.g.*, [**1**]) — perhaps motions can be achieved on a haptic exercise robot that more accurately represents the muscle activity of overground walking.

Recently, researchers have begun using perturbation to study the mechanics of limbs and muscles. In addition to observing motions, they perturb limbs with forces or motions to examine the unconscious response. Although only performed on arm motions as of yet, many of these studies use planar robots; a lower-limb haptic robot allows for study of the legs as well. Example research include the mass and load adaption experiments done by Bock [**2**], Krakauer *et al.* [**70**], and Sainburg *et al.* [**118**], as well as the after-effect studies of Thoroughman and Shadmehr [**138**], Osu [**98**], and Mussa-Ivaldi and Patton [**92, 103**].

2. Consumer Exercise Machines

Realistically, an all-in-one-exercise robot will not replace all of the cardiovascular machines in the consumer exercise market. While it can be designed to replace stair climbers, ellipticals, ski machines, and arc machines, and can be altered to replace bicycles, it will most likely never replace treadmills. To simulate a bicycle machine, the exercise robot would need a seat (that can be moved out of the way for upright exercise) and easy-to-rotate (perhaps by computer control) pedals. Simulating a treadmill, however, would be a difficult, and possibly dangerous, endeavor. Unlike during low-impact exercise, during running the user's feet periodically break contact with the ground (pedal). Attempting to position the pedals so that the user's feet can land on them is difficult at best, dangerous because of potential injury, and unsettling to the user. Therefore, it is not likely that any one exercise machine or robot will ever replace both the low-impact cardiovascular machines and treadmills.

With regard to stair climbers, workout speed is often measured as the rate at which the user lifts his mass, in meters per second. (That is, workout speed is the step frequency times step height.) Thus, power exerted by the user is the workout speed times the user's weight. With passive stair climbers, however, power can also be viewed as the rate of energy dissipated through damping, which gives the same result. On either machine, increased workout is achieved by increasing the downward velocity of the stairs. For the passive stair climbers, this means decreasing the pedals' damping and thus forcing the user to increase step rate or step height to stay off the floor. This is the opposite of what one finds with other exercise machines — usually, *increasing* the damping in an exercise machine increases the workout.

For ski machines, power can be interpreted as the sum of the arm and leg powers, each of which is the corresponding resistance coefficient times the corresponding velocity. Ski machines are completely passive, and stride length and rate are determined by the user. Increased power exertion is achieved by increasing damping, and typically the only inertia is that of the relatively lightweight ski boards.

Arc machines are also passive, with exertion increased by increased damping. Their pedals may be independent or dependent (recall the terminology of Section 1.2), and they may have a flywheel for additional inertia. Power can be interpreted as the resistance coefficient times the velocity.

Ellipticals are the newest additions to the exercise market. First appearing in the mid-1990's, ellipticals (also called cross trainers) have gained great popularity, with many fitness equipment manufacturers unveiling versions of the machine. From 2002-2003, the exercise market saw a 65% jump in the number of elliptical users, up to around 30% of the more popular treadmill [**28**]. Workout speed for ellipticals is measured in cycles per time, usually RPM. Because of the complexity of path shapes, power exerted on a elliptical is measured as the power dissipated through the damped flywheel. Increased exertion is achieved by increasing the damping. Unlike the two-pedaled stair climbers and ski machines, ellipticals have relatively high inertia in their flywheels and linkages that helps carry the user around the cyclic path.

3. Existing Exercise and Lower-Limb Robots

There are also several examples of locomotion devices in the literature, usually meant for use in virtual reality. These devices allow the user to explore virtual environments by
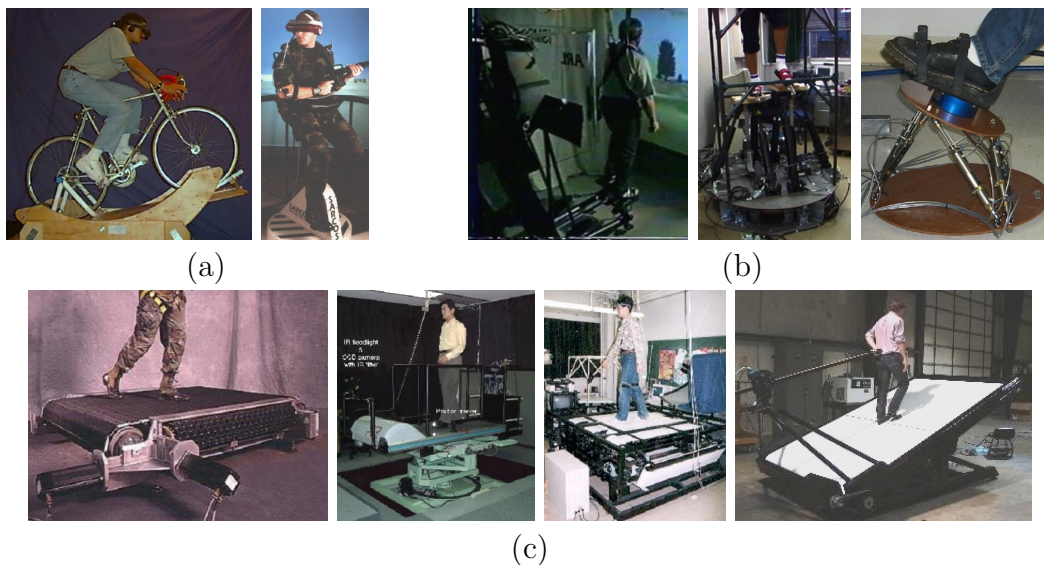
Figure C.2. Examples of locomotion devices using (a) pedaling [**17, 23**], (b) foot platforms [**58, 63, 3**], and (c) treadmills [**29, 88, 61, 56**].

pedaling, programmable foot platforms, or treadmills (although other techniques exist, *e.g.*, [**62**]). Figure C.2 presents some of these devices. Examples of pedaling devices are the device used by Brogan *et al.* [**17**] and the first-generation Sarcos Uniport built by Christensen *et al.* [**23**]. Devices using programmable foot platforms include the Sarcos Biport [**58**], the GaitMaster [**63**], and Rutgers' Mega-Ankle [**3**]. Finally, examples of treadmill-style devices are the Omni-Directional Treadmill [**29**], the ATLAS and ATR-GSS [**97, 88**], the Torus Treadmill [**61**], and the Sarcos Treadport [**57, 56**].

As can be seen by the dates of the literature, locomotion devices have generally evolved through the three types: from the simple bicycle, to the more realistic but incredibly complex foot-platform, to the relatively straightforward treadmill. In fact, Hayward and Hollerbach have even attempted to simulate stair climbing using a treadmill and torso force feedback, with unsuccessful, but encouraging, results [**53**]. While treadmills are

excellent for virtual reality applications, they are insufficient here because they do not have the path dimensionality desired in haptic exercise robots.

With regard to exercise, a few robotic devices have been built to replace free weights and similar upper-limb strength-training exercise devices. For example, Kazerooni and Her built a pantograph-style two-degree-of-freedom exercise robot driven by two motors [68]. Book and Ruis designed an active exercise machine using hydraulics [5, 6]. Similarly, Van Reet and Feemster modified a one-degree-of-freedom bicep and tricep machine with a motor, to help eliminate the noise of free weights on a submarine [142]. Matsuoka and Miller designed and built a three-degree-of-freedom passive device using magnetic particle brakes, for resistance exercise of the arm or leg, although it is not specifically designed for cyclic exercise [84]. None of these devices saw much investigation after being built. There are, however, some existing patents on these types of machines [116, 131].

In rehabilitation, the cardiovascular lower-limb exercise machines of choice are the cycle ergometer (*e.g.*, [109], [19], [35]) and treadmill (*e.g.*, [82]). Dietz *et al.* [33], and Jensen *et al.* [65], used split-belt treadmills to investigate human locomotion. Similarly, Raasch, Ting, Kautz, and their colleagues used a cycle ergometer modified for independent pedal control and dynamics [110, 139, 67]. Focusing on ankle rehabilitation, Yoon *et al.* have presented the most recent design: a reconfigurable, active, parallel robot for strength and balance training [150]. There is also a slew of robots designed for gait rehabilitation, such as the Haptic Walker [120], KineAssist [105], DGO [27], Gait Trainer [55], and STRING-MAN [132] (see Figure C.3).
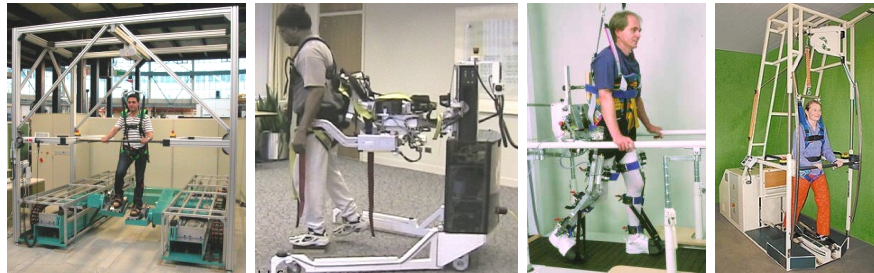
Figure C.3. Examples of robots for gait rehabilitation. [**120, 105, 27, 55**]

4. Haptic Devices

Haptic devices can be roughly categorized as either energetically active or passive. (Recall the terminology discussion in Section 1.2.) The following two sections look at various examples of each. This discussion is by no means exhaustive, but it does highlight the more relative, better-known, haptic robots. For a fuller description of *commercially available* haptic devices, see Laycock and Day's overview [**73**].

4.1. Energetically Active Haptic Devices

The first category of haptic device is Energetically Active. These robots use motors and other actuators to impart the physically felt constraints and dynamics, with power being lost to heat but replenished by the actuators. In general, active devices are mechanically simpler than their passive counterparts; however, safety is of greater concern, especially in devices that need to impart high forces. High-powered actuators can be extremely harmful when they or their electronics fail, as motors may suddenly torque in unexpected directions. Thus, active haptic devices implement several layers of hardware and software safety, and use as small of motors as possible. The smaller motors also decrease power consumption and cost.

Figure C.4. The PHANTOM device for haptic interaction (photo courtesy of SensAble Technologies).

Unfortunately, virtual surfaces created by actuators are not always of high quality. For the constraints to be stiff, the motors must be strong, which brings the safety issue into question. As with any device, the virtual surfaces are sometimes unrealistically soft and rough. Thus, although simple, inexpensive, and useful, these devices do not impart fully realistic virtual surfaces.

4.1.1. PHANTOM. The Personal Haptic Interface Mechanism, commonly known as the PHANTOM, is the most widely used haptic interface because of simplicity, inexpensiveness, and purchasability (see Figure C.4). Developed by Massie and Salisbury at M.I.T. [**83, 123**], the PHANTOM uses three relatively small motors and an intelligently designed pantograph-style mechanism to impart forces up to 1.5N-3.0N continuously (depending on the product model). The Phantom uses a fingertip thimble or stylus for contact, and has a three-dimensional translational workspace large enough for wrist motion.

Because it is active, the PHANTOM is able to simulate forces such as gravity and inertia, as well as virtual surfaces. These surfaces are stiff enough that typical, gentle users do not penetrate them significantly, but they are easily overcome if users increase their forces. In addition, the surfaces often feel sticky rather than smooth. While extremely successful for fingertip exploration, the PHANTOM design cannot be feasibly scaled for lower-limb exercise — the motors will have to be extremely large and thus unsafe for human interaction, and there is intentionally no inclusion of inertia.

4.1.2. Others. There is a variety of other active haptic devices meant for kinesthetic interaction with the arm. Although these devices are kinematically different from the PHANTOM, they are typically similar in abilities — they are good at simulating forces in environments from low to high damping, but inherently unsafe for large-scale interactions. They are also not designed specifically for cyclic, highly damped motions. Examples of these haptic devices include the DaVinci surgical system [**50**], Pathos [**69**], Delta [**45**], Virtual Touch [**52**], Freedom-7 [**54**], and the six-degree-of-freedom device created by Lee *et al.* [**75**].

4.2. Energetically Passive Haptic Devices

The second subset of haptic devices is Energetically Passive. These devices use dampers, brakes, energy-storage, and other passive elements to impart haptic sensations. They can store and return energy from the user but they cannot add additional energy into the system. Thus, in the last decade, there has been much emphasis on creating these passive robots because they are inherently safer than active ones, however they are typically more

mechanically complex. The complexity arises from the storing or transferring of energy within the device.

Energetically passive devices are limited by their passive nature. Devices that use brakes and clutches (such as the two described below) are kinematically simple, very strong, but poor at rendering smooth or arbitrarily oriented constraints. Devices that steer the user (like the cobots described below) create stiff, smooth, and sudden surfaces but are complex mechanically and infeasible for high forces. None of the passive robots described here achieve high quality dynamics, such as zero damping, because of loss of energy to mechanism and actuation friction. In fact, the more recent generations of cobots have been low power actuated (*i.e.*, minimally active, rather than passive) to overcome friction and to allow for simulation of arbitrary inertias and stiffnesses.

The following subsections present three classes of passive haptic robots that use three distinct architectures for prescribing virtual surfaces. They are specifically interesting because they offer creative alternatives to the traditionally active device.

4.2.1. PTER. The Passive Trajectory Enhancing Robot (PTER; see Figure C.5) [**4, 22, 7**], created by Wayne Book and colleagues at Georgia Tech, is an example of a passive robot that relies solely on clutches for creating forces and virtual surfaces. It is meant for interaction with the user's hand and arm, and consists of a handle attached through a pantograph (labeled **A**–**D** in the figure) to its base. PTER uses four clutches (labeled **1**–**4**) at its base for its two degrees of freedom. Two of the clutches connect two arms of the pantograph to ground, thus acting as brakes, while the remaining two clutches connect the two arms' rotations directly and inversely. In this manner, the clutches can apply torques
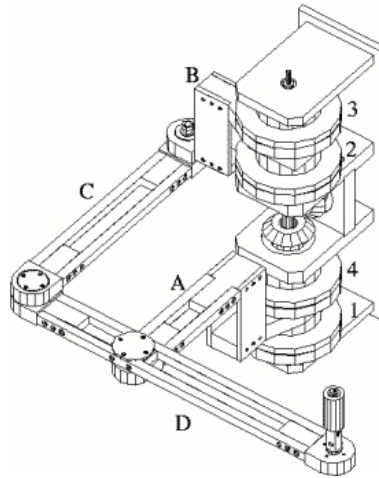
Figure C.5. Sketch of PTER, at Georgia Tech, with links labeled A–D and clutches labeled 1–4 (courtesy of Georgia Tech's website).

directly to each arm, apply torques to synchronize the arms' speeds and direction, and apply torques to pull the arms' speeds towards equal magnitude but opposite direction.

Prescribing high-quality virtual surfaces with PTER has been surprisingly difficult, mostly due to nonideal clutches and poor controllers. The initial design used off-the-shelf electromagnetic clutches that were later discovered to have extremely slow time constants (0.16-2.5 seconds), and poor modulation of torque [49, 91]. Replacement clutches were made in-shop using piezo-electric actuation and a clever torque measuring design, but were found to be limited by the time-constant of the power supply (0.1 seconds rise time and a "significantly slower" drop time), their cost, and their need for high tolerances [91]. Modification of the clutches to include measurement of torque introduced unwanted oscillations [134]. These difficulties meant that PTER could not react (*i.e.*, increase or decrease torque) quickly and accurately to human input.

Adding to the difficulties, the first few generations of controllers were deemed inadequate by the researchers. Initial on/off heuristic controllers created accurate but "very

'jerky"' surfaces [**30, 49**]. A velocity controller created much smoother surfaces, but at the cost of path accuracy [**49**]. It wasn't until PID torque controllers were applied to the modeled and physical clutches that PTER could accurately prescribe torques on the human's hand [**136, 133**], and it required a controller that optimizes every timestep for PTER to display accurate and smooth virtual surfaces [**135**]. With regard to virtual surfaces (*e.g.*, obstacle avoidance), Swanson and Book found that the locking PTER into a single degree-of-freedom, and toggling that freedom, created smoother and harder surfaces than by using the velocity controller [**134**].

That said, PTER does what very few robots have done before. It displays believable programmable virtual surfaces to the human via purely passive actuators and a mechanically simple design. Because PTER is holonomic, its unconstrained mode is achieved by simply turning off the actuators, and motion is instantaneous rather than steered. PTER can also implement haptic effects that involve damping within unconstrained or constrained mode, which steerable passive devices cannot do.

4.2.2. PADyCs. The Passive Arm with Dynamic Constraints (PADyC) family of robots use a novel technique to prescribe constraints on users' motions. Designed and built by Troccaz and Schneider, PADyCs use overrunning clutches and computer-controlled reference velocities [**140, 122, 121**]. One half of the basic mechanism used by PADyCs is shown in Figure C.6a — I refer to it in this explanation. A motor is attached to the inner shaft of the overrunning clutch mechanism, also called a freewheel, and prescribes a reference velocity (here, assume it is zero, *i.e.*, $\omega_i^+ = 0$). If the user tries to move the outer shaft faster than the inner shaft (here, if $\omega_{user} > 0$), the rollers get wedged between the shafts and the two shafts become locked. However, motion is unconstrained if it is
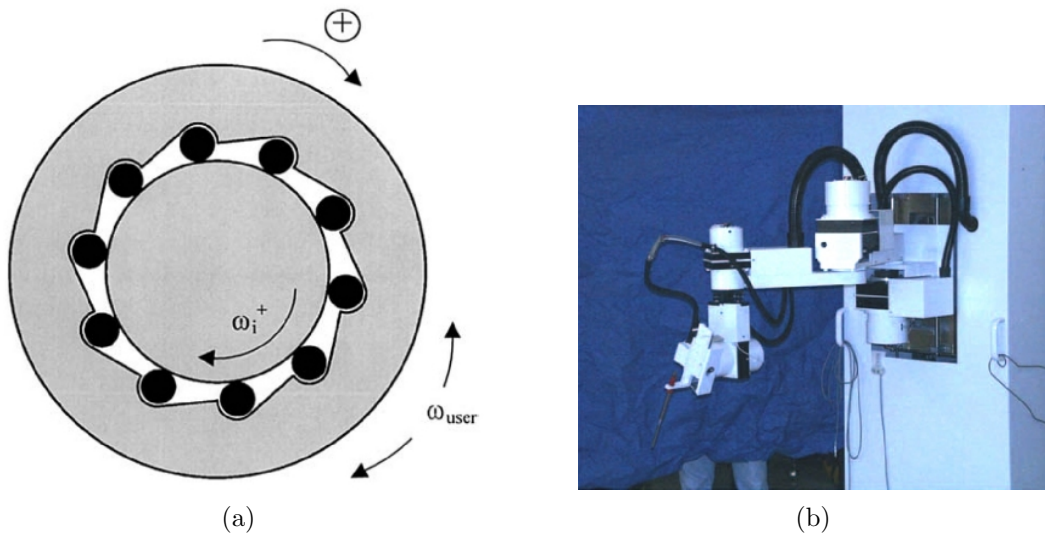
Figure C.6. The six-degree-of-freedom PADyC prototype (taken from [**122**]). (a) The PADyC overrunning clutch (a.k.a. freewheel) mechanism. (b) The prototype robot.

less than, or in the opposite direction of, the reference velocity (here, if $\omega_{user} < 0$). Each joint of a PADyC uses two of these freewheel mechanisms superimposed and oppositely oriented, each driven by its own motor that is electronically constrained to move in only one direction. Thus, each joint velocity is bounded between its two (opposite-direction) reference velocities: $\omega_i^- \leq \omega_{user} \leq \omega_i^+$. The most recent version of a PADyC is a six-degree-of-freedom prototype for use in robotic surgery (see Figure C.6b).

The design of PADyCs means that the user is free to move the robot within a bounded region of velocities, and by controlling those reference velocities and hence the bounds, the PADyC can prescribe virtual velocity constraints to the user. PADyCs are safer than devices directly driven by motors because PADyCs' motors cannot drive the joints — thus failure of one motor cannot cause unexpected motion of the robot.

The main limitations of the PADyC design are that it cannot directly prescribe forces to the user, such as for damping or gravity, nor can it enforce a velocity bound that does not include $\omega_{user} = 0$. The latter means that to constrain the endpoint to an arbitrary one-dimensional path, PADyCs must toggle between reference velocities, similar to PTER's implementation. With regard to exercise, PADyCs are capable of high forces and powers, but not specifically designed for cyclic motions, energy storage, or user exertion.

4.2.3. Cobots. Created by Colgate and Peshkin at Northwestern University [**25, 107**], cobots use the nonholonomic nature of wheels to create virtual constraints, as well as virtual dynamics (see Figure C.7a) [**144, 38, 32**]. When their power is off, cobots have at most one degree of freedom — the direction tangent to all of the wheels. With power on, cobots steer those wheels to achieve a higher dimensional workspace.[1] Thus, cobots create virtual constraints, such as walls, that are very smooth along the constraint but very stiff into the constraint. Cobots use little power and are safe, since they use small steering motors rather than large actuators to impart virtual constraints [**39, 40**]. When also actuated in the rolling direction, cobots (now, "powered cobots" [**89**]) can also impart virtual dynamics such as reprogrammable inertia, damping, and stiffness.

While cobots excel at imparting haptic environments, they are inherently limited by their friction transmissions [**39**]. To impart a constraint, cobots need their wheels to resist slip and creep in the perpendicular (*i.e.*, non-rolling) direction, via friction, and the slipping force a wheel can resist is directly proportional to the "preload" force pressing the wheel against the surface it's riding on. Thus, in high-force applications, such as exercise

---

[1]This is similar to driving a car: the car can easily roll forward and backward, but cannot easily slide sideways. However, by steering the car, one can move in higher dimensions.

(a)

(b)

(c)
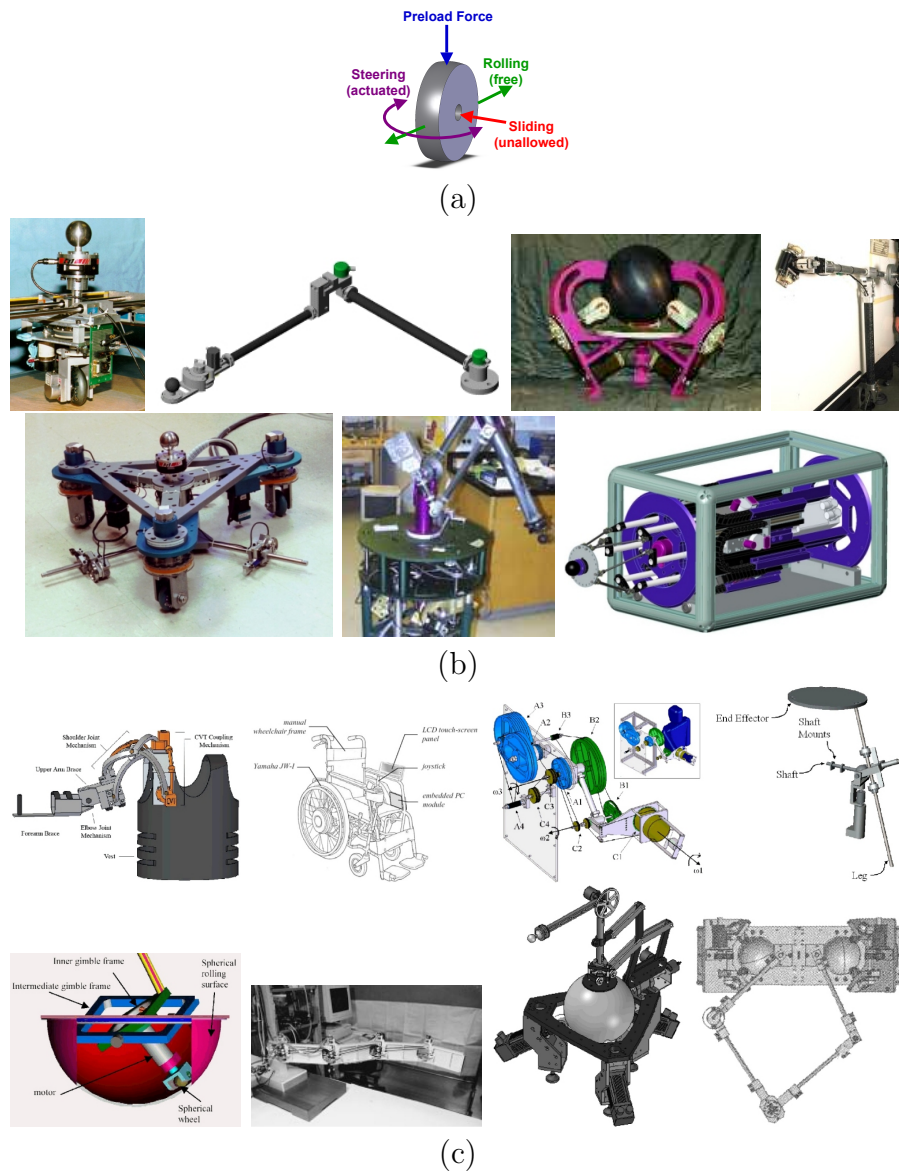
Figure C.7. Examples of cobots. (a) The basic cobot mechanism of a steerable wheel rolling on a surface. (b) Cobots designed and built be researchers at Northwestern University [**26, 149, 119, 21, 143, 90, 38**]. (c) Some cobots designed or built by other researchers [**15, 16, 24, 37, 64, 93, 145, 146**].

machines or rehabilitation, cobots require such a high preload force that they become impractical.

Examples of Colgate, Peshkin, and colleagues' cobots are shown in Figure C.7b. Over the last decade, they have built cobots that have various two-, three-, and six-dimensional achievable workspaces [**26, 149, 119, 21, 143, 90, 38**], and performed research into control [**106, 46, 41, 148**] and contact dynamics [**47, 18, 40**]. Likewise, other researchers have developed their own implementations of cobotic architecture, as seen in Figure C.7c [**15, 16, 24, 37, 64, 93, 145, 146**].

APPENDIX D

Preliminary Designs

I considered many preliminary designs, as well as some highly detailed designs. This section shows (by pictures only) many of the designs not covered in the body of this thesis.

1. General Designs

Please see Figure D.1.

2. Pedal Support Designs

Please see Figure D.2.

3. Two-Leg Designs

Please see Figure D.3.
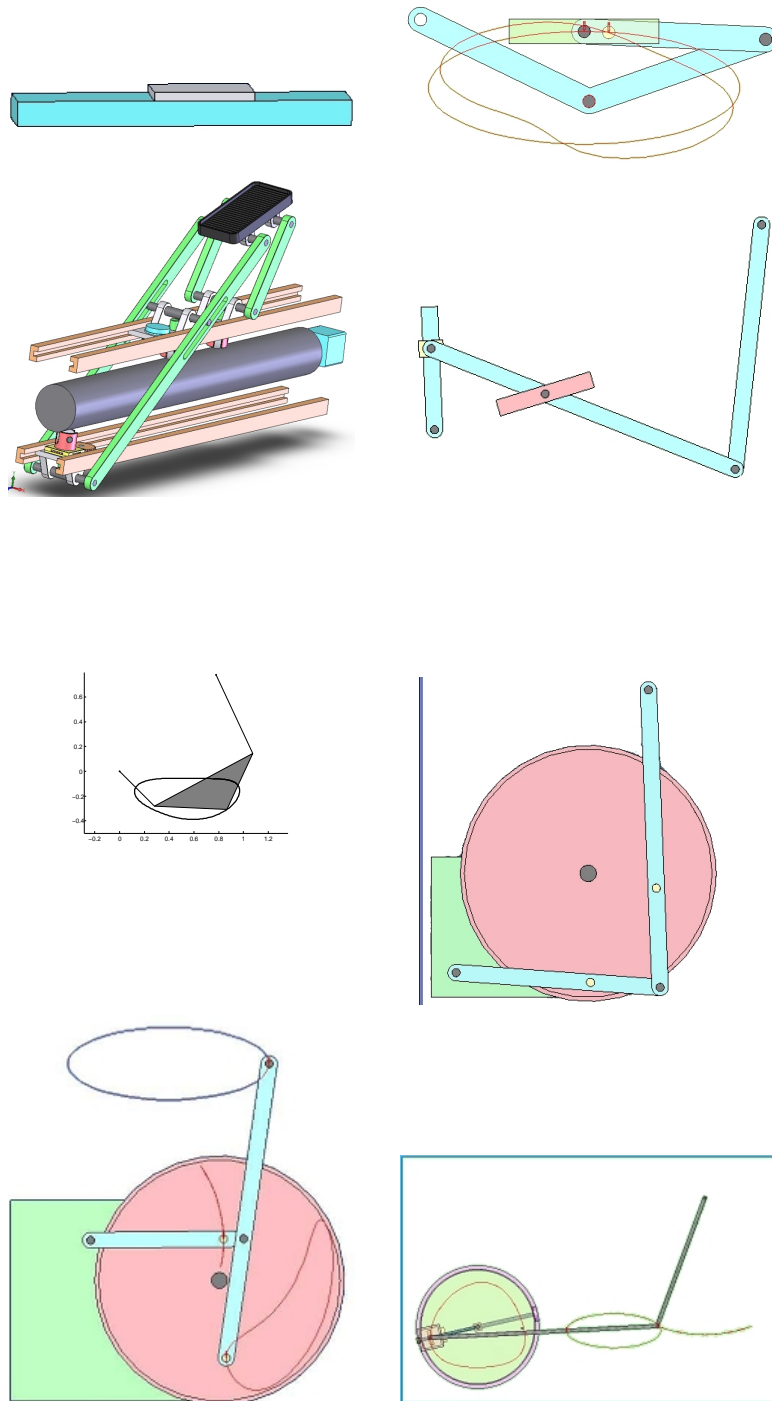
Figure D.1. General designs: (a) x-z rail (b) 2-revolute robot (c) Catapult (d) Elliptical plus prismatic (e) Four-bar coupler (f) Disk-L (g) Disk-T (h) Disk-Ring.
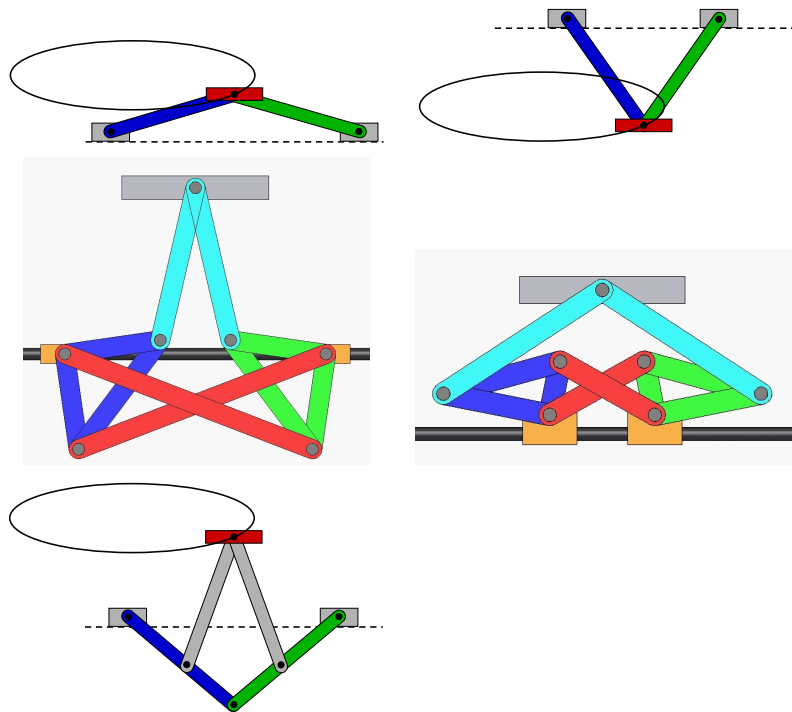
Figure D.2. Pedal support designs: (a) Triangle (b) Vee (c) Outer butterfly (d) Inner butterfly (e) Unmodified pantograph.
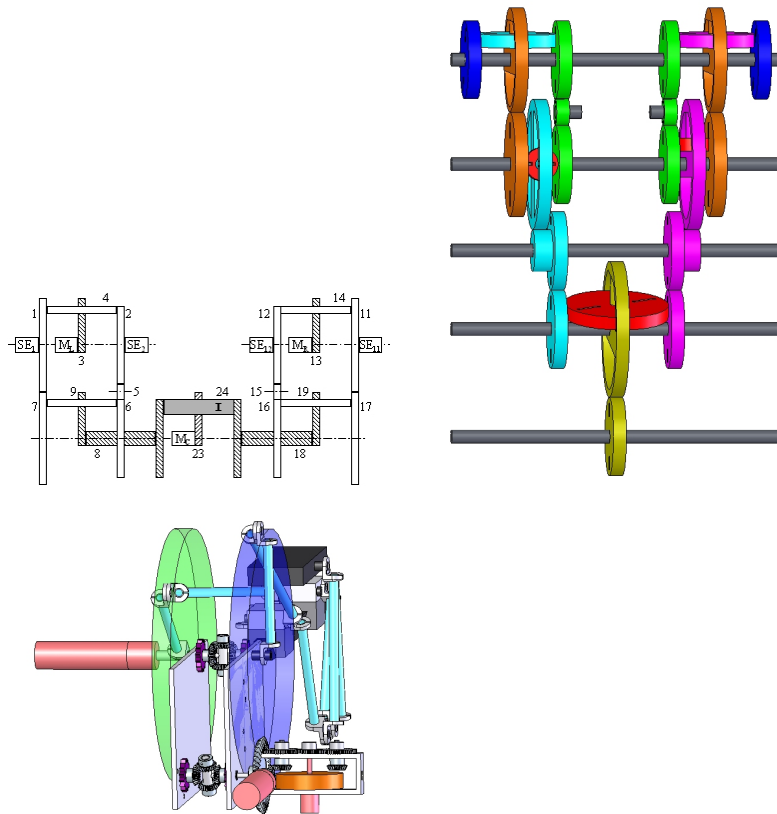
Figure D.3. Designs for a differential between the two legs of the device.

APPENDIX E

Device Kinematics and Dynamics

Given the mechanism shown in Figure E.1, with its dimensions for the Differential (r_{θ_1} and r_{θ_4}), Crank Arms (r_1, r_2, l_1, and l_2), and Modified Pantograph (a, b, c, and d). Let $\boldsymbol{x}$ be the position of the pedal, and $\boldsymbol{\theta_{34}}$ be the configurations coordinates of the robot, where

$$\boldsymbol{x} = \begin{bmatrix} x \\ z \end{bmatrix} \qquad \boldsymbol{\theta}_{34} = \begin{bmatrix} \theta_3 \\ \theta_4 \end{bmatrix}.$$
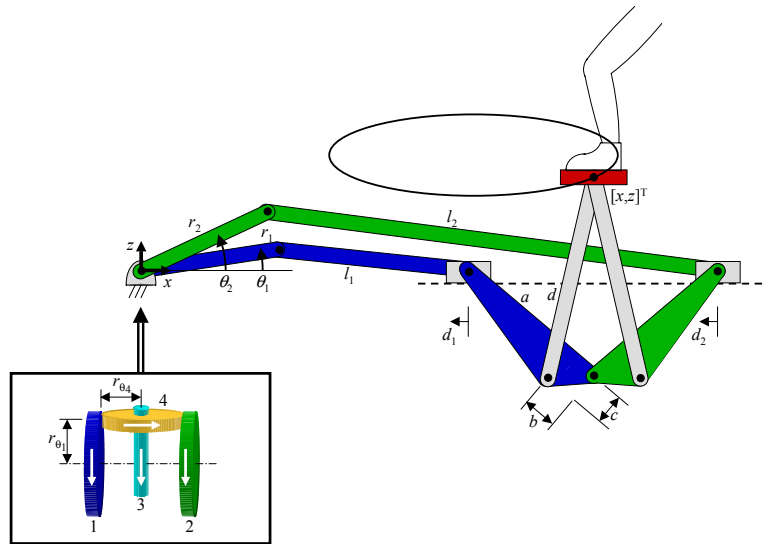
Figure E.1. A sketch of the device, and its parameters.
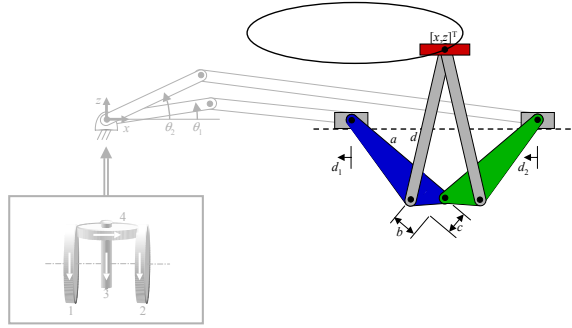
Figure E.2. The Modified Pantograph subsystem.

There exists a kinematic mapping,

$$\boldsymbol{x} = \boldsymbol{f}_{Full}(\boldsymbol{\theta}_{34}),$$

that consists of three mappings for the three subsystems (Modified Pantograph, Crank Arms, Differential):

$$\boldsymbol{x} = \boldsymbol{f}_P(\boldsymbol{d}) \qquad \boldsymbol{d} = \begin{bmatrix} d_1 \\ d_2 \end{bmatrix} = \boldsymbol{f}_C(\boldsymbol{\theta}_{12}) \qquad \boldsymbol{\theta}_{12} = \begin{bmatrix} \theta_1 \\ \theta_2 \end{bmatrix} = \boldsymbol{f}_D(\boldsymbol{\theta}_{34}).$$

1. Modified Pantograph

For the Modified Pantograph subsystem (Figure E.2), the kinematics are

$$e = \frac{1}{2}d_2 - \frac{1}{2}d_1$$

$$f = b\sin\alpha + c\cos\alpha = \frac{b}{a}e + \frac{c}{a}\sqrt{a^2 - e^2}$$

$$g = (a-b)\cos\alpha + c\sin\alpha = \frac{(a-b)}{a}\sqrt{a^2 - e^2} + \frac{c}{a}e$$

$$\begin{bmatrix} x \\ z \end{bmatrix} = \begin{bmatrix} \frac{1}{2}d_1 + \frac{1}{2}d_2 \\ \sqrt{d^2 - f^2} - g \end{bmatrix}.$$

The Jacobian is calculated by differentiating the kinematics with respect to time, defining the pantograph variable k_P :

$$\frac{\partial x}{\partial d_1} = \frac{1}{2}$$

$$\frac{\partial x}{\partial d_2} = \frac{1}{2}$$

$$\frac{\partial z}{\partial d_1} = \frac{1}{2}(d^2 - f^2)^{-\frac{1}{2}} \cdot (-2f \cdot \frac{\partial f}{\partial d_1}) - \frac{\partial g}{\partial d_1}$$

$$= \frac{-f}{\sqrt{d^2 - f^2}} \cdot \left(\frac{b}{a}\frac{\partial e}{\partial d_1} + \frac{c}{2a\sqrt{a^2 - e^2}} \cdot -2e\frac{\partial e}{\partial d_1}\right) - \left(\frac{(a-b)}{2a\sqrt{a^2 - e^2}} \cdot -2e\frac{\partial e}{\partial d_1} + \frac{c}{a}\frac{\partial e}{\partial d_1}\right)$$

$$= \left\{\frac{f}{\sqrt{d^2 - f^2}} \cdot \left(\frac{ce}{a\sqrt{a^2 - e^2}} - \frac{b}{a}\right) + \left(\frac{(a-b)e}{a\sqrt{a^2 - e^2}} - \frac{c}{a}\right)\right\} \cdot \frac{\partial e}{\partial d_1}$$

$$= \{...\} \cdot \frac{-1}{2} \equiv -k_P(d_1, d_2)$$

$$\frac{\partial z}{\partial d_2} = \{...\} \cdot \frac{\partial e}{\partial d_2} = \{...\} \cdot \frac{1}{2} = k_P(d_1, d_2).$$
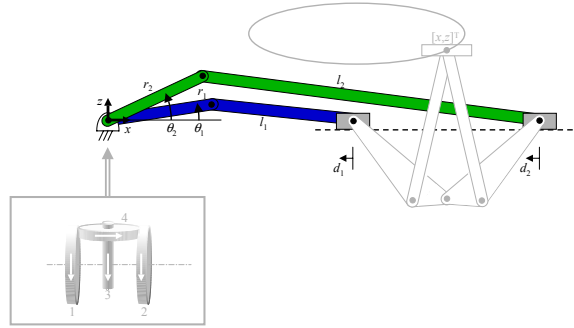
Figure E.3. The Crank Arms subsystem.

Therefore, the Jacobian and its inverse are

$$
\begin{bmatrix} \dot{x} \\ \dot{z} \end{bmatrix} = \begin{bmatrix} \frac{1}{2} & \frac{1}{2} \\ -k_p & k_p \end{bmatrix} \begin{bmatrix} \dot{d}_1 \\ \dot{d}_2 \end{bmatrix} = \boldsymbol{J}_P \cdot \dot{\boldsymbol{d}}
$$

$$
\begin{bmatrix} \dot{d}_1 \\ \dot{d}_2 \end{bmatrix} = \begin{bmatrix} 1 & -\frac{1}{2k_p} \\ 1 & \frac{1}{2k_p} \end{bmatrix} \begin{bmatrix} \dot{x} \\ \dot{z} \end{bmatrix} = \boldsymbol{J}_P^{-1} \cdot \dot{\boldsymbol{x}},
$$

where a dot over a variable represents differentiation with respect to time.

2. Crank Arms

For the Crank Arms, as shown in Figure E.3, the kinematics are

$$
l_1^2 = r_1^2 + d_1^2 - 2r_1 d_1 \cos \theta_1
$$

$$
d_1 = \frac{2r_1 \cos \theta_1 \pm \sqrt{4r_1^2 \cos^2 \theta_1 - 4 \cdot 1 \cdot (r_1^2 - l_1^2)}}{2 \cdot 1}
$$

$$
\begin{bmatrix} d_1 \\ d_2 \end{bmatrix} = \begin{bmatrix} r_1 \cos \theta_1 + \sqrt{r_1^2 \cos^2 \theta_1 + l_1^2 - r_1^2} \\ r_2 \cos \theta_2 + \sqrt{r_2^2 \cos^2 \theta_2 + l_2^2 - r_2^2} \end{bmatrix}.
$$

The $\pm$ in the above equation is known to be positive because of the crank arms' geometries.

The time derivatives (defining crank variables k_{C_1} and k_{C_2}) are

$$\frac{\partial d_1}{\partial \theta_1} = \left(-r_1 \sin \theta_1 - \frac{r_1^2 \sin \theta_1 \cos \theta_1}{\sqrt{r_1^2 \cos^2 \theta_1 + l_1^2 - r_1^2}} \right) \equiv k_{C_1}(\theta_1)$$

$$\frac{\partial d_1}{\partial \theta_2} = 0$$

$$\frac{\partial d_2}{\partial \theta_1} = 0$$

$$\frac{\partial d_2}{\partial \theta_2} = \left(-r_2 \sin \theta_2 - \frac{r_2^2 \sin \theta_1 \cos \theta_2}{\sqrt{r_2^2 \cos^2 \theta_2 + l_2^2 - r_2^2}} \right) \equiv k_{C_2}(\theta_2).$$

and the Jacobian and inverse are

$$\begin{bmatrix} \dot{d}_1 \\ \dot{d}_2 \end{bmatrix} = \begin{bmatrix} k_{C_1} & 0 \\ 0 & k_{C_2} \end{bmatrix} \begin{bmatrix} \dot{\theta}_1 \\ \dot{\theta}_2 \end{bmatrix} = \boldsymbol{J}_C \cdot \dot{\boldsymbol{\theta}}_{12}$$

$$\begin{bmatrix} \dot{\theta}_1 \\ \dot{\theta}_2 \end{bmatrix} = \begin{bmatrix} \frac{1}{k_{c_1}} & 0 \\ 0 & \frac{1}{k_{c_2}} \end{bmatrix} \begin{bmatrix} \dot{d}_1 \\ \dot{d}_2 \end{bmatrix} = \boldsymbol{J}_P^{-1} \cdot \dot{\boldsymbol{d}}.$$

3. Differential

From the Differential's geometry, it can be shown that

$$\begin{bmatrix} \dot{\theta}_3 \\ \dot{\theta}_4 \end{bmatrix} = \begin{bmatrix} \frac{1}{2} & \frac{1}{2} \\ \frac{1}{2} \frac{r_{\theta_1}}{r_{\theta_4}} & -\frac{1}{2} \frac{r_{\theta_1}}{r_{\theta_4}} \end{bmatrix} \begin{bmatrix} \dot{\theta}_1 \\ \dot{\theta}_2 \end{bmatrix}.$$
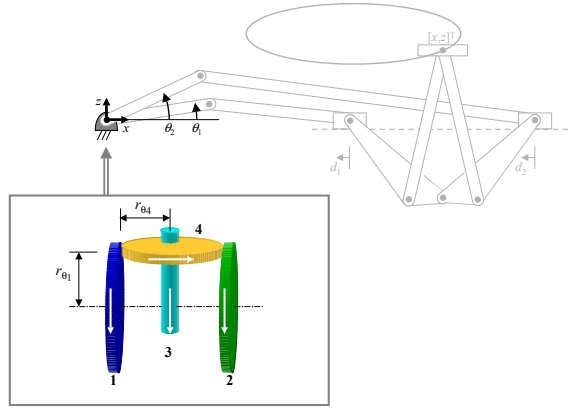
Figure E.4. The Differential subsystem.

This is the inverse Jacobian for the differential subsystem. That is,

$$\begin{bmatrix} \dot{\theta}_1 \\ \dot{\theta}_2 \end{bmatrix} = \begin{bmatrix} 1 & \frac{r_{\theta_4}}{r_{\theta_1}} \\ 1 & -\frac{r_{\theta_4}}{r_{\theta_1}} \end{bmatrix} \begin{bmatrix} \dot{\theta}_3 \\ \dot{\theta}_4 \end{bmatrix} \qquad\qquad = \boldsymbol{J}_D \cdot \dot{\boldsymbol{\theta}}_{34}$$

$$\begin{bmatrix} \dot{\theta}_3 \\ \dot{\theta}_4 \end{bmatrix} = \begin{bmatrix} \frac{1}{2} & \frac{1}{2} \\ \frac{1}{2}\frac{r_{\theta_1}}{r_{\theta_4}} & -\frac{1}{2}\frac{r_{\theta_1}}{r_{\theta_4}} \end{bmatrix} \begin{bmatrix} \dot{\theta}_1 \\ \dot{\theta}_2 \end{bmatrix} \qquad\qquad = \boldsymbol{J}_D^{-1} \cdot \dot{\boldsymbol{\theta}}_{12}.$$

The Jacobian can be integrated to obtain the kinematics:

$$\begin{bmatrix} \theta_1 \\ \theta_2 \end{bmatrix} = \begin{bmatrix} \theta_3 + \frac{r_{\theta_4}}{r_{\theta_1}}\theta_4 + \theta_1|_{t=0} \\ \theta_3 - \frac{r_{\theta_4}}{r_{\theta_1}}\theta_4 + \theta_2|_{t=0} \end{bmatrix}.$$

4. Full System

Combining the three subsystem's Jacobians,

$$\dot{\boldsymbol{x}} = \boldsymbol{J}_{Full}(\theta_{34}) \cdot \dot{\boldsymbol{\theta}}_{34}$$

$$= \boldsymbol{J}_P \cdot \boldsymbol{J}_C \cdot \boldsymbol{J}_D \cdot \dot{\boldsymbol{\theta}}_{34}$$

$$= \begin{bmatrix} \frac{1}{2} & \frac{1}{2} \\ -k_P & k_P \end{bmatrix} \begin{bmatrix} k_{C_1} & 0 \\ 0 & k_{C_2} \end{bmatrix} \begin{bmatrix} 1 & \frac{r_{\theta_4}}{r_{\theta_1}} \\ 1 & -\frac{r_{\theta_4}}{r_{\theta_1}} \end{bmatrix} \cdot \dot{\boldsymbol{\theta}}_{34}$$

$$= \begin{bmatrix} \frac{1}{2} & \frac{1}{2} \\ -k_P & k_P \end{bmatrix} \begin{bmatrix} k_{C_1} & \frac{r_{\theta_4}}{r_{\theta_1}} k_{C_1} \\ k_{C_2} & -\frac{r_{\theta_4}}{r_{\theta_1}} k_{C_2} \end{bmatrix} \cdot \dot{\boldsymbol{\theta}}_{34}$$

$$= \begin{bmatrix} \frac{1}{2}(k_{C_1} + k_{C_2}) & \frac{1}{2}\frac{r_{\theta_4}}{r_{\theta_1}}(k_{C_1} - k_{C_2}) \\ -k_P(k_{C_1} - k_{C_2}) & -k_P\frac{r_{\theta_4}}{r_{\theta_1}}(k_{C_1} + k_{C_2}) \end{bmatrix} \cdot \dot{\boldsymbol{\theta}}_{34}$$

$$\dot{\boldsymbol{\theta}}_{34} = \boldsymbol{J}^{-1} \cdot \dot{\boldsymbol{x}}$$

$$= \boldsymbol{J}_D^{-1} \cdot \boldsymbol{J}_C^{-1} \cdot \boldsymbol{J}_P^{-1} \cdot \dot{\boldsymbol{x}}$$

$$= \begin{bmatrix} \frac{1}{2} & \frac{1}{2} \\ \frac{1}{2}\frac{r_{\theta_1}}{r_{\theta_4}} & -\frac{1}{2}\frac{r_{\theta_1}}{r_{\theta_4}} \end{bmatrix} \begin{bmatrix} \frac{1}{k_{C_1}} & 0 \\ 0 & \frac{1}{k_{C_2}} \end{bmatrix} \begin{bmatrix} 1 & -\frac{1}{2k_P} \\ 1 & \frac{1}{2k_P} \end{bmatrix} \cdot \dot{\boldsymbol{x}}$$

$$= \begin{bmatrix} \frac{1}{2} & \frac{1}{2} \\ \frac{1}{2}\frac{r_{\theta_1}}{r_{\theta_4}} & -\frac{1}{2}\frac{r_{\theta_1}}{r_{\theta_4}} \end{bmatrix} \begin{bmatrix} \frac{1}{k_{C_1}} & -\frac{1}{2k_P}\frac{1}{k_{C_1}} \\ \frac{1}{k_{C_2}} & \frac{1}{2k_P}\frac{1}{k_{C_2}} \end{bmatrix} \cdot \dot{\boldsymbol{x}}$$

$$= \begin{bmatrix} \frac{1}{2}\left(\frac{1}{k_{C_1}} + \frac{1}{k_{C_2}}\right) & -\frac{1}{4k_P}\left(\frac{1}{k_{C_1}} - \frac{1}{k_{C_2}}\right) \\ \frac{1}{2}\frac{r_{\theta_1}}{r_{\theta_4}}\left(\frac{1}{k_{C_1}} - \frac{1}{k_{C_2}}\right) & -\frac{1}{4k_P}\frac{r_{\theta_1}}{r_{\theta_4}}\left(\frac{1}{k_{C_1}} + \frac{1}{k_{C_2}}\right) \end{bmatrix} \cdot \dot{\boldsymbol{x}}.$$

5. Dynamics Using All Masses

To derive the dynamic equations for the device where every link has a mass, I begin by writing the energy equation. (Alternatively, I could have started with the Lagrangian.) This derivation is for one leg only.

The kinematics for the pedal are as described in the previous sections. The first and second time derivatives of $\boldsymbol{x}$ are

$$\dot{\boldsymbol{x}} = \begin{bmatrix} \frac{\partial f_x}{\partial \theta_3} & \frac{\partial f_x}{\partial \theta_4} \\ \frac{\partial f_z}{\partial \theta_3} & \frac{\partial f_z}{\partial \theta_4} \end{bmatrix} \begin{bmatrix} \dot{\theta}_3 \\ \dot{\theta}_4 \end{bmatrix} = \boldsymbol{J}_{Full}\dot{\boldsymbol{\theta}}_{34}$$

$$\ddot{\boldsymbol{x}} = \boldsymbol{J}_{Full}\ddot{\boldsymbol{\theta}}_{34} + \left(\frac{d}{dt}\boldsymbol{J}_{Full} \right) \dot{\boldsymbol{\theta}}_{34} = \boldsymbol{J}_{Full}\ddot{\boldsymbol{\theta}}_{34} + \left(\frac{\partial \boldsymbol{J}_{Full}}{\partial \theta_3}\dot{\boldsymbol{\theta}}_3 + \frac{\partial \boldsymbol{J}_{Full}}{\partial \theta_4}\dot{\boldsymbol{\theta}}_4 \right) \dot{\boldsymbol{\theta}}_{34}$$

Note that I could have instead calculated $\frac{d^2}{dt^2}f_i$ which leads to the equivalent equation

$$\ddot{\boldsymbol{x}} = \dot{\boldsymbol{\theta}}_{34}^{T} \begin{bmatrix} \boldsymbol{H}_{f_x} \\ \boldsymbol{H}_{f_z} \end{bmatrix} \dot{\boldsymbol{\theta}}_{34}$$

where $\boldsymbol{H}_i$ is the three-dimensional Hessian matrix of state variable i.

The energy of link i (ignoring the subscript i) and its time derivative are

$$E = KE + PE = \frac{1}{2}\dot{\boldsymbol{x}}^T \begin{bmatrix} m & 0 & 0 \\ 0 & m & 0 \\ 0 & 0 & I \end{bmatrix} \dot{\boldsymbol{x}} + \boldsymbol{x}^T \begin{bmatrix} 0 \\ mg \\ 0 \end{bmatrix}$$

$$= \frac{1}{2}\dot{\boldsymbol{x}}^T \boldsymbol{m}\dot{\boldsymbol{x}} + \boldsymbol{x}^T \boldsymbol{w}$$

$$\frac{d}{dt}E = \dot{\boldsymbol{x}}^T \boldsymbol{m}\ddot{\boldsymbol{x}} + \dot{\boldsymbol{x}}^T \boldsymbol{w}$$

$$= \left(\boldsymbol{J}\dot{\boldsymbol{\theta}}_{34}\right)^T \boldsymbol{m}\left(\boldsymbol{J}\ddot{\boldsymbol{\theta}}_{34} + \dot{\boldsymbol{J}}\dot{\boldsymbol{\theta}}_{34}\right) + \left(\boldsymbol{J}\dot{\boldsymbol{\theta}}_{34}\right)^T \boldsymbol{w}$$

$$= \dot{\boldsymbol{\theta}}_{34}^T \boldsymbol{J}^T \boldsymbol{m}\left(\boldsymbol{J}\ddot{\boldsymbol{\theta}}_{34} + \dot{\boldsymbol{J}}\dot{\boldsymbol{\theta}}_{34}\right) + \dot{\boldsymbol{\theta}}_{34}^T \boldsymbol{J}^T \boldsymbol{w}$$

$$= \dot{\boldsymbol{\theta}}_{34}^T \left(\boldsymbol{J}^T \boldsymbol{m}\boldsymbol{J}\ddot{\boldsymbol{\theta}}_{34} + \boldsymbol{J}^T \boldsymbol{m}\dot{\boldsymbol{J}}\dot{\boldsymbol{\theta}}_{34} + \boldsymbol{J}^T \boldsymbol{w}\right)$$

where KE is the kinetic energy, PE is the potential energy, m is the mass of the sub-component, I is the rotational inertia of the subcomponent about its center of mass, and g is acceleration due to gravity.

The change of energy of the total device is equal to the power flow into the device:

$$\frac{d}{dt}E_{total} = P_{in}$$

$$\sum \frac{d}{dt}E_i = P_{34} + P_{user}$$

$$\sum \dot{\boldsymbol{\theta}}_{34}^T \left(\boldsymbol{J}_i^T m_i \boldsymbol{J}_i \ddot{\boldsymbol{\theta}}_{34} + \boldsymbol{J}_i^T m_i \dot{\boldsymbol{J}}_i \dot{\boldsymbol{\theta}}_{34} + \boldsymbol{J}_i^T \boldsymbol{w}_i \right) = \dot{\boldsymbol{\theta}}_{34}^T \boldsymbol{\tau}_{34} + \dot{\boldsymbol{\theta}}_{34}^T \boldsymbol{J}_{Full}^T \boldsymbol{F}_{user}$$

$$\sum \left(\boldsymbol{J}_i^T m_i \boldsymbol{J}_i \ddot{\boldsymbol{\theta}}_{34} + \boldsymbol{J}_i^T m_i \dot{\boldsymbol{J}}_i \dot{\boldsymbol{\theta}}_{34} + \boldsymbol{J}_i^T \boldsymbol{w}_i \right) = \boldsymbol{\tau}_{34} + \boldsymbol{J}_{Full}^T \boldsymbol{F}_{user}$$

$$\left[\sum \boldsymbol{J}_i^T m_i \boldsymbol{J}_i \right] \ddot{\boldsymbol{\theta}}_{34} + \left[\sum \boldsymbol{J}_i^T m_i \dot{\boldsymbol{J}}_i \right] \dot{\boldsymbol{\theta}}_{34}$$

$$+ \left[\left(\sum \boldsymbol{J}_i^T \boldsymbol{w}_i \right) - \boldsymbol{J}_{Full}^T \boldsymbol{F}_{user} \right] = \boldsymbol{\tau}_{34}$$

$$\boldsymbol{M}(\boldsymbol{\theta}_{34})\ddot{\boldsymbol{\theta}}_{34} + \boldsymbol{C}(\boldsymbol{\theta}_{34}, \dot{\boldsymbol{\theta}}_{34})\dot{\boldsymbol{\theta}}_{34} + \boldsymbol{N}(\boldsymbol{\theta}_{34}) = \boldsymbol{\tau}$$

That is,

$$\boldsymbol{M}(\boldsymbol{\theta}_{34}) = \sum \boldsymbol{J}_i^T m_i \boldsymbol{J}_i$$

$$\boldsymbol{C}(\boldsymbol{\theta}_{34}, \dot{\boldsymbol{\theta}}_{34}) = \sum \boldsymbol{J}_i^T m_i \left(\left[\frac{\partial \boldsymbol{J}_i}{\partial \theta_3} \quad \frac{\partial \boldsymbol{J}_i}{\partial \theta_4} \right] \dot{\boldsymbol{\theta}}_{34} \right)$$

$$\boldsymbol{N}(\boldsymbol{\theta}_{34}) = \left(\sum \boldsymbol{J}_i^T \boldsymbol{w}_i \right) - \boldsymbol{J}_{Full}^T \boldsymbol{F}_{user}$$